Electrical Characterization of Organic Devices
Case study: polythiophene-fullerene based solar cells

Von der Fakultät Mathematik und Naturwissenschaften der
Carl von Ossietzky Universität Oldenburg
zur Erlangung des Grades und Titels eines
Doktors der Naturwissenschaften
(Dr. rer. nat.)
angenommene Dissertation.

von Frau Dana Chirvase

Geboren am 2. September 1967
in Iasi, Rumänien

Erstgutachter: Prof Dr. Vladimir Dyakonov
Zweitgutachter: Prof. Dr. Jürgen Parisi
Drittgutachter: apl. Prof. Wilfried Tuszynski

Tag der Disputation: 15.12.2004

Contents

1. Motivation and outline.....1

2. General operation principles of organic solar cells.... 5
2.1 What are conjugated polymers?..... 5
2.2 Transport mechanisms of charge carriers..... 5
2.3 Basic principles of photochemistry..... 7
2.4 Materials used and device architecture.....10
2.5 How does an organic solar cell operate?..... 12
2.6 Solar radiation.....15
2.7 Theoretical framework of solar cell operation.....20
2.7.1 Power conversion efficiency.....20
2.7.2 Equivalent circuit of solar cells.....21
2.7.3 Short circuit current.....22
2.7.4 Open circuit voltage.....25
2.7.5 Influence of photoluminescence on the open circuit voltage.....26

3. Investigation of the influence of different metal electrodes on the main parameters of P3HT:PCBM based solar cells – The origin of the open circuit voltage.....29
3.1 Introduction.....29
3.2 Experimental.....31
3.3 Results and discussions.....31
4. Investigation on light intensity and temperature dependence of the main parameters of P3HT:PCBM based solar cells.....36
4.1 Experimental.....36
4.2 Light intensity dependence of the main parameters of P3HT:PCBM based solar cells...36
4.2.1 Short circuit current density, J_{sc}.....36
4.2.2 Open circuit voltage, V_{oc}.....37
4.2.3 Fill factor, FF.....39
4.2.4 Power conversion efficiency.....39
4.3 Temperature dependence of the main parameters of a P3HT:PCBM based solar cell.....41
4.3.1 Open circuit voltage, V_{oc}.....41
4.3.2 Short circuit current density, J_{sc}.....43
4.3.3 Power conversion efficiency, η and fill factor, FF.....44
5.Thermal annealing, a method for improving the efficiency of organic solar cells.....46
5.1 Introduction.....46
5.2 Absorption measurements.....48
5.2.1 Experimental.....48
5.2.2. Results and discussions.....48
5.3 Test on the persistence of improved electrical performance of P3HT:PCBM based solar cells upon thermal annealing.....51
5.3.1 Experimental.....51

5.3.2 Results and discussion.....52
5.4 Morphology measurements.....55
5.4.1 Experimental.....55
5.4.2 Results and discussion: atomic force microscopy….....55
5.5 Optimization of the amount of the PCBM acceptor in P3HT:PCBM based solar cells....61
5.5.1 Experimental.....61
5.5.2 Results and discussion.....61
6. Aspects related to the quality and stability of organic materials.....69
6.1. Quality of the organic material used in the fabrication of photovoltaic devices.....69
6.2 Experimental.....70
6.3 Results and discussions.....70
6.4 Deterioration at the contact electrode/semiconductor interface.....75
6.5 Light induced degradation.....77

7. Concluding remarks.....78

Appendix 1.....81

Appendix 2.....83

Bibliography.....85

ABSTRACT

Polymer based solar cells were fabricated by using Poly(3-hexylthiophene-2.5diyl)(P3HT) as a donor, combined with the fullerene derivative [6,6]-phenyl -C_{61} butyric acid methyl ester, (PCBM) as an acceptor, in a bulk heterojunction structure. Electrical and optical properties of these organic devices were studied together with the dependence of current-voltage characteristics on temperature and illumination intensity. The increase of the short circuit current density with temperature is evidence of a thermally activated transport mechanism, characteristic to disordered materials. This result explains the specific feature of organic solar cells to operate better in a warm climate, rather than at low temperatures, a totally different behaviour compared to conventional inorganic solar cells. The origin of open circuit voltage was investigated by varying the work function of the metallic electrode. From this experiment it was concluded that the open circuit voltage is very sensitive to the workfunction of metallic electrode. The hypothesis of Fermi level pinning of the workfunction of the metallic electrode to the LUMO level of the acceptor could not be confirmed in the case of P3HT:PCBM based solar cells. The thermal annealing applied to P3HT:PCBM based solar cells, was found to be a very effective method to increase the short current density, and therefore, the overall power conversion efficiency of the device. Morphology investigations (by using the Atomic Force Microscopy) for P3HT:PCBM based solar cells show the presence of large PCBM clusters (>500nm) built as a result of thermal annealing. Based on AFM results, as well as on current density-voltage (J-V) curves and external quantum efficiency measurements, the amount of the PCBM acceptor was optimized in the blend to a P3HT:PCBM weight ratio between 1:0.9 and 1:1. The best P3HT:PCBM based solar cell was fabricated with a P3HT:PCBM weight ratio of 1:1 and gave the following results: J_{sc}= 6.4mA/cm², V_{oc}= 0.59V, FF = 63.2%, η = 2.4% at room temperature and a white light intensity of 100mW/cm². Finally, it was shown that the electrical performance of P3HT:PCBM based solar cells can be considerably influenced by the quality of the organic material used for the fabrication.

ZUSAMMENFASSUNG

Es wurden Polymer-Solarzellen mit einer Bulk-Heteroverbindungsstruktur hergestellt, wobei P3HT als Donor und das Fullerenderivat PCBM als Akzeptor fungiert. Die elektrischen und optischen Eigenschaften dieser organischen Zellen wurden hauptsächlich über die Abhängigkeit ihrer Strom-Spannungs-Charakteristiken von Temperatur und Lichtintensität studiert. Die Zunahme der Kurzschlußstromdichte mit der Temperatur ist Beweis für einen thermisch aktivierten Transportmechanismus, der für ungeordnete Materialien charakteristisch ist. Dieses Ergebnis erklärt die hervorstechende Eigenschaft organischer Solarzellen in einem warmen Klima besser zu funktionieren, als bei tiefen Temperaturen. Konventionelle anorganische Solarzellen zeigen im Gegensatz dazu ein ganz anderes abweichendes Verhalten. Der Ursprung der Leerlaufspannung wurde durch Variation der Austrittsarbeit der Metallelektrode untersucht. Aus diesem Experiment konnte geschlossen werden, daß die Leerlaufspannung empfindlich von der Austrittsarbeit der verwendeten Metallelektrode abhängt. Die Hypothese des Fermi- Level- Pinnings der Austrittsarbeit der Metallelektrode an das Lumoniveau des Akzeptors hat sich im Falle der P3HT:PCBM Solarzellen nicht bestätigt. Die thermische Behandlung der P3HT:PCBM Solarzellen erwies sich als eine sehr effektive Methode zur Erhöhung der Kurzschlußstromdichte und damit auch als sehr wirkungsvoll zur Verbesserung des Gesamtwirkungsgrades der Zelle. Untersuchungen der Morphologie der P3HT : PCBM Solarzellen mittels AFM zeigen die Präsenz sehr großer PCBM Cluster (> 500 nm) als ein Resultat der thermischen Behandlung. Basierend auf diesen Ergebnissen, den J - V- Kurven und Messungen der externen Quantenausbeute wurde der Anteil des PCBM Akzeptors in der P3HT : PCBM -Mischung auf ein Gewichtsverhältnis zwischen 1:0,9 und 1:1 optimiert. Die beste P3HT:PCBM Solarzelle die hergestellt wurde, hatte ein Gewichtsverhältnis P3HT : PCBM von 1:1 und erzielte bei Raumtemperatur und einer Lichtintensität von 100 mW/cm² die folgenden Ergebnisse: J_{sc}= 6.4mA/cm², V_{oc}= 0.59V, FF = 63.2%, η=2.4% bei Raumtemperatur und einer Lichtintensität von 100mW/cm².
Zusätzlich konnte gezeigt werden, daß die elektrischen Eigenschaften von P3HT : PCBM Solarzellen wesentlich durch die Qualität des verwendeten organischen Materials beeinflußt werden.

Chapter 1 Motivation and Outline

1.1 Motivation

The quality of human life is related to the availability of energy resources. The present yearly energy consumption exceeds 6000GW [116] and is expected to grow more. Faced with this continuous demand, the earth's sources of non-renewable energy (coil, oil) are not expected to last long. According to recent predictions [1], the inevitable permanent decline in the oil production rate is expected to start in the next 10-20 years. On the other hand, the combustion of fossil fuels in the past had harmful effects on the nature balance of our planet. Today, the large quantity of almost $20x10^{12}$ kg of carbon dioxide which is released into the atmosphere cannot be absorbed by the plants and determines an increase of temperature by 0.3-0.6°C compared to that of the last 19^{th} century [2],[3],[4]. Renewable energy sources (wind, solar, geothermal, biomass) offer a relatively „environmentally friendly " solution, but the major drawback to date has been the cost.

To harness the huge amount of energy provided by the sun every second ($1395J/m^2$), this represents the main challenge that the solar photovoltaic technology faces to. Starting with the introduction of Si (maximum laboratory efficiency $\eta = 25\%$ and 12-16% on the market), as the prime semiconductor material used for solar cells in the late 1950s, followed by amorphous silicon a-Si:H (maximum laboratory efficiency $\eta = 13\%$) in the last years of 1970s, then the thin film technology, CIGS ($\eta = 19.2\%$) and CdTe ($\eta = 16.7\%$), now it is the turn of photochemistry and semiconductor physics to make a decisive contribution in this field.

Organic solar cells are based on an innovative advanced concept which mimics the natural photosynthesis in the conversion and storage of solar energy. Polymer based semiconductors have the main advantage to combine the opto-electronic properties of conventional semiconductors with excellent mechanical and processing properties of polymer materials.

The genesis of this new research field started in the 1970s, when a japanese scientist, H. Shirakawa prepared by accident the first polymer capable of conducting electricity – polyacetylene [5]. The combined efforts of two other american scientists, A. J. Heeger and A. J. MacDiarmid, led to the subsequent discovery that the polymer would undergo a huge increase in conductivity, only by oxidative doping [6]. The surprising discovery of the three laureates of the 2000 Nobel prize made a revolution in the semiconductor research field. At present, while terrestrial energy applications represented so far the primary aim of research investigation, small scale appliances and more recently, space applications using thin film solar cells on polymer substrate have increased special attention. This class of materials have been used to built efficient light emitting diodes [7], field effect transistors, optically pumped lasers, solar cells as well as power smart plastic (credit, phone) cards or photodetectors in large area scanners [117]. Therefore, applications based on conjugated polymers have as main target to cover the market energy needs related to the microelectronics sector and represent at the moment a very promising research field.

1.2 Outline

The present thesis is based on results obtained during 3.5 years of research within the Energy and Semiconductor Research Department at the University of Oldenburg, Germany, in the frame of the EU-RTN Project EUROMAP under contract HPRN-CT-2000-00127 financed by the European Union.

The main aim was to investigate electrical properties of conjugated polymers suitable for the fabrication of organic solar cells. A series of different donor/acceptor organic compounds was tested as potential candidates in the fabrication of efficient organic solar cells. They are: OC1C10-PPV, synthesised via sulfinyl route, and poly(alkyl-thiophenes) as donors and PCBM fullerene derivative and TCAQ tetracyano-antraquino-dimethane derivative, as acceptors. From all these materials, the best results were obtained with the following combinations in the preparation of organic solar cells: OC1C10-PPV:PCBM and poly(3-hexylthiophene-2.5diyl) (P3HT):PCBM. With the latter combination, i.e., P3HT:PCBM a systematic study was carried out and the most relevant results constitute the present thesis.

Chapter 2 presents the main properties of conjugated polymers and operation principles of organic solar cells, and is meant to be an easy and hopefully clear introduction, suitable also for readers with no experience in the field of organic photovoltaics. Organic optoelectronics, to whom belong also polymer based solar cells, involves more than another research field an interdisciplinary approach. Organic solar cells try to mimic the operation principle of photosynthesis from green plants. From this point of view, chemistry, physics and biology contribute equally, although in different languages, to the overall practical and theoretical understanding of natural processes in these types of devices. In this context the basic principles of photochemistry and the necessary minimum information related to solar radiation are explained. The generation process of charge carriers, transport mechanisms and device architecture (the bulk heterojunction concept) are also explained, followed by the theoretical framework of solar cell operation. The theoretical diode model borrowed from classical inorganic solar cells is applied to organic solar cells, due to the fact that at present, no theoretical and reliable model exists for these type of organic devices. The limitations of the classical model are mentioned.

Chapter 3 is focussed on the understanding of the origin of the open circuit voltage in the particular case of P3HT:PCBM based solar cells. The work function of the cathode was varied for P3HT:PCBM based solar cells by evaporating different metallic contacts (magnesium, aluminium, copper, gold) and the current density - voltage curves were measured under the same conditions.

In the **Chapter 4,** the current density-voltage characteristics of P3HT:PCBM based solar cells fabricated with different metallic electrodes were measured for different temperatures and light intensities. The variation of the main electrical parameters (open circuit voltage, short circuit current density, fill factor and efficiency) with light intensity and temperature was analysed.

Chapter 5 presents the application of a practical method used for improving the efficiency of organic solar cells i.e., the thermal annealing. By heating the P3HT:PCBM solar cells at a certain temperature and for a certain period of time, morphological changes can be induced in the bulk active layer of the organic device, having as main result a huge increase in the short circuit current, but almost no influence on the open circuit voltage. Additionally, the fill factor increases and the overall electrical characteristics of the solar cell improves towards an ideal diode curve. Different annealing temperatures and times have been tested with respect to the

stability of the improved electrical performances of annealed P3HT:PCBM based solar cells. Finally, for the particular case of thermal annealing at the temperature of T_a = 130°C and annealing time of 20s, an interesting phenomenon was discovered, i.e, cystallisation of the PCBM compound as a result of annealing. The influence of PCBM clusters on the electrical properties of annealed P3HT:PCBM solar cells was studied by performing external quantum efficiency, (EQE), current density –voltage and absorption measurements. Conclusions were correlated with atomic force microscopy (AFM) images and led finally to the optimization of the amount of PCBM in the bulk organic layer.

Chapter 6 presents an important aspect related generally to the deterioration of organic solar cells and illustrated with experimental results in the case of P3HT:PCBM based solar cells. By producing cells under identical preparation conditions, but by using different batches of the same P3HT material, considerable differences are reported in the electrical performances of these devices. These differences have been attributed to different degrees of purity, organic materials are generally subject to, as a result of synthesis.

Therefore, one important remark should be mentioned here: All results and conclusions obtained in this thesis are valid with respect to the particular preparation procedures, conditions and materials used in the fabrication of P3HT:PCBM based solar cells, and should not be taken as absolute or extrapolated when comparing different results in the literature.

Polymer electronics generally, and particularly organic solar cells are at present at the level of fundamental research. The efforts in the present thesis were focussed less on obtaining the highest power conversion efficiency (maximum obtained here was 2.4%, measured at 100mW/cm² and room temperature), but more on understanding the physical processes. Negative results were considered in the same way as positive ones, contributing together to the understanding of what is an organic solar cell. And this because one cannot be in the light without being before in the dark, and without opening new doors. This was the working spirit of this thesis. In the hope that even, if the complete light of understanding was not reached, some small pieces of the huge puzzle called “organic solar cells” were clarified, I would like to express my gratitude to the people who helped me to perform this research:

Acknowledgements

I would like to thank both Prof. Dr. Jürgen Parisi and Prof. Dr. Vladimir Dyakonov, for making possible for me to perform this research at the University of Oldenburg and supporting me in the frame of the EUROMAP project.

I thank Dr. Jürgen Schumacher, for raising my interest in the semiconductor field during his interesting solar energy lecture given in 1998/1999 in the frame of the Renewable Energy postgraduate course, and for his answer one year later, when I asked him if it is possible to start a PhD at the University of Oldenburg. “Yes, give me time three days” he answered to me. Thank you again!

I thank Prof. Dr. Martin Holtaus, who encouraged me as well as Prof. Jürgen Parisi, during my study and examination of Quantum Mechanics, topic of which as non-physicist I was very afraid.

I thank Dr. Leonid Govor for all discussions and useful recommendations related to my work and for his permanent help.

I thank Dr. Konrad Blum and Michael Golba for supporting me to work with the students in the lab within the Renewable Energy Program.

I thank from all my heart all my collegues from the EHF group, especially Ingo Riedel, who teached me everything he knew in the field of organic solar cells and who supported me permanently in the labs during these three years. Many thanks go to my colleague from Zimbabwe, Zivayi Chiguvare, (The Knowledge Threshold) for so many interesting discussions starting from physics, chemistry, philosophy, religion to politics and for his permanent support in our common work. I thank also all my colleagues Jens Reemts, Marco Munzel, Susanne Böger, Liz von Hauff, Verena Mertens, Carsten Deibel, Martin Knipper, Johannes Sieger, Amir Gashti and Elzbieta Chojnowski for their permanent help and friendly atmosphere in our research group. Many thanks go to Holger Koch for his assistance in the lab in critical moments, as well as to Hans Holtorf, Tania Miesner, Andrea Geisler and Wilhelm Jürgen. I also thank Prof. Wittstock and Mrs. Erni Hassel Schneider for their help during atomic force microscopy (AFM) measurements. I thank to Michael Niggemann from ISE Freiburg for performing scanning electron microscopy (SEM) measurements.

I thank my best friend, Uzodinma Okoroanyanwu, (The Good Way to the Sun) from Advanced Micro Devices – USA, who forwarded to me so many interesting books and articles, and spend a lot of time explaining from a chemist perspective the physical processes in polymers.

I thank all members of the Euromap Project from Germany, Austria, Italy, Belgium, Italy and Spain and the EU Commission, for offering me the opportunity to work in such an international environment. And, I thank to be given the opportunity to travel to so many interesting places in Europe: to investigate the morphology structure of arab architecture in Spain and Portugal, to admire the stained glass of gothic cathedrals in Germany, Austria, France, Belgium, to climb the medieval towers in Carcassone, Avignon, to wonder about Mont St. Michel or Sacre Coeur, to drink beer in Kassel, in the same pub where Bruder Grimm wrote their stories and, and..

And last but not least, I thank from all my heart my parents from Romania for their care, permanent efforts and support in the long process of my general education which started since I was born.

Chapter 2

General operation principles of organic solar cells

2.1 What are conjugated polymers?

Plastics have been known so far as isolators, that means they do not conduct electricity, they are polymers, molecules that form long chains of a repeating unit called monomer. In order to become electrically conductive, the material must be similar to a metal with electrons free to move along the polymer chain. The electron configuration of the six electrons in a carbon atom in its ground state is $1s^2 2s^2 2p^2$. The three valence electrons in the $2s^2 2p^2$ combine to a hybridized structure when forming covalent bonds, giving rise to **σ -** sigma bonding orbitals which actually form the scheleton of the polymer chain. The fourth electron resides in a delocalized p_z orbital oriented perpendicular to the backbone (the plane of the **σ -**sigma orbitals) as it is illustrated in **Figure 2.1**. The p_z orbitals of neighboring atoms overlap to form π bands in which electrons are permanently changing their place while the C atomes are fixed. The delocalization of the electrons in the p orbitals is not homogeneous. Between every second carbon atom, there is a shorter bond length (corresponding to a double bond) i.e. conjugated polymers have alternating single bonds C - C and double bonds C = C. It is this alternation of single and double bonds which determines the opening of the band gap due to the Peierls distortion and explains the fact that conjugated polymers in their neutral state are semiconductors and not metals. As a result of the oscillation of the π electrons, the electromagnetic radiation is absorbed. The process is similar to what happens in the photosynthesis process in plants. Is there, for example, only a conjugated double bond, the molecule will absorb only ultraviolet light. For more conjugated double bonds, the molecule will be able to absorb at different wavelengths of the visible light. As a conclusion, the π electrons are, therefore, responsible for the propagation of electrical and chemical influences similar to biological systems.

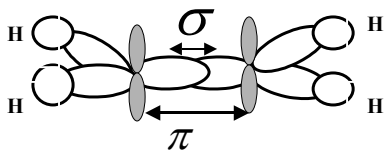

FIGURE 2.1 Electrons in the π orbitals are quasi free and are responsible for the conducting properties of conjugated polymers

The electronic conductivity of conjugated polymers can be changed by doping from a semi-conducting regime in the neutral polymer to a semi-metallic regime. Chemical or electrochemical reduction injects unpaired electrons into the lowest levels of the conduction band. Conversely, oxidation would remove electrons from the top of the valence band to give positive holes and unpaired residual electrons.

2.2 Transport mechanisms of charge carriers

Polymers can exist as amorphous or as crystalline materials but, in the most cases, they consist of mixtures of crystalline and amorphous parts and therefore are considered generally

disordered materials. They are molecular materials, i.e. each polymer chain is its own individual entity and the interaction with other polymer chains is usually weak. Polymer chains can take up different conformations and can be oriented mechanically. In contrast to many materials, polymers do not have an unique molecular weight but are described in terms of weighted average molecular weights, representing the average and the distribution about the mean. With strongly interacting atoms such as covalently bonded silicon, a band structure describing the allowed energy levels can be set up. Disordered materials do not have a band structure. In this case, many localized states are introduced into the conduction band, which can eventually merge together to form bands. These bands are the **HOMO** (**h**ighest **o**ccupied **m**olecular **l**evel) and **LUMO** (**l**owest **u**noccupied **m**olecular **l**evel) corresponding to the valence band and conduction band from the classical inorganic semiconductors respectively.

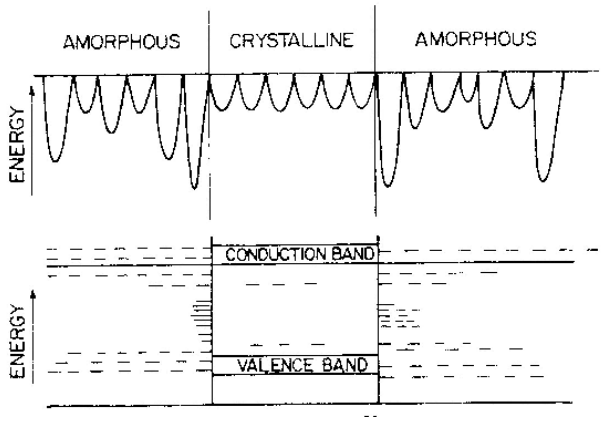

FIGURE 2.2: The energy diagram of a polymer with crystalline and amorphous regions. (Reprinted from reference [60])

The more heavy the doping, the broader the bands should become. When partially filled bands are formed, the charge transport should be of metallic character. In **Figure 2.2** it is presented the energy diagram of a polymer with amorphous and crystalline regions. There are interfacial states at the crystalline-amorphous boundary, which can act as traps for the charge carriers in the crystalline region. The morphological structure (amorphous, crystalline or semicrystalline) determines the transport mechanisms of charge carriers.

There are two distinct types of charge transport: band transport and hopping transport. The type of charge transport mechanism present in an organic material sample can be experimentally determined by the variation of conductivity with temperature. Metals, in which band transport takes place, have a finite conductivity value at zero temperature. Due to the extended states known as bands, the charge carriers move freely being scattered only by impurities in the material and, at higher temperatures, by phonons. After scattering, the direction of propagation of charge carriers is random. In band transport, phonons are the source of resistance and increasing temperature favors a more intense phonon scattering.

In the case of disordered materials like conjugated polymers, the charge carriers follow the hopping transport mechanism by tunneling or hopping between localized states in the energy band gap. In the latter case, since charge carriers are localized, they need an external activation energy to hop from one side to another. The activation energy is provided by the phonons. In this case the hopping conductivity increases with temperature according to the following law:

$$\sigma = \sigma_0 \exp\left(\frac{-E_a}{kT}\right) \qquad \textbf{(2.1)}$$

where E_a represents the activation energy, T is the temperature and k is the Boltzmann constant.

The probability of a hopping event depends on the physical distance to another site/chain and the difference in energy between the sites. The degree of charge carrier localization depends on the amount of structural disorder in the material and, in this case, well ordered films are expected to have better charge transport properties.

2.3 Basic principles of photochemistry

The main process which occurs in organic based devices is based on the photoexcitation of electrons as a result of absorption of the photon energy in the organic bulk material (**Figure 2.3**). In the present paragraph, the basic principles of photochemistry are explained, which are necessary for the understanding of organic solar cell operation mechanism.

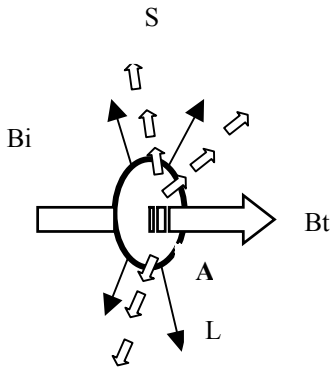

FIGURE 2.3: Photophysical processes of a beam of light interacting with matter: absorption (A), scattering (S), luminescence (L); the rest of the beam is transmitted. The absorbed light A disappears altogether and becomes excitation energy of a sample

Photoexcitation of ground state species leads to the formation of excited states, which are more chemically reactive. And one aspect of the reactivity of excited molecules is to induce transitory or permanent changes in the neighboring molecules by transferring electrons.

When a molecule absorbs visible or ultraviolet light, electrons in the highest occupied orbitals undergo transitions to unoccupied orbitals lying at higher energies. By absorbing a photon of light, the ground state is converted into an electronically excited state (E=hν).

The energy states of molecules, correspond to electronic, vibrational, rotational and translational degrees of freedom. The dominant energy transitions are described usually by the Jablonsky diagram. Each electronic state in the Jablonsky diagram (**Figure 2.4**) corresponds to a bonding or anti-bonding molecular orbital. The orbitals associated with a carbon-carbon bond can be either σ or π type. In the σ bond, electrons are localized between the carbon atoms while the π bonds establish a delocalized electron density above and below the atomic plane. The corresponding antibonding orbitals are designed σ^* or π^* and are of higher energy. There are also valence shell electrons that do not participate in the formation of molecular bonds.

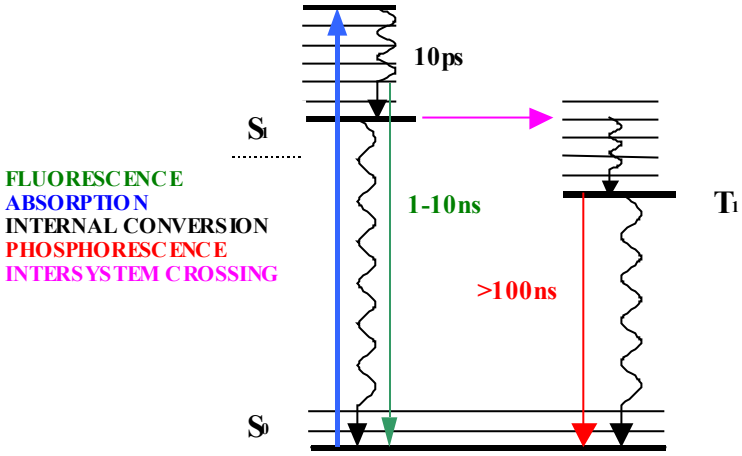

FIGURE 2.4: Jablonsky diagram of organic molecules depicting typical energy levels and energy transfer

In the formation of an excited single state, photoexcitation takes place from the lowest vibrational level of the ground state into any one of the higher vibrational levels of the excited single state. During absorption, the geometry of the molecule does not change although the electrons may undergo rapid motions. This transition to the upper excited single states is referred as Franck-Condon transition. The mass of the electron is smaller than the mass of the nucleus, the electronic transition proceeds much faster (10^{-16}s) than the typical nuclear vibration (10^{-12}-10^{-14}s)[9]. After its formation, the Franck Condon state undergoes some vibrational relaxation to an equilibrium geometry. Usually this process happens in a time interval of 10^{-12}-10^{-14}s. The equilibrated exited state participates in a photochemical reaction. The singlet excited state is a very reactive species and it may release energy or undergo chemical transformations.

The energy releasing pathways illustrated in the **Figure 2.4** are the following:

- **Radiative** –are transitions to lower states including light emission

Fluorescence is the light emission accompanying the transition from the lowest vibrational state of the excited single state to any of the vibrational levels of the ground state. Phosphorescence is the radiative recombination from the triplet excited state to the ground state.

fluorescence $\quad M^*_{(S1)} \longrightarrow M_{(S0)} + h\nu_f$

phosphorescence $\quad M^*_{(T1)} \longrightarrow M_{(S0)} + h\nu_p$

- **Nonradiative** – are transitions involving the release of heat

In a nonradiative transition, the energy of the excited singlet state is dissipated as heat to the surrounding medium. This transition is referred to as an internal conversion. One of the nonradiative transition is the intersystem crossing which implies the formation of the vibrationally triplet state from the singlet excited.

non radiative deactivation $\quad M^*_{(S1)} \longrightarrow M_{(S0)} +$ **heat**

intersystem crossing $\quad M^*_{(S1)} \longrightarrow M^*_{(T1)}$

non radiative deactivation $\quad M^*_{(T1)} \longrightarrow M_{(S0)} +$ **heat**

In addition to radiative and nonradiative transitions, one excited state can participate in a number of inter- and intramolecular reactions. Examples of intramolecular processes include ejection of an electrode (photoionization), decomposition into smaller fragments (photodecomposition) or spontaneous isomerization (photoisomerization). Intermolecular pathways, involve reactions with ground state molecules. Among all these reactions**,** the most relevant for the understanding of the operation of organic solar cells are the **energy transfer** and the **electron transfer.**

Before approching the real operation of an organic solar cell, another aspect should be mentioned: Energy and electron transfer are classified as quenching pathways. In the photochemistry, **quenching** is defined as the deactivation of an excited sensitizer by an external component. The external component is called quencher and is usually a molecule in the ground state.

In the case of **energy transfer**, the quencher (acceptor A) receives the energy from the excited sensitizer (donor D) and becomes excited.

Energy transfer

$$D^* + A \longrightarrow D + A^*$$

In the case of **electron transfer**, the donor is excited first, the excitation is delocalized on the D–A complex before charge transfer is initiated, leading to an ion radical pair and finally charge separation can be stabilized possibly by carrier delocalization on the $D^{+\cdot}$ or $A^{-\cdot}$ species by structural relaxation. **Figure 2.5** shows the two deactivation mechanisms of an excited molecule.

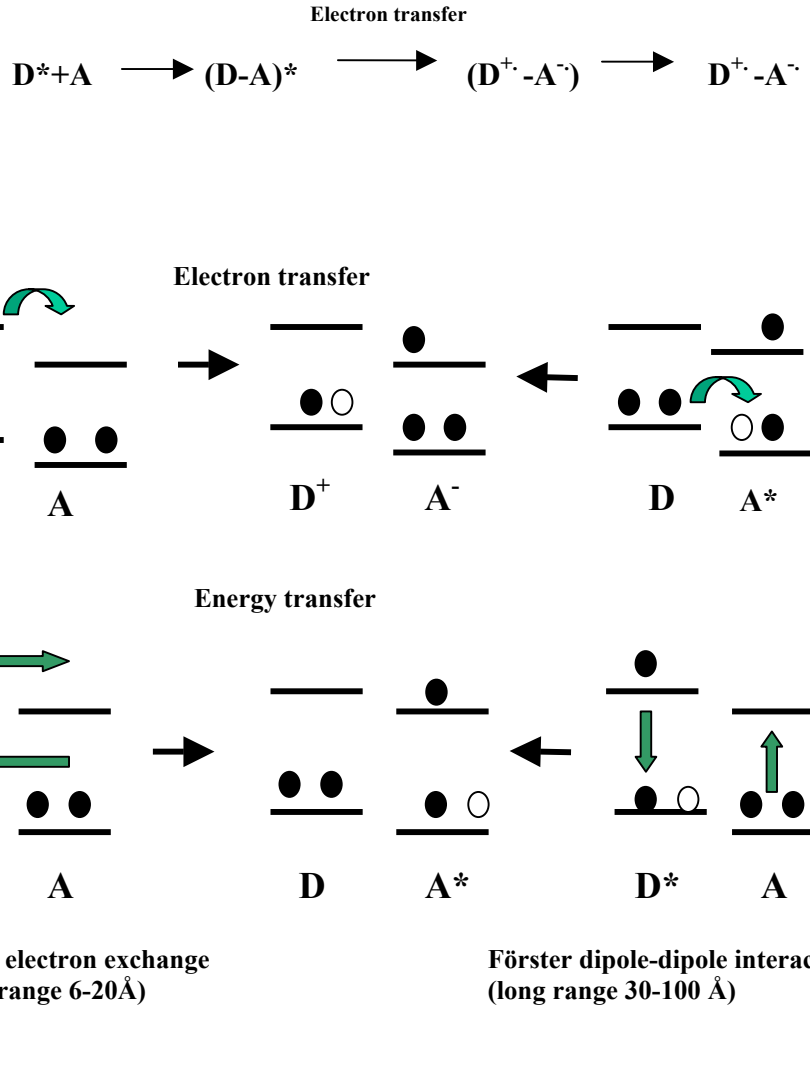

FIGURE 2.5: Illustration of the two mechanisms of deactivation of an excited molecule:
a) electron transfer
b) energy transfer (Dexter electron exchange and Förster dipole-dipole interaction between donor and acceptor)

2.4 Materials used and device architecture

- **Device arhitecture**

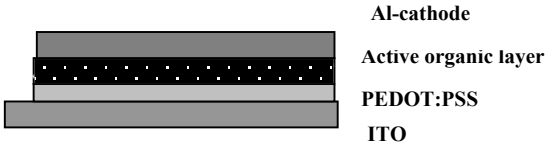

FIGURE 2.6 Device architecture of an organic solar cell

A polymer based device consists of a thin layer of organic material sandwiched between two electrodes: the anode (ITO) and the cathode (metallic electrode) (**Figure 2.6**). A thin layer of poly(3,4-ethylenedioxythiophene polystirene sulfonate) PEDOT:PSS[10] is introduced as intermediate layer between the active organic layer and the anode in order to smooth the roughness surface of ITO. In solar photovoltaic applications, the way how the two organic compounds (donor and acceptor) are integrated in the organic active layer determine the electronic properties of the device. The common device architectures are:

- **bilayer structure**

Two separate layers of donor and acceptor are spin coated on top of each other and the thin active layer consists of two separate regions. The excitons are dissociated at the interface donor acceptor. Due to the limited contact surface, recombination processes occur, leading to a low generation efficiency within the organic active layer and reflected in a low current in the outer circuit.

- **bulk heterojunction structure**

The organic compounds are mixed together in a blend structure, in order to achieve specific structural and physical properties of the polymeric mixture in the solid state. The mixing of donor/acceptor creates many direct contacts and therefore many possibilities for exciton dissociation and an increased probability for charge generation in the bulk and therefore a higher current in the outer circuit [11].

The organic solar cells which are presented in the thesis, were fabricated in a bulk heterojunction structure, by using the following organic materials: **Poly(3-hexylthiophene, 2.5diyl)** (hereinafter referred to as **P3HT**) as a **donor,** and a soluble fullerene derivative **[6,6]-phenyl-C61 butyric acid methyl ester (PCBM)** as electron **acceptor** (**Figure 2.7**).

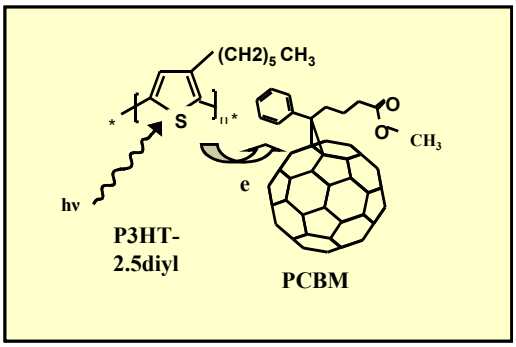

FIGURE 2.7: Materials used for the fabrication of polythiophene based solar cells. The donor is the conjugated polymer Poly(3- hexylthiophene- 2.5diyl) (P3HT) and the acceptor is a fullerene derivative, [6,6]-phenyl-C61 butyric acid methyl ester (PCBM)

- **Donor**

Of the many conjugated polymers, poly(3-alkylthiophenes) have been found to be an unusual class of polymers with good solubility and environmental stability. Practical applications include electrochromic devices, chemical and optical sensors, light emitting diodes, field effect transistors[12]. For the information related to the synthesis of poly(3 alkylthiophenes) the reader is referred to the article published by Rieke [13]. Field effect mobilities of Poly(3 alkylthiophene) in the range of 0.05-0.1 $cm^2V^{-1}s^{-1}$ were reported in the literature [72]. From the class of poly(3 hexylthiophene), a particular polymer, poly(3-hexylthiophene-2.5diyl) [15] was used in the present thesis for the the fabrication of polythiophene based solar cells.

- **Acceptor**

Fullerenes C_{60} and fullerene derivatives are the most promising acceptor materials used for organic photovoltaic applications. The band gap is suggested to be 2.3eV (mobility gap) but the optical absorption extends from the gap energy to the lower energy side (optical gap is 1.6eV).[16][17] Theoretical calculations demonstrated a band gap of 2.15 eV [18]. For organic donor/acceptor based solar cells, a C_{60} molecule is an ideal candidate due to its strong acceptor properties. C_{60} can accept according to the cyclic voltametry investigations, up to 6 electrons [19]. The efficient photoresponse of organic cells based on conjugated polymers/fullerene is due to a very fast charge transfer from the donor molecule to the acceptor [20],[21]. This process is faster than other recombination mechanisms, that's why the quantum efficiency of this process is expected to be close to unity. High conversion efficiencies were reported for organic solar cells 2.5% [22], 3.6% [23] and recently 5% [24], obtained by Siemens. The role of C_{60} in an organic solar cell (bilayer or bulk heterojunction) is not only to take electrons from the polymer (donor) and to separate the exciton, but also to contribute to the conversion of the short wavelength components of sunlight. One of the disadvantages introduced by the C_{60} molecules is its low solubility and miscibility. This is the reason why the soluble fullerene derivative [6,6] -phenyl-C_{61} butyric acid methyl ester (PCBM) [25] has become almost a standard C_{60} substitute material for a number of researchers working on solution processed based organic devices.

- **Electrodes**

In organic devices, **i**ndium **t**in **o**xide (ITO) is usually used as anode. ITO is a degenerated semiconductor comprising a mixture of In_2O_3 (90%) and SnO_2 (10%) with a bandgap of 3.7eV and a Fermi-level between 4.5 and 4.9eV [3]. The large bandgap allows no absorption of wavelengths longer than about 350 nm. The high optical transmittance of ITO is a direct consequence of being a wide bandgap semiconductor. The fundamental absorption edge generally lies in the ultraviolet region of the solar spectrum, and shifts to shorter wavelengths with increasing carrier concentration. Indium acts as n-type dopant, leading to very low sheet resistances for already only 100nm thick layers of ITO. The surface can be modified via plasma etching. In single layer OLED and in organic solar cells, the factors limiting the life time of the devices are: the oxidation of the organic emitting layer by oxygen diffusion out of ITO, the presence of electric shorts due to rough ITO surface and the unbalanced electron hole injection. Therefore, a thin layer of Poly(3,4-ethylene dioxithiophene) (PEDOT) was introduced between ITO and the emissive layer. (PEDOT) is one of the best known π- conjugated polymers because of its excellent electrical conductivity (550 S/cm) [26],[27] electrooptic properties (it is transparent and stable) as well as

processability. PEDOT itself, prepared with standard oxidative chemical or electrochemical polymerization methods, was found to be insoluble. This problem was solved by adding during polymerization a water based polyelectrolyte PSS (polystirene sulphonic acid).

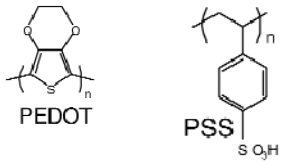

FIGURE 2.8 : PEDOT:PSS layer is used as hole injecting layer in organic photovoltaic devices

PEDOT and PEDOT:PSS (**Figure 2.8**) are used in commercial applications as antistatic coatings in photographic films [28] and in the field of organic based optoelectronics for light emitting diodes (LED) and solar cells [29],[30]. Because PEDOT is transparent to visible light, this additional layer does not diminish the light output in case of organic light emitting diodes (OLED) or the absorption of light in case of organic solar cells, but instead, it leads to an increase in the lifetime of the device and improvement of the efficiency. The positive effects of PEDOT:PSS arise from the smoothing of the ITO surface, and reduction of the hole barrier at the interface ITO/semiconductor.

Aluminium is commonly used as cathode in organic devices. The main disadvantage is the high electron barrier and the degradation under oxygen atmosphere. This is the reason why a thin layer (5-10Å) of an insulating material (for exemple LiF) is commonly introduced between the the organic layer and the aluminium electrode. The main effect is the reduction of the barrier for electrons by aligning the LUMO level of the organic material with the work function of the aluminium electrode. In the same time, LiF acts as a dipole enhancing the electron transport over the barrier. Another feature of aluminium is that it bonds chemically to some polymers creating defect sites by disrupting the alternating bond conjugation at the interface that can trap injected charge carriers [31]. LiF does not dissociate in the Al/LiF/polymer structure, but serves also to protect the polymer from interacting with aluminium.

2.5 How does an organic solar cell operate

The operation of organic solar cells starts with absorption of light, similar to what happens in the process of photosynthesis in green plants. In both cases, in photosynthesis and in organic solar cells, an important requirement for a high photoconversion efficiency is the matching of the absorption spectrum of organic molecules with the emission solar spectrum. In the case of green plants, the absorption spectrum of the chlorophyll ***a*** indicates two absorption peaks at 450nm (blue light) and 650nm (red light) [32] the last one corresponding also to the maximum of the emission solar spectrum.

In the case of organic solar cells, the most known conjugated polymers have an absorption peak around 550nm. The most used acceptor, the fullerene C_{60} and its derivative (6,6)-phenyl-C_{61} butyric acid methyl ester (PCBM), show a maximum absorption edge at 350 nm and a very small peak at 700 nm. By using both components in a donor/acceptor solar cell system, it can be clearly noticed that an important amount of the solar energy remains unused. This is the reason why the use of low band gap polymers represents a solution for this problem by shifting the absorption spectrum towards higher wavelenghts.

The main principle responsible for the operation of an organic solar cell is a double conversion from solar energy into chemical energy, and then from chemical energy into electrical energy as it is indicated in **Figure 2.9**:

A photon having the energy $E=h\nu$, excites an electron from the valence band (HOMO) of either the donor or the acceptor creating not a free charge carrier, but rather an electron-hole pair, (exciton). Excitons are normally bound, and would not break up. If, however, a semiconductor with higher electron affinity is placed in close contact with the first material,

it can be energetically favourable for the electron to leave the exciton and jump to the acceptor molecule. In this process, the conjugated polymer acts as an electron donor and the fullerene derivative as electron acceptor, in what can be considered a molecular heterojunction. Conjugated polymers acting as donor (PPV, polythiophene, polyfluorene etc.) are considered to be p-doped semiconductors, because as a result of photoexcitation and charge transfer they remained with an excess of holes. Organic molecules as fullerene or fullerene derivative, are considered to be n-doped semiconductors, because after accepting electrons they are negatively charged. In this case one can speak about a photodoping process.

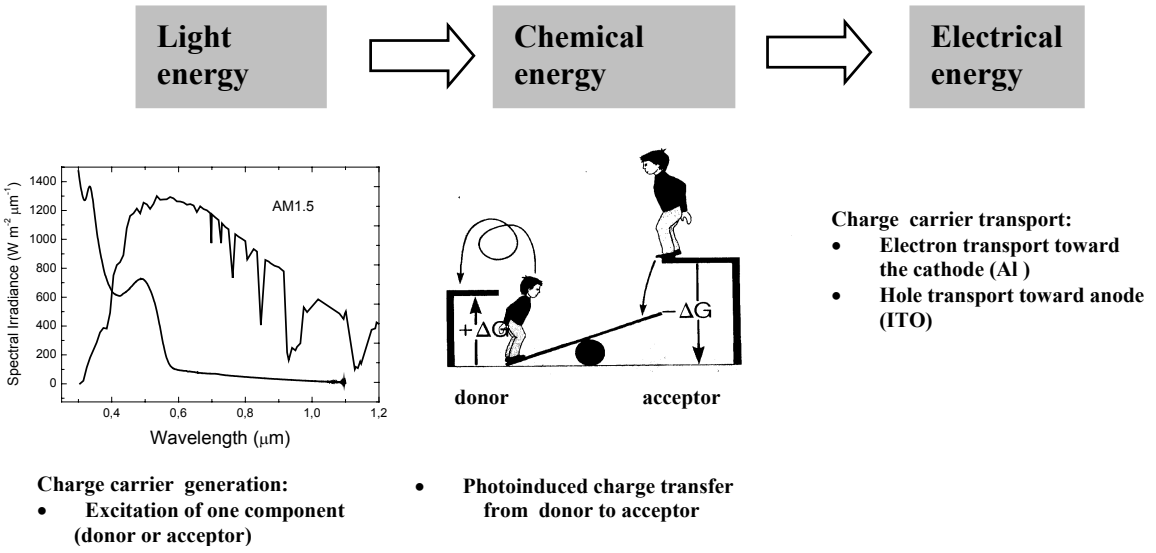

FIGURE 2.9: a) The high efficiency of energy conversion from solar energy into chemical energy is determined by the capability of organic materials used (donor and acceptor) to absorb energy in the corresponding emission solar spectrum range. The conversion of solar energy into chemical energy is responsible for generation and separation of charge carriers (electrons and holes) which are c) then transported towards electrodes.
b) Illustration of the principle of energy coupling between donor and acceptor by using a mechanical model.
Each component of the chemical reaction the donor and the acceptor possess its own energy which is related to its redox potential, that means to the capability to donate (oxidize), or to accept (reduce) electrons . The free Gibbs energy of the chemical reaction, defined as the difference between the energy of each component determine if this one proceeds spontaneously (exothermic) or needs additional energy from the environment (endothermic).

Photoinduced charge transfer from the donor to the acceptor represents in this case the mechanism of exciton dissociation. The result is a metastable charge separated state. It is worth to be mentioned that simultaneously with the charge carrier transfer from the $LUMO_{donor}$ to the $LUMO_{acceptor}$, other competitive processes like radiative (photoluminescence) or non-radiative (intersystem crossing) recombinations may occur. Because the charge transfer time from donor to acceptor is found to be around 50 fs [33], that means very quickly compared to other recombination processes which take place in a time interval of microseconds [22], the efficiency of this process is considered to be 100%.

The condition of the exciton dissociation from the donor to the acceptor is [34]:

$$\mathbf{I_D^* - A_A - U_C < 0} \qquad \mathbf{(2.2)}$$

where $\mathbf{I_D^*}$ is the ionization potential of the donor excited state (P3HT), $\mathbf{A_A}$ represents the electron affinity of the acceptor PCBM and $\mathbf{U_c}$ represents the Coulombic attraction force of the exciton (**Figure 2.10**). In case this condition is not fulfilled, the electron excited in the LUMO level of the P3HT may be attracted on the LUMO level of PCBM but without exciton dissociation, there is a high probability of back recombination, i.e the electron recombines back with the hole in the HOMO level of P3HT and is therefore lost in the photogeneration

process. Back recombination does not represent the only recombination mechanism. If the exciton produced in the donor as a result of photoexcitation, is not dissociated, its fate is to recombine radiatively through photoluminescence with a hole in the valence band of the donor. Not only electrons in the valence band of the donor are excited, but also in the n-type acceptor material.

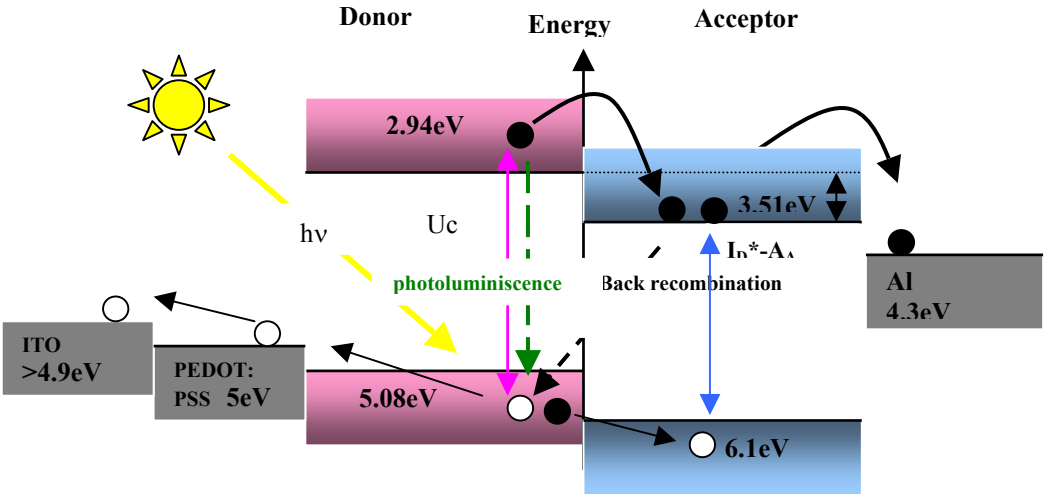

FIGURE 2.10: Operation principle of an ideal polymer/fullerene heterojunction organic solar cell: Photons with energy $h\nu > E_{LUMOdonor} - E_{HOMOdonor}$ excite electrons into $LUMO_{donor}$ which are then transferred to $LUMO_{acceptor}$ from which they can be collected by negative electrode with work function closed to $LUMO_{acceptor}$. Holes are collected by positive electrode with work function closed to $HOMO_{donor}$.

Similarly, an electron excited in the valence band of the acceptor will create also an exciton. The hole left in the valence band of the acceptor, will be replaced by an electron taken from the valence band of the donor. In any case, the electron transfer takes place from $LUMO_{donor}$ to $LUMO_{acceptor}$ (for an exciton produced in the donor) or from $HOMO_{donor}$ to the $HOMO_{acceptor}$ (for an exciton produced in the acceptor) as it was shown in the **Figure 2.5**.

As it was previously mentioned, the photoluminescence stands for the radiative recombination mechanism in organic devices. In the case of organic solar cells, the role of the acceptor (C_{60} or other fullerene derivatives) is to quench the photoluminescence. In this way, the electrons contribute to the photogenerated current in the outer circuit. **Figure 2.11** shows the photoluminescence quenching in poly(3-hexylthiophene-2.5diyl)(P3HT) as a result of adding in the blend of a strong electron affinity, the fullerene derivative (PCBM). The photoluminescence quenching is a measure of the photogeneration efficiency.

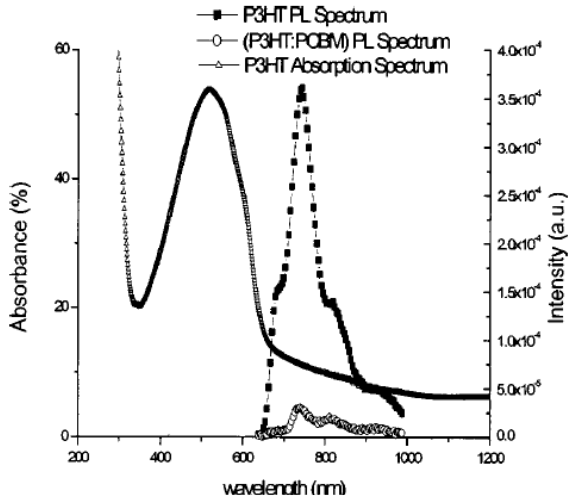

FIGURE 2.11: Photoluminescence quenching is evidence of photoinduced electron transfer from P3HT to PCBM. The absorption spectrum of P3HT indicates an absorption edge at about 580 nm corresponding to a HOMO–LUMO energetic difference of 2.14 eV.

A higher current in the outer circuit will imply a lower photoluminescence. On the other hand, a higher photoluminescence reflects a high number of electrons accumulated in the conduction band close to the cathode (-) and a high number of holes accumulated in the valence band near the ITO electrode (+), and therefore determines the open circuit voltage in the device. This aspect will be discussed in the **paragraph 2.7.5**.

2.6 Solar radiation

The sun is the main energy supplier for all natural processes on the earth and in the atmosphere. During the nuclear fusion reaction in the sun, which converts hydrogen into helium, a big amount of energy is released into space 3.9 $*10^{26}$J/s [35]. This huge amount of energy is emitted primarily as electromagnetic radiation in the ultraviolet to infrared region (0.2 to 3μm). The intensity of solar radiation in free space at the average distance from the sun is defined as solar constant and has a value of 1353W/m² [36]. The temperature within the photosphere is 5800K and the energy of the sun corresponds to the radiation emitted by a black body at this temperature. This radiation corresponds to a solar spectrum emitted outside the atmosphere and is defined as AM 0 spectrum. The AM 0 spectrum is relevant for satellite and space vehicle applications. The AM 1 spectrum represents the sunlight at the earth surface when the sun is overhead and corresponds to an incident power of 925W/m². About 70% from the sun radiation can penetrate the atmosphere. The reasons for this attenuation are due on one side to the scattering by the molecules (Rayleigh scattering), most effective at the short wavelengths, and by the aerosols and dust particles, and on the other side by the absorption of radiation due to CO_2, H_2O and ozone O_3 (ultraviolet absorption) found in the atmosphere. Additionally, the length of the light path through the atmosphere reflected in the air mass, determines also the degree of attenuation and is highly dependent on the latitude and time of the year.

The AM 1.5 spectrum was standardized by both the International Organization of Standardization (ISO 9845-1:1992) and by the American Society for Testing and Materials (ASTM E892-87:1992), although the latter standard is more commonly referred to, in respect of solar cell testing (**Figure 2.12**). For convenience, the flux of the standardized AM1.5 spectrum has been corrected to 1000W/m². However, despite availability of standards, great care has to be taken when results reported in the literature are compared. For example, often AM 1.5 conditions are reported, but this may only mean that a radiance of 1000W/m² was used, with the proper spectral distribution being neglected. The standard solar spectrum used for solar cell efficiency measurements, AM 1.5 corresponds to an angle θ of 48° according to the formula:

$$AM = \frac{1}{\cos\theta} \qquad \textbf{(2.3)}$$

where θ is the angle measured from the zenith as it is shown in the **Figure 2.13**.

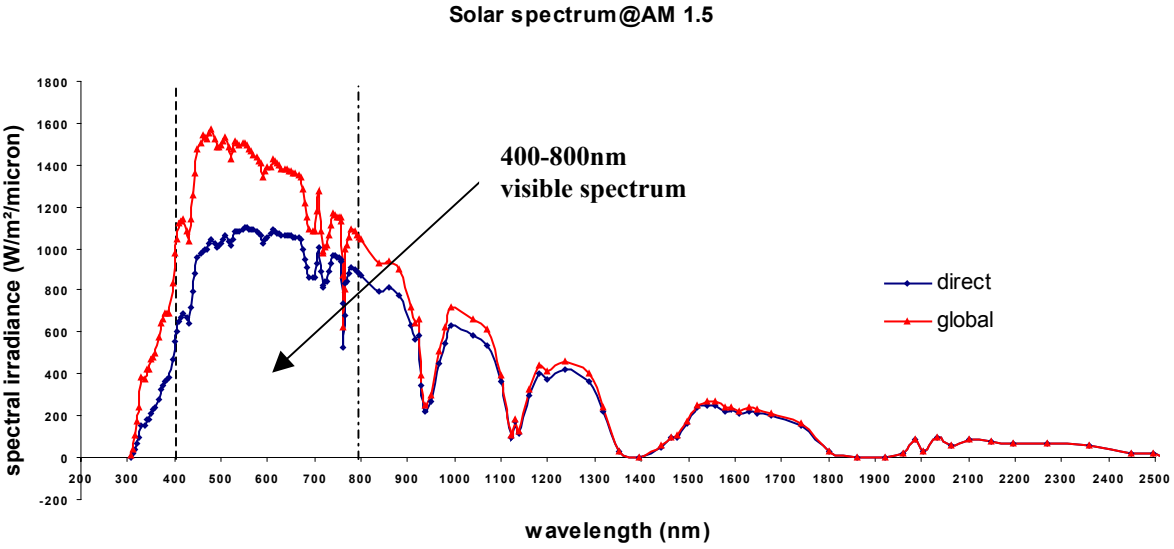

FIGURE 2.12: Spectral distribution of solar irradiation. Air mass AM 1.5 global and direct spectrum. Water (H_2O), ozone (O_3) and carbondioxide (CO_2) are the main absorbers of the direct solar radiation in the earth`s atmosphere

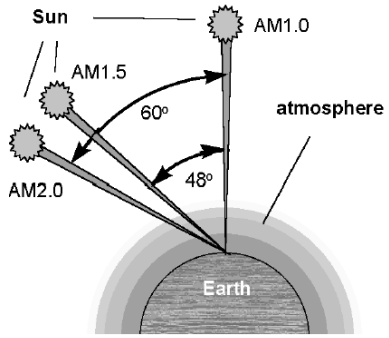

FIGURE 2.13: AM1.5 corresponds to the solar incident radiation angle of 48° and is the standard solar spectrum used commonly in the literature for solar cell efficiency

The global AM1.5 solar spectrum includes the direct solar spectrum, AM1.5 at the earth surface plus the diffuse components (**Figure 2.12**). Depending on the applications, different parts of the solar spectrum become more important. In the case of solar energy conversion, the range between the visible and near infrared light (400-800nm) is the relevant part since it contains most of the solar power. Therefore, the organic compounds should absorb in the high wavelength visible range in order to have a good photogeneration of charge carriers.

From the photophysical point of view, as reliable monocromatic efficiency for solar cells is the external quantum efficiency (EQE), which is defined as the conversion efficiency of the solar radiation in electrical energy.

EQE_λ is defined as the number of electrons measured in the outer circuit divided by an incident photon of a given wavelength (**Figure 2.14**).

$$EQE_\lambda = \frac{number_of_electrons}{number_of_incident_photons} \qquad \textbf{(2.4)}$$

The external quantum efficiency is different from the engineering power conversion efficiency mentioned in the **paragraph 2.7.1.**

In case the solar cell presents low series resistances (<100 Ohm), a simple method [37] can be applied for the evaluation of the short circuit current from EQE measurements.

$$EQE_\lambda = \frac{I_\lambda}{eN_\lambda} \qquad \textbf{(2.5)}$$

$$N_\lambda = \frac{\lambda E_\lambda}{hc} \qquad \textbf{(2.6)}$$

where: e is the electron charge and N_λ is the incident photon flux density (photons/cm²/s/nm), I_λ is the photocurrent, E_λ is the solar energy corresponding to a certain wavelength λ, h is the Planck constant and c is the speed of light.

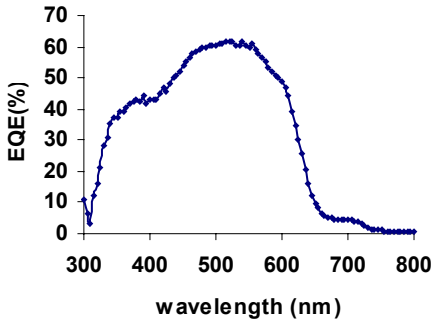

FIGURE 2.14: External quantum efficiency (EQE) of a ITO/PEDOT:PSS/P3HT:PCBM/Mg solar cell. At 390nm the main absorption peak due to PCBM is observed while at 520nm the main absorption peak of P3HT can be identified indicating a maximum EQE of 60%

The short circuit current given by the solar cell can be estimated by performing an integration over the whole wavelength range.

$$I_{sc} = \int I_\lambda d\lambda \qquad \textbf{(2.7)}$$

$$I_{sc} = \int_{\lambda_1}^{\lambda_2} eEQE_\lambda N_\lambda d\lambda \qquad \textbf{(2.8)}$$

In **Figure 2.15** it is shown the incident photon flux density corresponding to the AM1.5 global solar spectrum. It can be seen that the integration of the photon flux density curve in the region 300-800 nm of the visible range where the P3HT:PCBM absorbs, gives a maximum short circuit current density of 25.98mA/cm² which can be obtained by a solar cell. In the case of the measured solar cell the short circuit current density calculated by integration in the same range is 8.22mA/cm², value which is in agreement with the experimental result of 8.235mA/cm² obtained from the J-V curve at 100mW/cm².

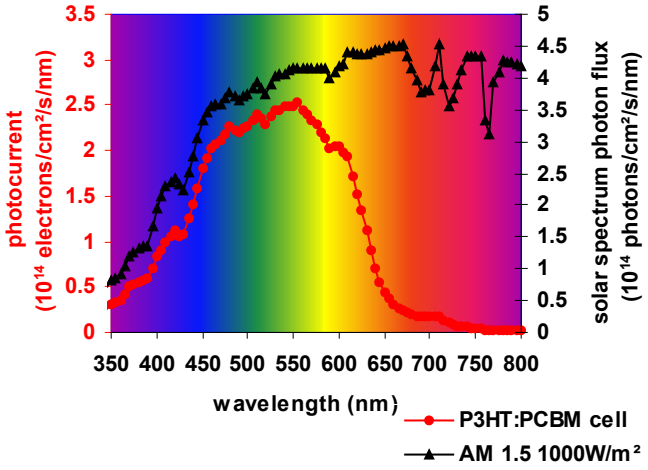

FIGURE 2.15: The AM1.5 solar spectrum photon flux (black curve) and the photocurrent for the P3HT:PCBM solar cell calculated from external quantum efficiency curve

AM-1.5 solar spectrum
Jsc=25.98mA/cm²
(integrated 320-800nm)

P3HT:PCBM based cell
Jsc=8.22mA/cm²
(integrated 320-800nm)

In **Figure 2.16** it is represented a comparison of the theoretical limit of the short current density for classical inorganic solar cells (case a) and organic solar cells (case b) calculated from the global AM 1.5 spectrum. In the case b), the band gap range (1.5-3.5eV) corresponds to the absorption region of organic molecules. Conjugated polymers have a band gap higher that 2eV. By comparing the two graphs, it can be noticed that organic solar cells are far below from the point of view of current compared to the inorganic ones. This is the main reason why the synthesis of low band gap polymers which should present a red shift in the absorption spectrum is one strategy of increasing the short circuit current, and therefore the efficiency of organic solar cells .

In the particular case of P3HT:PCBM solar cells, both organic components absorb, P3HT has a maximum peak around 560nm while the maximum absorption peak of PCBM belongs to the blue region around 350nm. In the P3HT:PCBM organic blend, the main absorber is P3HT to whom it corresponds an optical band gap $HOMO_{P3HT}$-$LUMO_{P3HT}$ = 2.14eV.

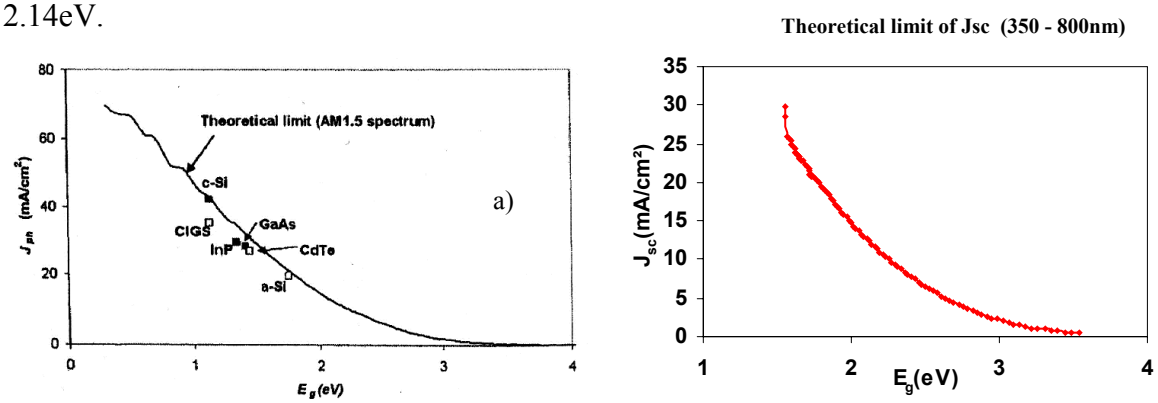

FIGURE 2.16: Theoretical limit (AM-1.5 spectrum) of the short current density Jsc(mA/cm²) in the case of classical inorganic solar cells (a) and organic solar cells (b). In the case b) the calculated current was obtained by performing the integration of the solar spectrum photon flux density in the range (350-800nm) where the organic material absorbs. The visible solar spectrum (400-800nm) correspond to the band gap range of 3 – 1.55eV.

The calculation of the theoretical limit of short circuit current is not enough to appreciate the overall limitation of the power conversion efficiency of solar cells. Open circuit voltage and fill factor determine both the overall efficiency. For classical inorganic solar cells, the following expression [38],[39] approximates with resonable accuracy the open circuit voltage.

$$V_{oc} = \frac{E_g}{q}\left(1 - \frac{T_c}{T_s}\right) + \frac{kT_c}{q}\ln\frac{f_\omega}{f_0} + \frac{kT_c}{q}\ln\left(\frac{T_s}{T_c}\right) \qquad \textbf{(2.9)}$$

where T_c is the temperature of the solar cell, T_s = 5767K is the temperature of the sun,

$$f_\omega = \left(\frac{R_{sun}}{R_{sun_earth}} \right)^2 = \frac{\omega_s}{\pi} = 2.18 * 10^{-5} \qquad \textbf{(2.10)}$$

R_{sun} =696*10^3 km is the radius of the sun and R_{sun_earth}=149.6*10^6 km is the distance between earth and sun.

The coefficient f_0 is 1 or in some cases 2, depending on the refractive index of the solar cell ($f_0 = 1+n^2$) and on different device geometry.

The formula (2.9) takes into account that at open circuit voltage the solar cell behaves similar to an ideal thermodynamic engine with Carnot efficiency ($1-T_c/T_s$). Due to the fact that equation (2.9) depends only on material characteristics and on other constant parameters, it can be extrapolated also in the case of organic solar cells. The dielectric constant for polythiophene [40] is considered in the literature to be 3 and for in the case of PCBM [41] is 3.9.

In **Figure 2.17** are represented the theoretical limits for open circuit voltage in case of inorganic (a) and P3HT:PCBM based solar cells (b). The shaded area represents the inaccesible open circuit voltage region.

In the case of organic solar cells the maximum open circuit voltage which can be expected is determined by the difference between the $HOMO_{donor(p3HT)}$ and the $LUMO_{acceptor(pcbm)}$. This idea will be discussed in detail in the **chapter 3.** From the **Figure 2.10** it can be noticed that the band gap, E_g taken into account in the formula is $HOMO_{donor(p3HT)}$ - $LUMO_{acceptor(pcbm)}$ = 1.57eV, so in this case a maximum voltage of 1.48V can be maximum expected at 300K.

In case of inorganic solar cells for an ideal J-V characteristics, the fill factor cannot be determined analytically but it has been shown [42] that it depends on the ratio voc = eV_{oc}/kT.

$$FF = \frac{voc - \ln(voc + 0.72)}{voc + 1} \qquad \textbf{(2.11)}$$

As it is well known, the maximum thermodynamic efficiency for the conversion of unconcentrated solar irradiance into electrical free energy in the radiative limit, and thermal equilibrium between electrons and phonons, was calculated by Shockley and Queisser in 1961 [43] to be about 31% (**Figure 2.18**).

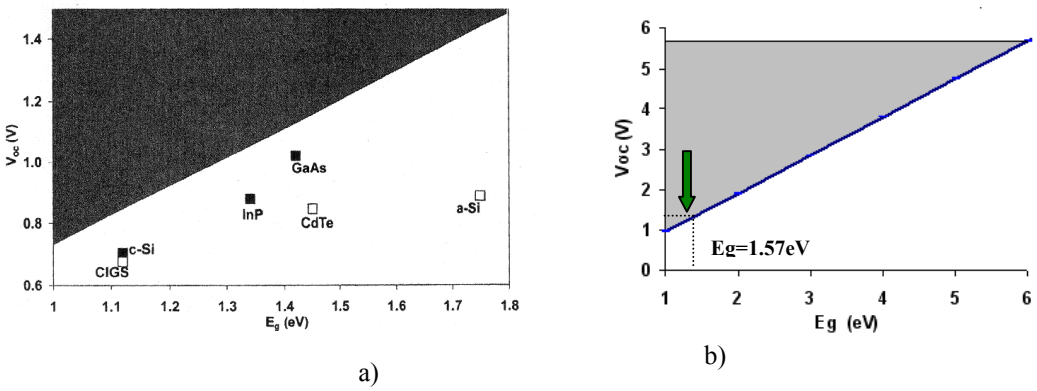

FIGURE 2.17: Theoretical limit (AM1.5spectrum) of the open circuit voltage Voc(V) in the case of classical inorganic solar cells (a) and P3HT:PCBM based solar cells (b).

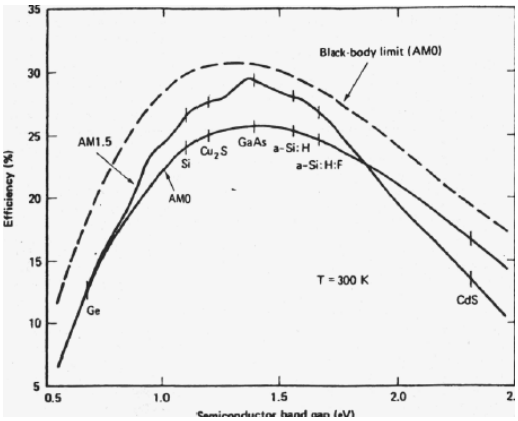

FIGURE 2.18: Theoretical limit of power conversion efficiency for classical inorganic solar cells. (Reprinted from the reference 3)

This efficiency is attainable in semiconductors with bandgaps ranging from about 1.25 to 1.45 eV.

Organic solar cells, as it will be shown in the following paragraph, do not follow a 100% Shockley J-V diode dependence in the 4th quadrant, where current and voltage can be extracted from the solar cells. In the most cases, the performance of the solar cell is influenced by defects at the contacts or shunts reflected in a poor fill factor. The equation (2.11) cannot be applied in this case and therefore, a limit for the theoretical power conversion efficiency is not indicated here.

2.7. Theoretical framework of solar cell operation

2.7.1 Power conversion efficiency

The operating regime of the solar cell in which the cell delivers power corresponds to the voltage range from 0 to V_{oc}. The cell power is given by P = I*V. The power, P reaches a maximum at the cell's operating point or maximum power point. This point occurs at a certain voltage V_m and current I_m (**Figure 2.19**).
The fill factor is defined as the ratio :

$$FF = \frac{I_{\max} * V_{\max}}{I_{sc} * V_{oc}}$$ and describes the 'squareness' of the I-V curve. **(2.12)**

The power conversion efficiency of the cell is the power density delivered at operating points as a fraction of the incident light power L

$$\eta = \frac{I_{sc} * V_{oc} * FF}{L}$$ **(2.13)**

The four quantities I_{sc}, V_{oc}, FF and η are the key performance characteristics of a solar cell.

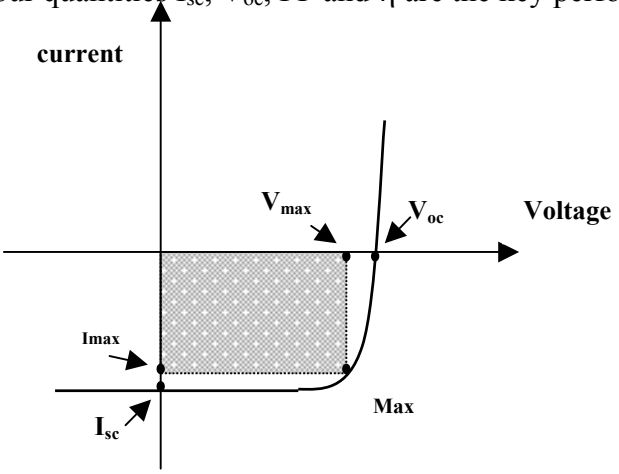

FIGURE 2.19 The current –voltage characteristics of an ideal cell. The maximum power, $I_{max}*V_{max}$ is given by the area of the inner rectangle. For a fill factor equal 100% the current –voltage curve would follow the outer rectangle $I_{max}*V_{max}$

2.7.2 Equivalent circuit of solar cells

The operating principle of classical inorganic solar cells may be represented by the equivalent circuit in **Figure 2.20**. For organic solar cells, the physical processes might be different but the loss mechanisms are similar.

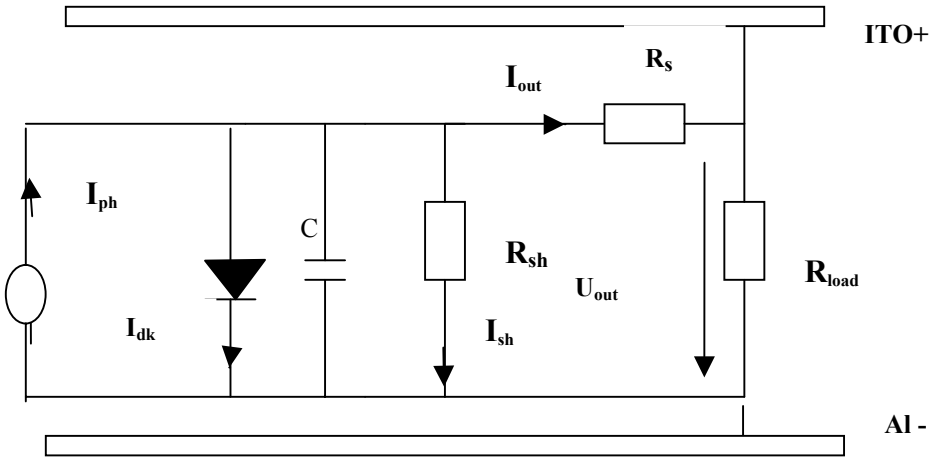

FIGURE 2.20 : Equivalent circuit of a solar cell

The main components of the equivalent electrical circuit are the following:

- A constant current source which generates the constant current I_{ph} under illumination. The photogenerated current is closely related to the photon flux incident on the cell, and its dependence on the wavelength of the light is reflected in the external quantum efficiency or spectral response as the ratio between the number of free charge carriers created in the outer circuit and the number of incident photons.

- An ideal diode following the Shockley relation:

$$I_{dk}(V) = I_0\left[\exp(\frac{qV}{kT}) - 1\right] \qquad \textbf{(2.14)}$$

where I_0 is the saturation current, q is the electron charge, V is the applied voltage, k is the Boltzmann constant and T is the temperature.

In the ideal case, the short circuit current I_{sc} is equal to the photogenerated current I_{ph} and the open circuit voltage has the following expression:

$$V_{oc} = \frac{kT}{q}\ln\left(1 + \frac{I_{ph}}{I_0}\right) \qquad \textbf{(2.15)}$$

The maximum achievable short circuit current has been discussed in the paragraph 2.7. The rectification behaviour expressed by the ideal diode model is due to the built in field in the solar cell ($HOMO_{donor}$ - $LUMO_{acceptor}$) and the difference in the work function of the metallic electrodes. The I-V characteristic of a solar cell represents a superposition between the dark diode curve and the constant photogenerated current i.e., the dependence is shifted downwards in the negative part of the y axis by a value equal to the short circuit current I_{sc}.

- The shunt resistance R_{sh} accounts for the recombination processes near the dissociation sites and at the interface with the metal electrodes. For the ideal case, R_{sh}

should be >> than the series resistence R_s. Sometimes, an additional parallel resistance is added to the circuit in **Figure 2.20** in order to simulate the shorts due to pinholes. Due to the fact that at small voltages the ideal diode does not conduct, according to the Kirchoff's laws, the outer current is controlled by the sum of series and parallel resistances.

$$R_s + R_{sh} = \frac{V_{out}}{I}\Big|_{I \Rightarrow I_{sc}} \qquad \textbf{(2.16)}$$

- Series resistance R_s includes the bulk and the interface organic material/metallic electrode resistance. The conductivity of the charge carriers is influenced by the thickness of the organic layer, and by the density of traps. At high voltages, the conduction is determined mostly by the series resistance :

$$R_s = \frac{V_{out}}{I}\Big|_{I \Rightarrow \infty} \qquad \textbf{(2.17)}$$

For an ideal solar cell having a pronounced diode dependence of the current with voltage, R_s=0 and $R_{sh} = \infty$. In real cases, the increased series resistance and a low parallel resistance determine a modification of the shape of the I-V curve. Organic solar cells are more sensitive to the influence of these resistances and distortions of the I-V curve are more pronounced when R_s and R_{sh} are comparable as values.

- The capacitor C reflects the charging/discharging processes in the solar cells which are more pronounced in the case of thin layer films with a large active area.

$$C = \varepsilon \frac{A}{d} \qquad \textbf{(2.18)}$$

- The short circuit current depends on the photogeneration of charge carriers and is proportional with the incident light intensity, while the open circuit voltage V_{oc} is proportional with the load resistance. The main method to determine other operating points on the I-V curve is to apply an additional voltage V_{app}. A positive voltage, V_{app} applied with **+ on the anode (ITO) and – on the cathode (Al)** is referred as **forward bias,** while a negative one **(- on ITO and + on Al)** is referred to as **reverse bias**. When V_{app}=V_{oc} the total voltage measured in the outer circuit is zero i.e., we have short circuit conditions (I_{sc}). At V_{app} = 0 we get the maximum voltage in the outer circuit V_{oc}, we are at open circuit voltage conditions and the current is 0.

2.7.3 Short circuit current

As it was mentioned before, the real J-V curve of an organic solar cell is far from being an ideal Shockley type and is characterized by three operating regimes.

Under reverse bias conditions, the ideal diode is blocked and the I-V curve is determined by the sum R_s+R_{sh}. While the voltage increases and becomes positive, the conduction is driven by the ideal diode. This is the active region of the solar cell which determines the efficiency. At higher positive voltages, space charge region is formed and the I-V characteristics undergoes a transition from a Shockley type diode behaviour to a dependence proportional with the second power of the voltage. (Mott&Guerney's law):

$$J = \frac{9}{8}\varepsilon_0 \varepsilon_r \theta \mu \frac{V^2}{d^3} \qquad \textbf{(2.19)}$$

where θ is the trap density, μ represents the mobility, ε_r represents the relative permittivity of the organic material, d is the thickness of the active layer.

The measurements and the evaluation of the solar cells in this dissertation are focussed on the reverse bias and the Shockley type region, before the space charge limited region is reached.

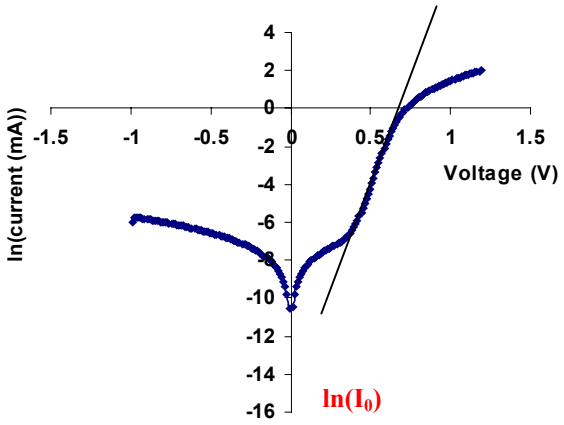

FIGURE 2.21 : Evaluation of the saturation current and ideality factor from the dark J-V curve

Considering the equivalent circuit in **Figure 2.20,** the current in the outer circuit can be obtained by solving the Kirchhoff laws:

$$I_{ph} = I_{dk} + I_{out} + I_{sh} \qquad \textbf{(2.20)}$$

$$I_{out}R_s + V_{out} - I_{sh}R_{sh} = 0 \qquad \textbf{(2.21)}$$

Considering the dark current : $I_{dk} = I_0\left(e^{q(V_{out} - I_{out}R_s)/nkT} - 1\right)$ **(2.22)**

The evaluation of the saturation current and the ideality factor can be determined from a semilogarithmic representation of the current versus applied voltage, according to the formula (2.23) and it is given by the extrapolation towards zero voltage of the linear part of the J-V curve at positive voltages [44] as it is indicated in **Figure 2.21**.

$$\ln(I) = \ln(I_0) + \frac{q}{n(T)kT}V \qquad \textbf{(2.23)}$$

From the equations (2.20), (2.21), (2.22) the current in the outer circuit can be obtained :

$$I_{out} = \frac{R_{sh}}{R_s + R_{sh}}\left[-\frac{V_{out}}{R_{sh}} - I_0\left(e^{q(V_{out} - I_{out}R_s)/nkT} - 1\right) + I_{sc}\right] \qquad \textbf{(2.24)}$$

The I-V characteristic of the solar cell is given by the solution of the transcedental equation (2.24) and requires numerical methods. If the variable x is introduced as defined in (2.25), then the equation to be solved is indicated below :

$$x = I_{out} \tag{2.25}$$

$$f(x) = \frac{R_{sh}}{R_s + R_{sh}}\left[-\frac{V_{out}}{R_{sh}} - I_0\left(e^{q(V_{out} - xR_s)/nkT} - 1\right) + I_{sc} \right] - x \tag{2.26}$$

$$A(x) = I_0 e^{q(V_{out} - xR_s)/nkT} \tag{2.27}$$

$$f(x) = -\frac{V_{out}}{R_s + R_{sh}} - \frac{R_{sh}}{R_s + R_{sh}} A(x) + \frac{R_{sh}}{R_s + R_{sh}}\left(I_{sc} + I_0\right) - x \tag{2.28}$$

The first derivative of the function f(x) is :

$$f'(x) = -\frac{R_{sh}}{R_s + R_{sh}}\left[A(x) \ln\left(\frac{A(x)}{I_0}\right)\left(-\frac{qR_s}{nkT}\right) \right] - 1 \tag{2.29}$$

A method to solve this equation is the Newton iterative method. This method consists in calculating the variable x according to the formula:

$$x = x_0 - \frac{f(x)}{f'(x)} \tag{2.30}$$

where x_0 is a random value.

The final value for the current is obtained as a result of many iterations, while the initial random value x_0 is replaced with the x value obtained in the previous iteration. In this way the I-V curve can be simulated and compared with the experimental one, assuming that the values for the short circuit current, series and parallel resistances, saturation current, ideality factor, and temperature are known.

Figure 2.22 shows the experimental and simulated J-V curves under dark and illuminated conditions (100mW/cm²). From the simulated curves, the ohmic region can be distinguished (open circles red for illuminated and open circles blue for dark), which transforms into the Shockley dependence at a voltage around 0.4V (red for illuminated and blue for dark curves). At higher forward bias >>1.2V the Shockley dependence is expected to transform itself into space charge limited current dependence following the Mott&Guerney law (not shown).

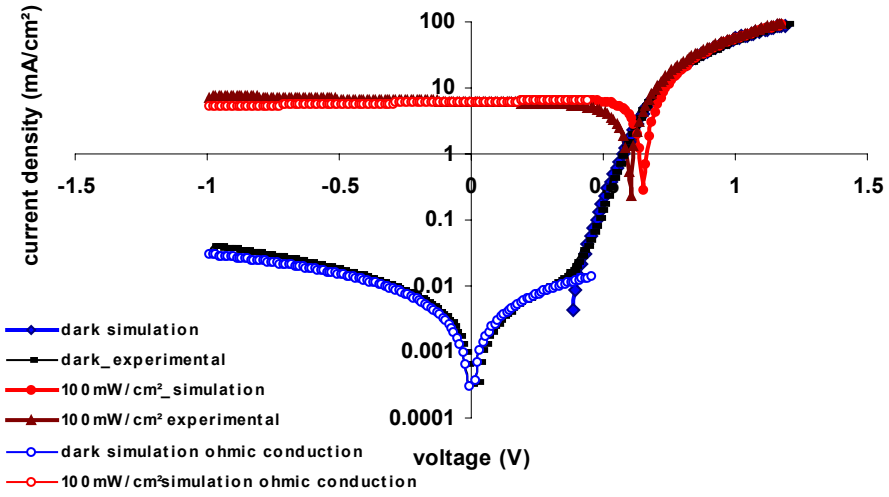

FIGURE 2.22: Experimental and simulated J-V curves under dark and illumination conditions

From the simulation curves in **Figure 2.22,** it can be noticed that the 1 diode model does not match perfectly the experimental curves in the case of P3HT:PCBM based solar cells. An error difference of approximatively 50mV is obtained for the open circuit voltage in the case of simulated curves compared with the experimental ones. The same result was confirmed by other studies [45]. The authors solved this problem by applying a correction factor to I_{dk}, taking into account the mean carrier distance of the charge carriers according to the formula:

$$mean_dist = \tau * \mu * \frac{(V - V_{bi})}{L} \qquad \textbf{(2.31)}$$

where τ is the average lifetime of the carriers, μ is the carrier mobility and V_{bi} is the built in field whose maximum value is considered to be given by the difference in the work function of the electrodes.

This method was not applied in the present case, due to the uncertainty in the evaluation of the average lifetime and mobility of charge carriers. Additionally, due to the PCBM clusters formed as a result of thermal annealing of P3HT:PCBM based solar cells, there is a large variation in the thickness of the active layer. (for details see **Chapter 5**).

2.7.4 Open circuit voltage

The region in the 4th quadrant is the region where the voltage and the current can be extracted from the solar cell. When the photocurrent cancels the dark current, the open circuit voltage is obtained.

$$I_{out} = 0 \qquad \textbf{(2.32)}$$

$$V_{oc} = \frac{nkT}{q} \ln\left(\frac{I_{sc}}{I_0} + 1\right) \qquad \textbf{(2.33)}$$

From the equation (2.33), it can be noticed that the value of open circuit voltage is influenced by the saturation current. A small saturation current determines an increase in the open circuit voltage. Taken into account the shunts, the open circuit voltage is decreased by the parallel resistance:

$$V_{oc} = \frac{nkT}{q} \ln\left(\frac{I_{sc} - \frac{V_{oc}}{R_{sh}}}{I_0} + 1 \right) \qquad \textbf{(2.34)}$$

A peculiarity of organic solar cells is that high currents, injected into the organic layer have as main result the "burning" of shunts, which means that a low resistance region is physically destroyed and the pinholes actually burnt. By using this method, the performance of the solar cell can be improved.

2.7.5 Influence of the photoluminescence on the open circuit voltage [46]

Another aspect referring to organic solar cells is related to the influence of the photoluminescence on the open circuit voltage.

In solar cells and detector applications, photoluminescence is considered to be a loss of energy, rather than a requirement for efficiency conversion. Under open circuit conditions, energy dissipation by photoluminescence is a measure of the device's ability to bypass other losses in producing work from light and influences in this way the open circuit voltage. In a quantum system, light is absorbed in the material in order to produce electrons in the conduction band which can recombine then radiatively by giving up the excitation energy in the form of emitted luminescent photons. The electrons can also decay non-radiatively through traps or through Auger recombination to produce a phonon or lattice vibration. Alternatively, if the electron survives these recombination processes it may be collected by the external circuit to produce a voltage. This voltage is the difference between the quasi Fermi levels E_{fn} and E_{fp} of electrons and holes in the conduction and valence band, respectively.

Analogous to a chemical reaction, the interaction of electrons with photons is characterized by the Gibbs free energy per particle or chemical potential. The photoluminescence efficiency, Θ_{PL} is defined as the rate of the photons emitted from the material (I_{0R}), divided by the incident photons absorbed (I_{sc}) plus the thermal excitations (Io/Θ_{PL}), i.e. radiative recombination/total recombination.

$$\Theta(\mu, T) = \Theta_{PL} = \frac{I_{oR}}{I_{sc} + I_0 / \Theta_{PL}} \qquad \textbf{(2.35)}$$

$$\Theta_{PL} = \frac{I_{oR} - I_0}{I_{sc}} = \frac{I_0 \exp(\mu / kT) - I_0}{I_{sc}} = \frac{I_{dk}}{I_{sc}} \qquad \textbf{(2.36)}$$

where μ represents the chemical potential ($\mu = qV_{oc}$). The photoluminescence quantum yield is a measure of the ratio between dark current and short circuit current. From the equation (2.36) the expression for the open circuit voltage V_{oc} is easily derived:

$$V_{oc} = \frac{kT}{q} \ln\left(\frac{I_{sc}}{\frac{I_0}{\Theta_{PL}}} + 1 \right) \qquad \textbf{(2.37)}$$

which is exactly the expression identical with the equation obtained from the diode equation. In this case the photoluminescence quantum yield Θ_{PL} becomes a correction factor for the saturation current. For a 100% photoluminescence, the corresponding photoluminescence quantum yield is $\Theta_{PL} = 1$.

The operation of a solar cell can be understood as a balance between the driving force (thermodynamics) represented by the chemical potential, and kinetic or rate process represented by the current I_{out}.

Thermal excitations + ambient absorbed + solar absorbed = luminescent photons + phonons + current extracted

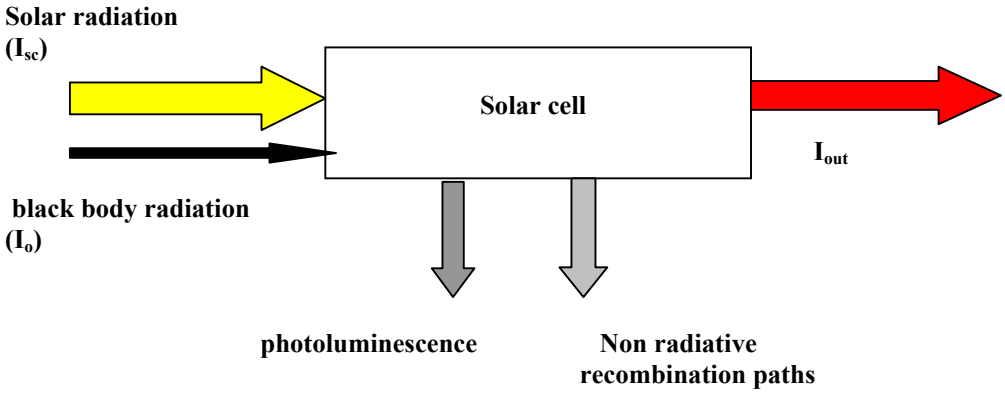

FIGURE 2.23: Representation of a solar cell from the thermodynamic point of view. Solar radiation and ambient black body radiation stand for short circuit current and saturation current respectively. Competitive processes as photoluminescence and non-radiative recombination paths decrease the output photocurrent.(Reprinted from reference [46])

As the current extracted increases, the observed voltage and thus luminescent and non-radiative flux will decrease. **Figure 2.23** shows the flow of current through a solar cell.

The power conversion efficiency of a solar cell is determined by the open circuit voltage, short circuit current and fill factor**.** For a thin absorber layer, the reduction of the thickness has as main effect a lower emissivity coefficient, a higher photon flux which stands for a high photoluminescence quantum yield , and therefore a lower saturation current I_0. Therefore the open circuit voltage will increase. In the same time for thin absorber layers, the absorption coefficient will be low which determines a small electron collection quantum yield, η_c according to the formula 2.38 and therefore small short circuit current I_{sc}:

$$\eta_c(photon_energy) \approx \frac{1}{1 + \left[\frac{1}{\alpha(photon_energy) L_d} \right]} \qquad \textbf{(2.38)}$$

$$L_d = \left(kT\mu\tau / q \right)^{1/2} \qquad \textbf{(2.39)}$$

where α(photon_energy) is the absorption coefficient, L_d is the diffusion length and μ is the carrier mobility. The constant τ is the carrier lifetime, which can be deduced from time resolved luminescence measurements.

The lowering of the luminescence with extracted current or chemical species produced is observed experimentally in semiconductors [47]. Organic dyes for example are known to have a photoluminescence efficiency near 1. Since the mobility of these materials is low and the resistivity R_s is high, these materials produce high voltages but low currents. A highly fluorescent material can have a low charge carrier mobility and still generate a high open circuit voltage [46]. The thickness of an absorber layer in a solar cell should be designed in such a way as to absorb most of the solar photons but not as thick as to quench totally the photoluminescence. Luminescence is seen as a loss in the process of conversion of light into useful work but also a measure of voltage.

As a conclusion the overall efficiency of a solar cell is determined by the electrical performance in the 4th quadrant of the main parameters of the solar cell, i.e by the open circuit voltage, short circuit current and fill factor, the last one determining the shape of the I-V curve.

From this point of view sometimes the requirements for a high open circuit voltage and a high short circuit current are opposite as indicated in table 2.1 bellow:

Table 2.1 Main requirements for a high power conversion efficiency of a solar cell

	V_{oc}	J_{sc}
band gap	**High**	**Small**
saturation current	**Small**	**Small**
photoluminescence	**High**	**Small**

A high band gap of the organic material determines a high open circuit voltage. In case this high band gap is identical with the absorption band gap, this fact will determine a higher energy necessary for electrons to be excited from the valence into the conduction band i.e, the short circuit current will be smaller. A high photoluminescence rate will determine a high open circuit voltage while a condition for a high short circuit current is the quenching of the photoluminescence.

Chapter 3

Investigation of the influence of different metal electrodes on the main parameters of P3HT:PCBM based solar cells – The origin of open circuit voltage

3.1 Introduction

The origin of the open circuit voltage for organic devices is not completely understood at this moment and contradictory opinions are found in the literature. The conventional description of the open circuit voltage in the case of polymer diodes, for example, relies on the metal-insulator-metal (MIM) model of charge carriers separation [48]. In the view of the MIM model, the active organic layer is considered to be insulator, and therefore depleted of charge carriers. According to the MIM model, the open circuit voltage, V_{oc} is considered to be determined by the built-in potential, due to the difference in the work functions of the electrodes. By considering as electrodes ITO (4.7eV) and Al (4.3eV), a maximum of 0.4eV for the open circuit voltage should be expected. For organic photovoltaic devices, the open circuit voltage observed experimentally is in the range of 0.4-0.95eV [49],[50],[113] i.e, far much higher than 0.4V. This is an indication that the MIM model cannot be applied.

In organic materials, the photon energy transmitted to the electrons determine their excitation from the valence band into a higher energy state. Photoexcited charge carriers can decrease then their energy, till they reach the lowest unoccupied molecular level LUMO, corresponding to the conduction band. The energy loss is converted into phonons i.e heat, a process called thermalization (**Figure 3.1**). Therefore, theoretically, the difference between the HOMO and LUMO level of the organic material determines the maximum open circuit voltage which can be achieved by the organic device.

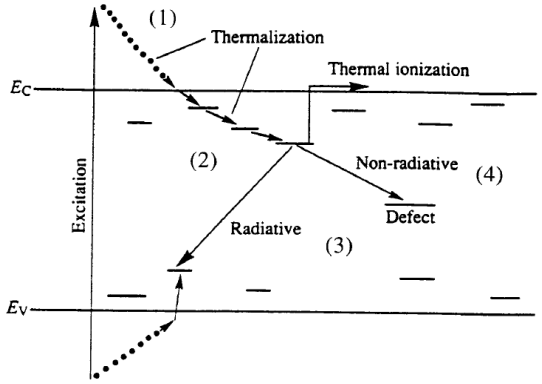

FIGURE 3.1: Illustration of the photoexcitation dynamics in a-Si:H. The photoexcited charge carriers relax through thermalization (1) on the conduction band and are transported through a hopping mechanism (2) towards the electrodes or they recombine radiatively through photoluminescence (3) or catched by deep traps they recombine non-radiatively (4) Reprinted from reference [66]

For the particular case of bulk heterojunction organic solar cells, different experiments were realized in order to find out what determines the open circuit voltage in the device. For PPV based solar cells, a series of acceptors, having different electron affinities were used and additionally, the metallic electrode was varied [51],[52],[53]. The open circuit voltage of the devices was found to be correlated directly with the acceptor strength of the acceptor, while it was rather insensitive to variations in the workfunction of the negative metallic electrode.

A similar result [50] was obtained when different PPV based polymers, having different ionization potentials were used as a donor, combined with the PCBM acceptor in a set of organic solar cells fabricated under the same conditions. The open circuit voltage was found to be strongly correlated with the ionization potential of the PPV based polymers. These experimental results suggested that the V_{oc} is rather determined by the difference between $HOMO_{donor}$ and $LUMO_{acceptor}$. The fact that no influence of the workfunction of the electrodes was found, suggested the following conclusion: The Fermi levels of the metallic electrode and of the acceptor are pinned together.

Other experiments, referring this time to polyfluorene based solar cells produced in a laminated bilayer structure, trying to explain the origin of the open circuit voltage based on a MIM model, proved a different conclusion. The open circuit voltage, V_{oc} was found to consist of the work function difference of the anode and cathode, plus an additional component due to the light intensity [54]. This was a clear indication that the built in voltage created by the electrodes influences V_{oc}. By using low work function metallic electrodes like Ca [55] or Mg, high open circuit voltages were reported. The main disadvantage in this case is the fast oxidation of the contact, due to the unavoidable exposure to the O_2 atmosphere. The thin oxide layer formed between the organic layer and the metallic electrode increases the contact resistance and, consequently, the barrier which has to be passed by the electrones. In case of Ca, without the presence of O_2, an additional effect may occur i.e, the diffusion of Ca into the organic layer as it was reported by some groups [56].

For polythiophene/fullerene solar cells, studies [57] reported that the maximum open circuit voltage, V_{oc} is not limited by the work function difference of the electrodes, but is much higher than this difference.

Different to classical p-n junction solar cells with separated p- and n- regions, the bulk heterojunction solar cell architecture consists of a mixture of an organic p-type and n-type semiconductor, generating nanoscaled p-n junctions for charge separation in the bulk. As it was assumed also by other groups [114], the organic blend in a bulk heterojunction can be considered as a virtual semiconductor characterized by the $LUMO_{acceptor}$ as conduction band and the $HOMO_{donor}$ as valence band. The open circuit voltage of the bulk heterojunction cell is due to the difference between the ionization potential of the donor and the electron affinity of the acceptor, ($HOMO_{donor}$-$LUMO_{acceptor}$) plus a term including the energy necessary for the exciton dissociation and the passing over the barriers between the organic bulk and the electrodes [3].

In what degree the workfunction of the electrodes influences the open circuit voltage, depends on the particular organic compounds used in the device fabrication and cannot be generalized for all cases. For P3HT:PCBM based solar cells, the following experiment was realized in order to clarify this problem:

3.2 Experimental

P3HT:PCBM based solar cells were produced in a P3HT:PCBM weight ratio of 1:2 by using the fabrication procedure indicated in the **Appendix 2** (**recipe 2**). The cells were thermally annealed for 20s at T_a = 130°C. The annealing procedure is applied in order to improve the charge transport properties of organic bulk heterojunction layer and will be discussed in detail in **Chapter 5**. Different metallic electrodes were used as cathode, in order to modify the built in field introduced by the work function difference of the electrodes upon the active organic layer, and to see its influence on the open circuit voltage, V_{oc}. The following metallic electrodes were chosen: Mg (3.66eV), Al (4.3eV), Cu (4.65eV), Au (5.1eV). After thermal annealing, the external quantum efficiency, (EQE) and J-V curves were measured.

3.3 Results and discussions

Figure 3.2 shows in linear and semilogarithmic representation the experimental J-V curves of annealed P3HT:PCBM based solar cells under dark and illumination conditions (100mW/cm²). In **table 3.1** are indicated the electrical parameters for P3HT:PCBM based solar cells fabricated with different metallic electrodes (Mg, Al, Cu and Au).

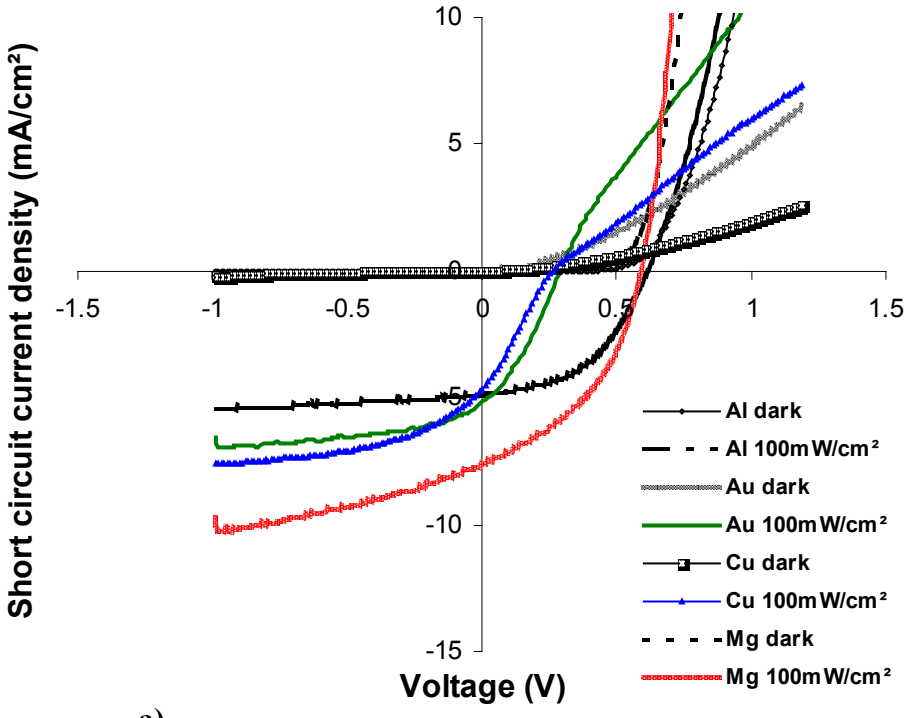

a)

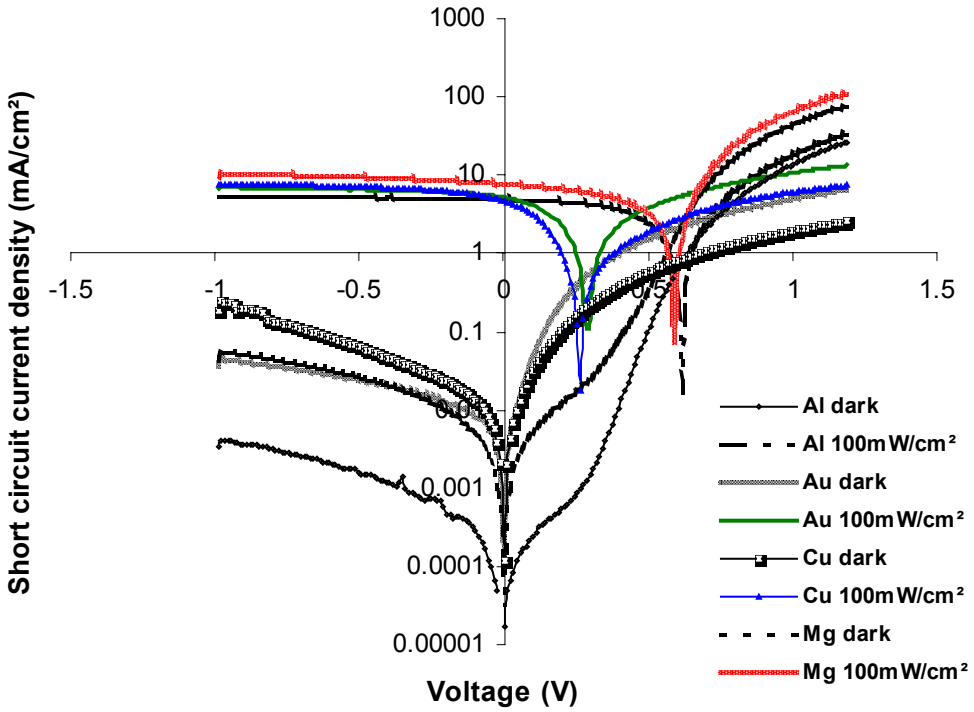

b)

FIGURE 3.2: J-V curves of annealed P3HT:PCBM based solar cells fabricated with different metallic electrodes (Mg, Al, Cu, Au) in linear a) and semilogarithmic representation b) (100mW/cm², 289K).

Table 3.1 Electrical parameters for thermally annealed P3HT:PCBM based solar cells fabricated with different metallic electrodes (T=289K)

Cathode	Work function (eV)	J_{sc}(mA/cm²)	V_{oc}(V)	FF(%)	η(%)
Mg	3.66	7.66	0.595	43.07	1.96
Al	4.3	4.91	0.617	47.8	1.44
Cu	4.65	4.65	0.265	26.17	0.322
Au	5.1	5.16	0.298	32.52	0.5

From **Figure 3.2** and **table 3.1** it can be noticed that in the case of P3HT:PCBM based solar cells fabricated with Mg and Al electrodes, close values for open circuit voltages were obtained, while for the cells produced with Au and Cu electrodes, the open circuit voltages are in the same range, but considerably low. In order to explain the differences obtained in the values of V_{oc}, the transport mechanism of the charge carriers over the interface semiconductor/metal must be considered.

The photoexcited electrons are injected from the conduction band into the cathode (metallic electrode), and the holes remained in the valence band are injected to the anode (ITO-PEDOT:PSS). **Figure 3.3** represents an illustration of the 'virtual' bulk material with the

corresponding energy levels of the both p- and n-type organic compounds. The 'virtual' material can be considered as a theoretical model, but in reality, there are many direct contacts between each organic compound and both electrodes. As a result of these direct contacts, a band bending occurs at the interface of between each organic compounds (P3HT and PCBM) and both electrodes (anode and cathode).

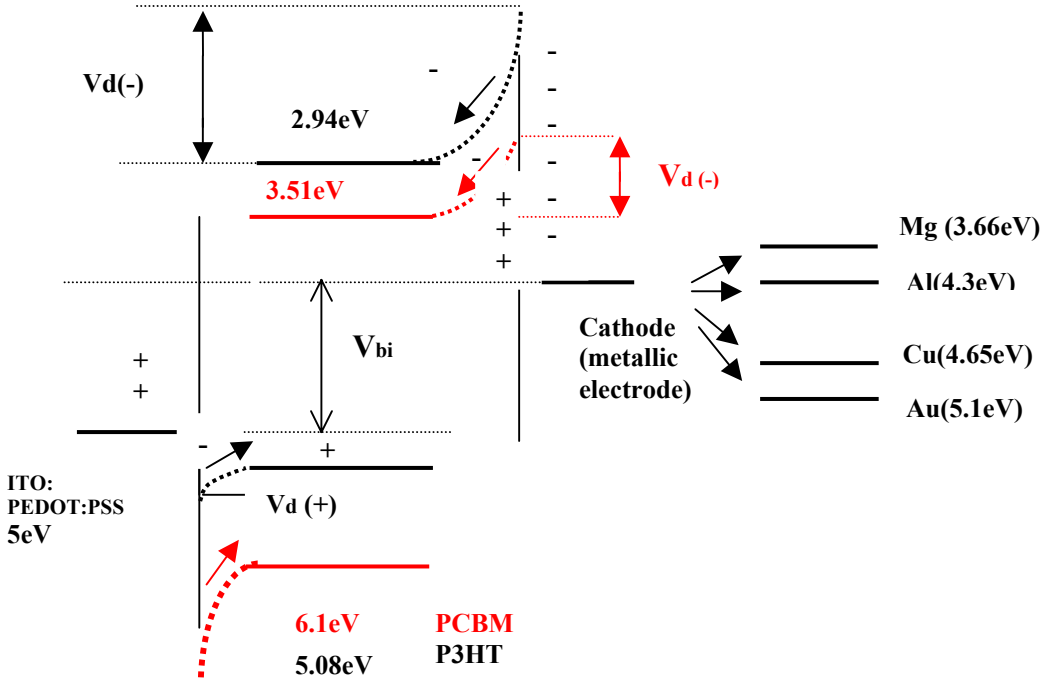

FIGURE 3.3 : Illustration of band bending which occurs in P3HT:PCBM based solar cells, at the interface organic material-electrodes.

The band bending at the interface organic materials/electrodes was explained by the theory of Schottky and Mott (1938) [36]. The rectification mechanism occurred at the interface between two semiconductors, or between semiconductor/metal with different work functions follows a direction, which can be explained by supposing that electrons passed over a potential barrier through the normal process of drift and diffusion. The diffusion process over the interfacial region takes place until the Fermi levels in both materials are equalized. At equilibrium, the current contributions to each side of the junction must be equal. Blocking contacts are formed when p- or n- type semiconductors make contact with metals with work functions less or greater than those of the semiconductor, respectively (Schottky contact shown in the **Figure 3.3**). Ohmic contact is formed when the work functions of the metals are greater (for p-type) or less (for n-type) than those of the semiconductors (not shown in the picture). For ohmic contacts, the metal becomes an infinite reservoir of charge carriers which can be injected in the organic semiconductor material, until the Fermi levels are equalized on both sides of the interface.

In **Figure 3.3** it can be noticed that there are 4 interface combinations between every organic component and the two electrodes (anode and cathode). It is the smallest barrier at each interface which dominates the injection [58].

- **P3HT: anode (ITO/PEDOT:PSS) interface**
  Electrons from the anode will be injected into the valence band of P3HT, and fill the holes remained there as a result of photoexitation of charge carriers over the band gap. Due to the fact that the difference $HOMO_{P3HT} - \phi_{ITO\text{-}PEDOT:PSS}$ is very small (0.08eV), the contact can be considered ohmic.

- **PCBM : anode (ITO-PEDOT:PSS) interface**
  A larger barrier than in the previous case, occurs for the electrons injected from the anode into the valence band of PCBM. The valence band of the PCBM acceptor, is likely to be filled with electrons either obtained through electron transfer from the P3HT donor, or most probably, with its own unexcited electrones. This fact will determine a charge space, i.e, a blocking contact occurs for the electron injection from anode into PCBM.

- **PCBM:cathode (metallic electrode) interface**
  In this case, due to the diffusion potential created between the PCBM and the cathode, the large number of electrons attracted in the conduction band of PCBM through the photoinduced charge transfer from P3HT, will be injected into the metal. The barrier will be proportional to the difference ϕ_m-$LUMO_{PCBM.}$

- **P3HT:cathode (metallic electrode) interface**
  A barrier, similar to that of the previous case will be formed between P3HT and the cathode. This barrier will be determined by the difference ϕ_m-$LUMO_{P3HT}$. Due to the fact that in the conduction band of P3HT, the photoexcited charge carriers are likely to be attracted by the strong acceptor PCBM, and taking into account a larger barrier created with the cathode (ϕ_m-$LUMO_{P3HT}$ > ϕ_m-$LUMO_{PCBM}$), there is a lower probability for the electrons to be transported directly from P3HT to the metallic electrode, unless there is a direct contact between them.

In the 4 cases of P3HT:PCBM based solar cells fabricated with different metallic electrodes, the differences obtained in V_{oc} are evidence of a strong influence of the cathode work function. Taking into account that $HOMO_{donor}$-$LUMO_{acceptor}$ is the same in all 4 cases, the variation of V_{oc} can be explained through modification of the barrier at the PCBM:metallic electrode interface. In the case of the cell fabricated with a Mg electrode, the contact can be considered ohmic because the difference $LUMO_{PCBM}$-ϕ_{Mg} = 0.04eV is very small. (The condition for a bulk limited conduction was reported [59] to occur when the difference between the Fermi levels of semiconductor and metal is < 0.3-0.4eV).

The highest current obtained for the cell fabricated with a Mg electrode can be explained through a better extraction of electrons by the cathode. And this huge increase in J_{sc} is probably the reason why the V_{oc} for Mg cell is a little bit lower than that of the cell fabricated with Al. When Cu and Au electrodes are used, a higher barrier PCBM/cathode is obtained, and the experimental results indicated a very small open circuit voltage of less than 300mV. From the normal representation of the J-V curve, it can be noticed a very high series resistance and a low fill factor.

J_{sc} for P3HT :PCBM based solar cells fabricated with different metallic electrodes was calculated by using a method [37] (**chapter 2**) based on the solar spectrum and external quantum of photogenerated charge carriers, (EQE) measurements. These values were compared with those obtained experimentally from the J-V curve. These results are shown in the **table 3.2** and

correspond to **Figure 3.4**. The highest current is obtained for the cell produced with a Mg electrode. In the case of other electrodes Al, Cu and Au, J_{sc} is in the same range of values for all 3 cells, but lower.

Table 3.2: Peak values of external quantum efficiency and short circuit current density both estimated from EQE and measured on P3HT:PCBM based solar cells fabricated with different metallic electrodes

	J_{sc} (mA/cm²) Calculated (300-800nm)	J_{sc} (mA/cm²) Measured (T=289K)	EQE (%) Max at 540nm
AM 1.5 1000W/m²	25.98	-	
Magnesium	8.225	7.66	61.5
Aluminium	5.667	4.91	41.6
Copper	6.01	4.65	44.3
Gold	5.068	5.16	39.64

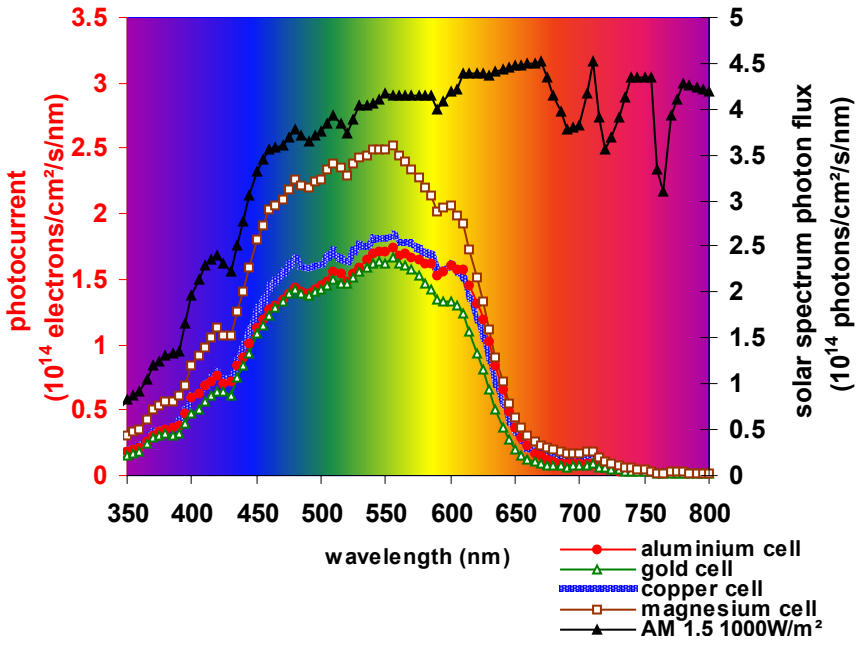

FIGURE 3.4: Photocurrent (10^{14} electrons/cm²/s/nm) calculated from solar spectrum and external quantum efficiency curves of annealed P3HT:PCBM based solar cells fabricated with different metallic electrodes as cathode (Mg, Al, Cu, Au). The graph plotted with black triangles represents the solar spectrum photon flux (10^{14} photons/cm²/s/nm)

Chapter 4

Investigation on light intensity and temperature dependence of the main parameters of P3HT:PCBM based solar cells

4.1 Experimental

In the following, the experiment performed in chapter 3 was used, in order to appreciate the influence of light intensity and temperature on the main parameters of P3HT:PCBM based solar cells fabricated with different electrodes (Al, Cu, Au and Mg). Current density - voltage characteristics of P3HT:PCBM based solar cells were measured in a range of temperatures from 120K-370K and for different light intensities, following the procedure mentioned in the **appendix 2**.

4.2 Light intensity dependence of the main parameters of P3HT:PCBM based solar cells

4.2.1 Short circuit current density, J_{sc}

In general, for semiconductors, the photogenerated current depends on the incident light intensity following the law:

$$J_{sc} \approx L^n \quad (4.1)$$

$$n = f(N_f/N_t) \quad (4.2)$$

where L is the light intensity and N_f and N_t are the densities of free and trapped carriers, respectively. The value of the coefficient n depends on the number, distribution and type of traps present (i.e., shallow or deep traps), on the carrier generation and conduction mechanisms and on diffusion and recombination processes generally [60]. For organic insulators in the dark, $0.5 \leq n \leq 1$. For high light intensities, when $N_f \geq N_t$, bimolecular recombination of the photogenerated free charge carriers dominates and $n = 0.5$. A saturation of the short circuit current occurs when the light intensity is so high that space charge limited current (SCLC) exists. A superlinear dependence ($n > 1$) was in some cases observed [61]. Poor contacts or contamination of the interface metal/semiconductor can have an influence on the recombination processes and affect the value of n. In the particular case of P3HT and fullerene composites, photophysical studies [62],[63] found out a strong bimolecular recombination.

The **Figure 4.1** shows the dependence of the short circuit current density on light intensity of P3HT:PCBM based solar cells fabricated with different metallic electrodes. Generally, in organic semiconductors, the photogenerated current scales with the light intensity. The logarithmic representation of J_{sc} with the light intensity at all temperatures shows a linear dependence. From the slope of the graph the coefficient n can be derived (**Figure 4.1 case e**). In all 4 cases the coefficient n was found to have a value around 1 at room temperature. This is an indication that the bimolecular recombination in this temperature range can be neglected.

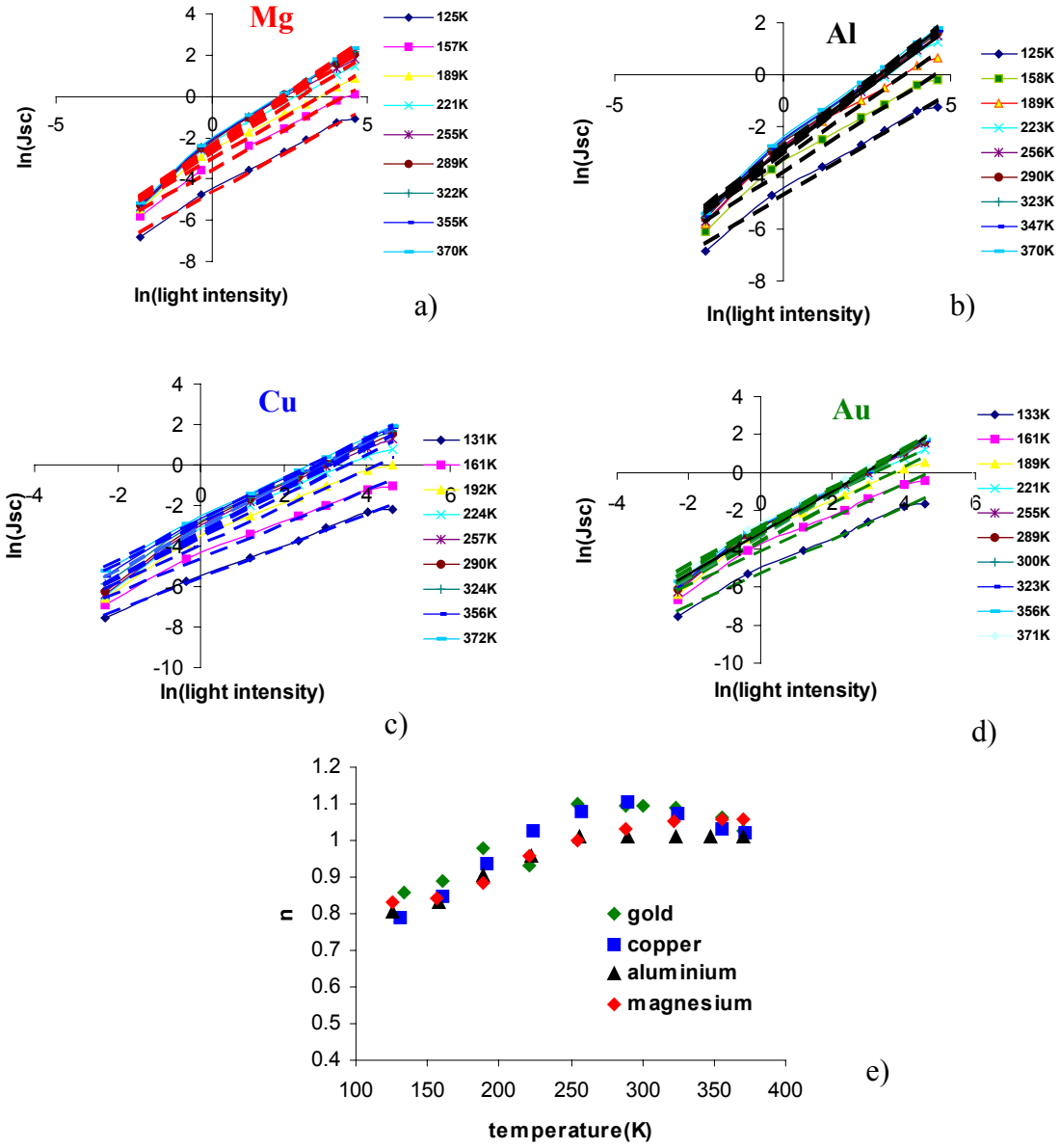

FIGURE 4.1: Light intensity (mW/cm²) dependence of the short circuit current density (mA/cm²) in logarithmic representation at different temperatures for the 4 P3HT:PCBM based solar cells fabricated with different electrodes a) Mg b) Al c) Cu d) Au . In the figure e) it is represented the dependence of the coefficient n with the temperature.

This fact can be understood by the positive influence of temperature on the transport of charge carriers leading to the avoidance of recombination processes. The same conclusion was found in the case of P3HT:PCBM based solar cells by other groups [62].

4.2.2 Open circuit voltage, V_{oc}

When the light intensity is increased, then more free charge carriers are photogenerated, i.e., more negative charge carriers are accumulated at the cathode and more holes at the anode, increasing the potential difference over the organic material layer. In this case, a higher open circuit voltage is obtained.

In a linear representation of open circuit voltage versus light intensity, there is a nonlinear increase of V_{oc} at low values followed by a saturation region at higher values of light intensity. Since the photogenerated current is a function of the light intensity according to the formula (4.1) and the V_{oc} is given by the following equation:

$$V_{oc} = \frac{kT}{e} \ln\left(\frac{I_{sc}}{I_0} + 1\right) \quad \textbf{(4.3)}$$

It is expected that $V_{oc} \approx \ln(L)$ **(4.4)**

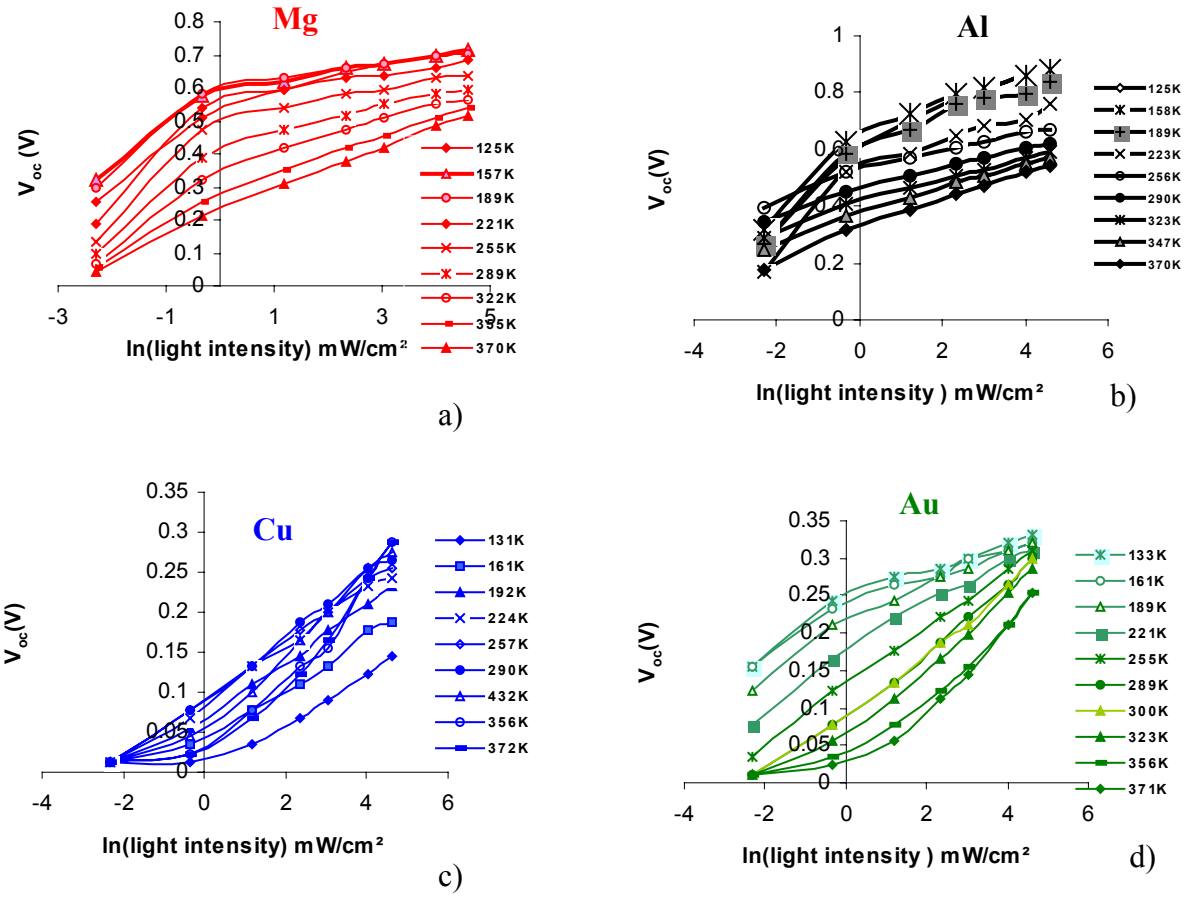

FIGURE 4.2: Variation of the open circuit voltage with the light intensity at all measured temperatures for the P3HT:PCBM based solar cells with different electrodes: a) Mg b) Al c) Cu d) Au

The **Figure 4.2** shows in semi-logarithmic representation, the light intensity dependence of the open circuit voltage for different temperatures for P3HT:PCBM based solar cells fabricated with different metallic electrodes (Mg, Al, Cu, Au). For Mg and Al electrodes, the V_{oc} follows a linear dependence with the ln(light intensity) only at high temperatures. This behaviour is probably due to the influence of temperature on the transport of charge carriers over the barriers. If the light intensity is high, a lot of free electrons are produced and at high temperatures are easily transported over the barrier. In the case of Al and Mg due to their lower work functions compared to Au and Cu, the barriers between organic layer and metallic electrode are lower and

the built in field introduced by the anode/cathode work function difference is larger. Higher values are obtained for V_{oc}.

4.2.3 Fill factor, FF

The fill factor normally has a complicated dependence on the series and parallel resistance and is determined in organic materials by the trapping effects [64], recombination and diffusion properties within the bulk of organic material and at the electrode surfaces. Any modification of these parameters with the light intensity will affect the fill factor. In most organic materials, due to the fact that recombination processes are enhanced at higher light intensities, the fill factor decreases. This particular behaviour can be recognized also in the case of P3HT:PCBM based solar cells (**Figure 4.3**). The fill factor is higher for the cells fabricated with Al and Mg electrodes, about >50% and quite low in the other two cases (for cells with Au and Cu being around 30%). This result can be explained in the last two cases by the high barriers (high series resistance) for the electrons at the interface PCBM/cathode in the case of Au and Cu. If the charge carriers are not able to overcome them, they will recombine (low parallel resistance). In these cases recombination processes are pronounced and determine a low fill factor.

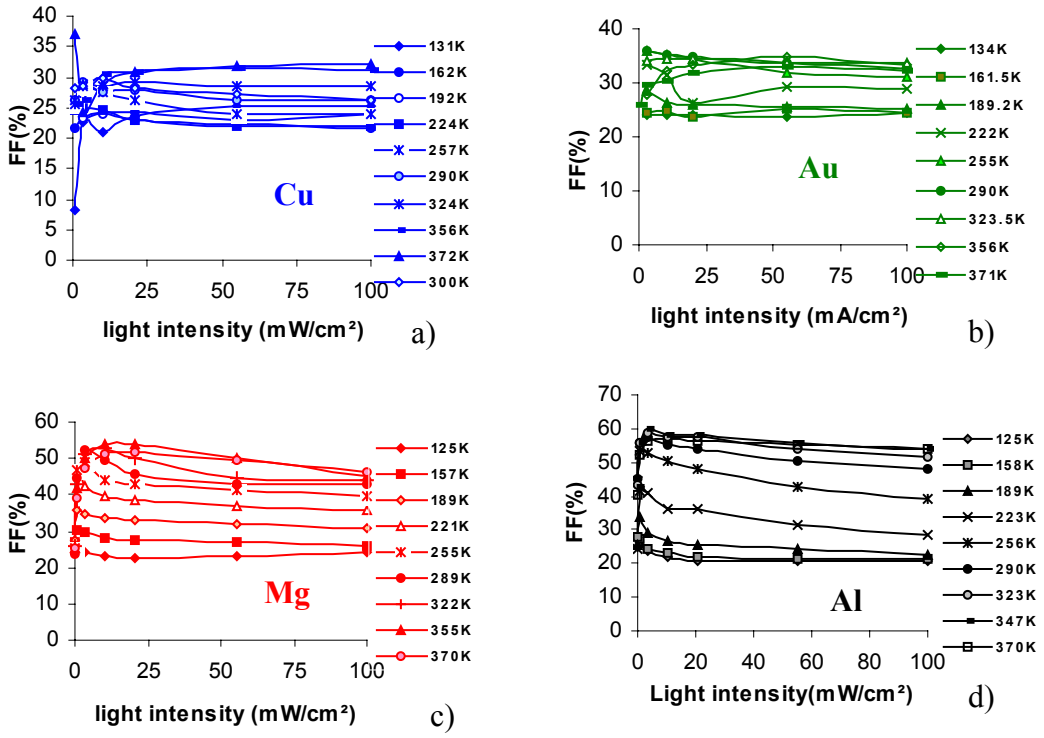

FIGURE 4.3 : Dependence of the fill factor with the light intensity for P3HT:PCBM solar cells with different contacts a) Cu b) Au c) Mg d) Al

4.2.4 Power conversion efficiency, η

Power conversion efficiency is the most important parameter, relevant for the electrical performance of the solar cells and depends on all above mentioned parameters (J_{sc}, V_{oc}, FF and light intensity). **Figure 4.4** shows the efficiency dependence on light intensity. A maximum of the efficiency occurs at 3mW/cm² at lower temperatures. This is an indication of the limited capability of the organic bulk material to transport the charge carriers due to dominant recombination processes. As the temperature increases, the maximum of the power conversion

efficiency is shifted to 50mW/cm² (**Figure 4.4 cases c and d**) and, at temperatures >350K, it reaches a saturation region.(**Figure 4.4 cases a and b**).

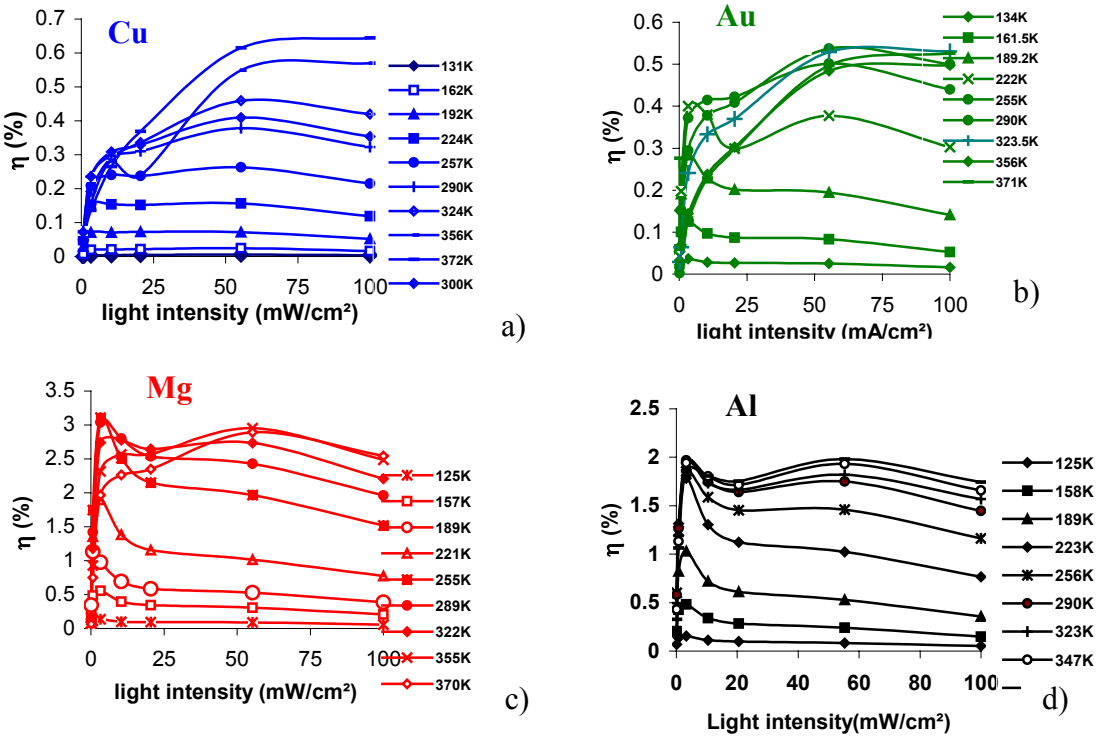

FIGURE 4.4: Dependence of efficiency with the light intensity for P3HT:PCBM solar cells with different contacts a) Cu b) Au c) Mg d) Al

4.3 Temperature dependence of the main electrical parameters of the P3HT:PCBM based solar cell

4.3.1 Open circuit voltage, V_{oc}

In the most organic solar cells tested so far, the open circuit voltage increased with decreasing temperature as it is depicted in **Figure 4.5 (case a, b, c)**. Few exceptions exist as the case d) of **Figure 4.5** when the cell was fabricated with a copper cathode.

In order to understand this behaviour the following formula should be considered:

$$V_{oc} = \frac{kT}{e}\left(\ln\frac{I_{sc}}{I_0}+1\right) \approx \frac{kT}{e}\ln\left(\frac{I_{sc}}{\frac{I_0}{\phi}}\right) \qquad \textbf{(4.5)}$$

where

$$I_0 = I_{0\max}\exp\left(\frac{-E_g}{kT}\right) \qquad \textbf{(4.6)}$$

From equations (4.5), (4.6) the following expression for the open circuit voltage is obtained:

$$V_{oc} = \frac{E_g}{e} - \frac{kT}{e}\ln\frac{I_{0\max}}{\phi I_{sc}} \qquad \textbf{(4.7)}$$

where E_g represents the band gap of the organic material. As it was explained in chapter 2, the photoluminescence quantum yield, ϕ is considered in formula (4.7) as a correction factor.

With decreasing temperature, the short circuit current density, J_{sc} decreases, due to the poor transport of charge carriers through the bulk, reflected in the dominant recombination processes (high ϕ). Therefore, the second term on the right side of equation (4.7) decreases, determining theoretically a higher V_{oc} at low temperatures. The dependence V_{oc} versus temperature can however not be completely linear, because in equation (4.7) there is also a variation of the band gap with temperature.

$$E_g = E_{g,0} - \frac{aT^2}{b+T} \qquad \textbf{(4.8)}$$

where $E_{g,0}$ is the band gap at T=0K and a,b are constants.

A similar dependence of the open circuit voltage with temperature was obtained by Katz [65] who proposed a straight line for $V_{oc}(T)$ by neglecting the influence of the the band gap with temperature. The matching of their proposed equation with experimental data suggests that the variation of the band gap with temperature might be negligible when compared to that of the second term of the right hand side of equation (4.7). Practically, as a result of recombination processes, V_{oc} can be found to deviate from the theoretical value expected to increase with

decreasing temperatures (**Figure 4.5 case d**). A similar deviation from the theoretically high V_{oc} value at low temperature was reported [113] also in the case of OC1C10-PPV:DPM-12 based solar cells fabricated with Al as metallic electrode.

For disordered materials, at low temperatures, the photoluminescence decay and intensity are longer and higher, respectively.This fact is illustrated in **Figure 4.6** in the case of a-Si:H. The pronounced recombination processes at low temperatures can explain the experimental reduction of V_{oc} values within this temperature range.

As a conclusion, according to equation (4.7), the theoretical limit of organic solar cells is given by the band gap E_g of the organic material and corresponds in the case of a bulk heterojunction structure to the difference $HOMO_{P3HT}$-$LUMO_{PCBM}$.

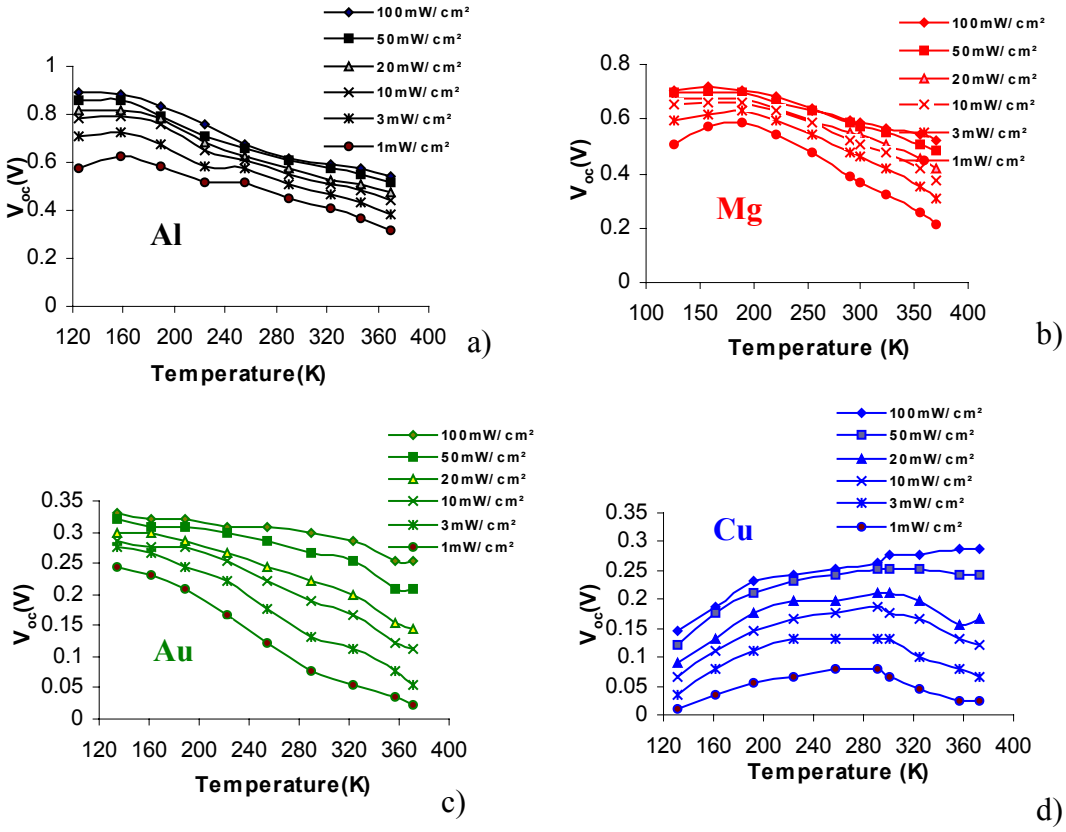

FIGURE 4.5: Dependence of the open circuit voltage, Voc with the temperature for P3HT:PCBM solar cells with different electrodes a) Al b) Mg c) Au d) Cu

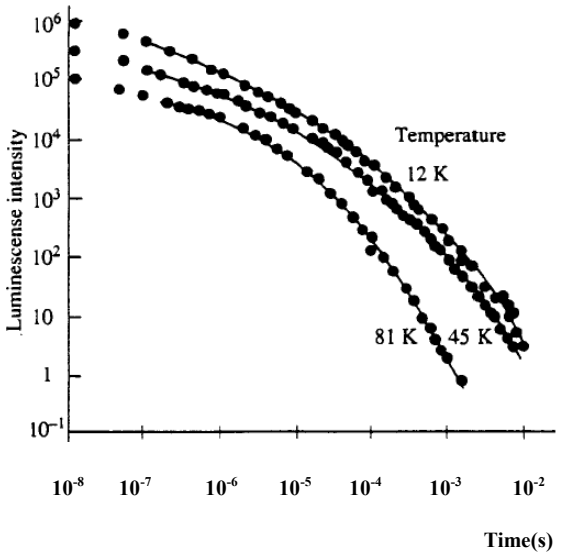

FIGURE 4.6: Illustration of the photoluminescence decay in a-Si:H (Reprinted from reference [66])

4.3.2 Short circuit current density, J_{sc}

The dependence of the short circuit current density with temperature, shows for all cases of P3HT:PCBM based solar cells an increase with increasing temperature (**Figure 4.7**). This particular variation $J_{sc} = f(T)$ was reported also for OC1C10-PPV based solar cells [103] and represents a typical behaviour of organic solar cells. This result, can be explained by the following arguments:

In a solar cell the output current is proportional to the number of photogenerated charge carriers and to their mobility. In the most conventional inorganic semiconductors, the mobility varies with temperature according to the following law [67]:

$$\mu \approx T^{-n} \qquad \textbf{(4.9)}$$

where n = -3/2 for impurity scattering and n = 3/2 for lattice scattering.

Generally, the main mechanisms that influence electron and hole mobility are lattice scattering and impurity scattering. In lattice scattering, a carrier in a crystal is scattered by a vibration of the lattice, depending on temperature. The frequency of such scattering events increases with temperature, since the thermal agitation of the lattice becomes greater. Therefore, one should expect the mobility to decrease as the sample is heated.

For organic semiconductors, the transport of charge carriers occurs via localized states, where the hopping of charge carriers from one site to another is assisted by the phonons. The conductivity and mobility are thermally activated and increase both with temperature.

$$\sigma = \sigma_0 \exp\left(\frac{-\Delta E}{2kT}\right) \qquad \textbf{(4.10)}$$

$$\mu = \frac{\sigma}{zen} \qquad \textbf{(4.11)}$$

where σ is the conductivity ($ohm^{-1}cm^{-1}$), μ is the mobility, *ze* the net charge of the carriers, n the concentration of charge carriers, ΔE the activation energy, k the Boltzmann constant and T the temperature.

The activation energy has two contributions, the band gap value energy necessary to excite electrons from HOMO to LUMO, and the energy to delocalize the charge carriers i.e., the energy necessary for an electron to escape from a trap [115]. At low temperature, the probability to find a phonon of sufficient energy to facilitate a hopping to the nearest site will be low. As the temperature increases, the charge carrier mobility and, therefore, the conductivity should also increase. As a general conclusion for organic materials, at low temperatures, few charge carriers are thermally generated and are not easily transported, therefore, the current is low.

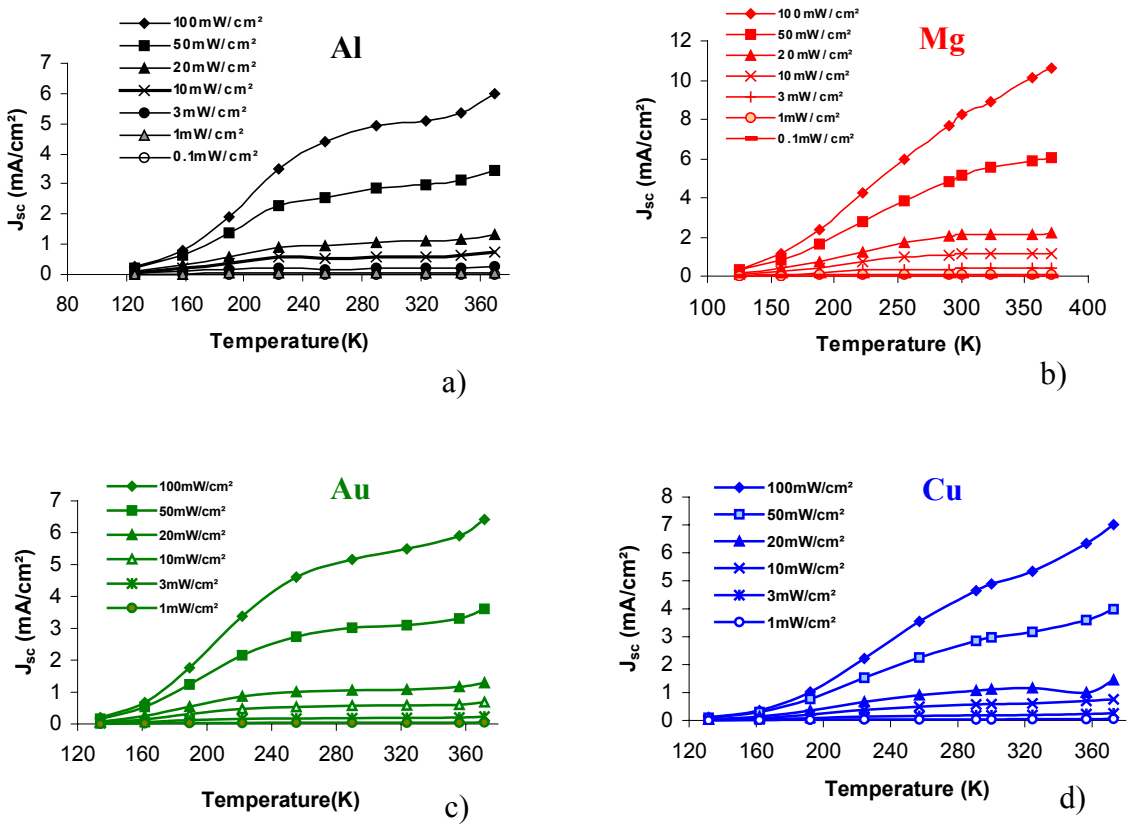

FIGURE 4.7: Dependence of the short circuit current density on temperature for the P3HT:PCBM based solar cells with different electrodes a) Al b) Mg c) Au d) Cu

4.3.3 Efficiency, η and Fill factor, FF

The variation of the power conversion efficiency, η and the fill factor, FF with temperature shows in both cases, an increased value at high temperatures in all P3HT:PCBM based solar cells independent of the metallic electrode used for the cell fabrication (**Figure 4.8**). This result can be explained by a reduced recombination probability and a reduced series resistance at high temperatures. The photogenerated charge carriers are transported easier through the bulk and over the contacts respectively, due to the thermally activated hopping mechanism and contribute to the output current.The increase of efficiency at higher temperatures is a direct result of the dependence of the main parameters (short circuit current, open circuit voltage, fill factor) with temperature according to the formula $\eta=FF*J_{sc}*V_{oc}/L_d$, where $L_d = L/a$ is the power density of the incident light, L and *a* is the active area of the device. The small decrease of V_{oc} and the huge

increase of J_{sc} and FF at higher temperatures determine the improvement of the efficiency. The efficiency improvement with increasing of temperature is generally a peculiarity for organic solar cells which is not observed in the case of inorganic solar cells [68]. It is important to be mentioned that the heating of the solar cells at high temperatures can be caused naturally by the absorption of the solar radiation which imply that organic solar cells are likely to have better performances under a warm climate than under standard test conditions.

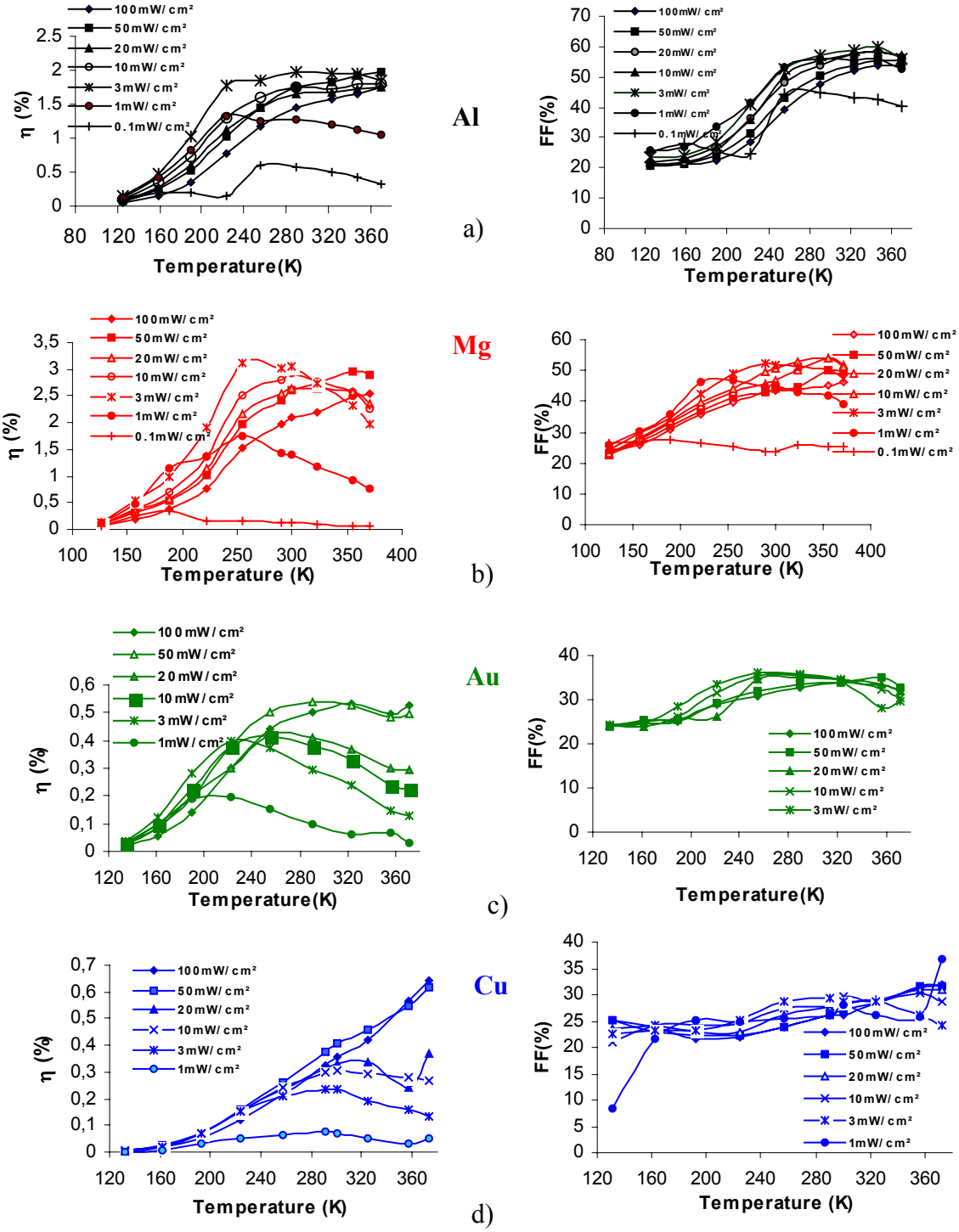

FIGURE 4.8: Dependence of efficiency and fill factor on temperature for P3HT:PCBM based solar cells with different metallic electrodes: a) Al b) Mg c) Au d) Cu

Chapter 5

Thermal annealing, a method for improving the efficiency of organic solar cells

5.1 Introduction

A good performance of an organic solar cell is determined by an optimum balance among the following requirements: light absorption, photogeneration, transport and extraction of charge carriers. Light absorption, reflected in the photogeneration efficiency of charge carriers is determined by the absorption coefficient of the organic materials and by the band gap. Extraction of charge carriers is considerably influenced by the appropriate choice of electrodes, and by their interface with the organic active layer. Transport properties of the bulk organic material, reflected by the mobility of charge carriers, depends on the morphology of the active layer. This is the aspect which will be discussed in the present chapter.

Conjugated polymer chains can be imagined having a structure similar to spaghetti arranged in a random way. Fullerene derivatives, imagined as beans, are added and mixed homogeneously with the polymers chain by using a particular solvent, and a special preparation procedure (**Figure 5.1**).

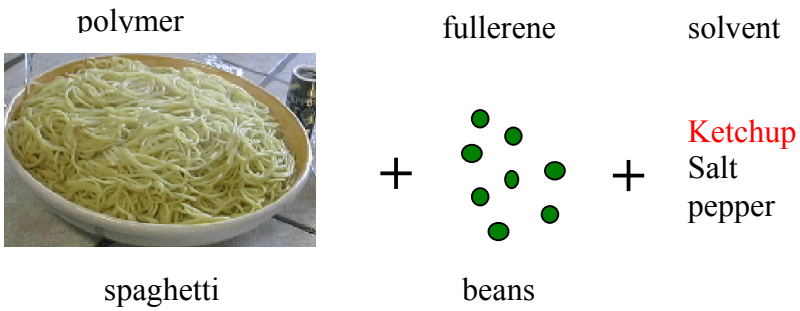

FIGURE 5.1: The simple analogy to describe the structure of most polymers is a dish of cooked spaghetti reduced in size 100 000 times. Each spaghetti represents a long polymer chain. The acceptor (fullerene) can be imagined as beans coming in a close contact with the polymer chain. The optimization of the morphology is highly determined by the solvent and the preparation procedure

When two organic materials (polymer and methanofullerene) are blended, the mixing does not happen spontaneously. The natural trend of both organic compounds is to demix and to form a separate phase consisting of respective components. When the polymer blend is not given enough time to complete the phase separation, an intermediate state of mixing is frozen into a solid state giving rise to the typical morphology of a blend. There are two methods of avoiding phase separation:

a) through morphology optimization

The polymers are dissolved in a common solvent, and form an homogeneous solution which is then dispensed (spin coated) (**Figure 5.2**) on a substrate rotating at a 1000-4000 rpm in the surface plane.

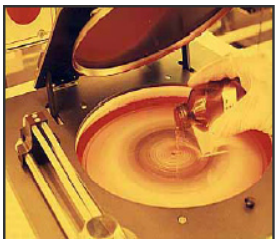

FIGURE 5.2: Spin coating is the wide spread option for obtaining organic thin films

The formation of thin organic films as a result of spin coating takes place according to the following scenario [69]:

During spin coating, the domains that are rich in the least soluble component, solidify first and form walls, while the remaining solution resides between the walls. When the solvent continues to evaporate, the second domain collapses in the wells formed between the walls. The overall morphology and domain size is strongly influenced by the blend ratio, the rate of solvent evaporation is determined by the solvent properties, solvent polymer interactions, and spin coating conditions (speed, temperature).

Conjugated polymers dissolved in good*,[71] solvents tend to have an open conformation, allowing easy access for chromophore to come into interchain contact. Conjugated polymer chains in poor solvents, tend to form tight coils, making difficult for chromophores to become physically adjacent, even though the chains tend to clump together. If a solvent is good or bad, this can be appreciated in relation to the polymer used. For example for PPV based solar cells, THF [71] and toluene [22] were found to be bad solvents compared to chlorobenzene. PPV based solar cells processed from chlorobenzene gave higher currents [22]. In the case of polythiophene, the influence of the solvent was confirmed by the electrical performace of P3HT based field effect transistors. Different field mobilities measured for field effect transistors fabricated with different solvents are reported [72] below:

Field effect mobility for P3HT prepared from (THF)= $6.2 * 10^{-4}$ (cm^2/Vs)
(toluene)= $3.6*10^{-3}$(cm^2/Vs)
(chlorobenzene)=$4.7*10^{-3}$ (cm^2/Vs)
(chloroform)= $9.2*10^{-3}$ (cm^2/Vs)

b) through thermal annealing

The process of thermal annealing has been demonstrated to considerably increase the efficiency of P3HT:PCBM based light emitting diodes [73] and solar cells [81]. As a result of heating, the morphological structure of the organic active layer can be modified towards a better organisation, having as main consequence a better transport of charge carriers and therefore a higher current and a better power conversion efficiency.

Several attempts towards improving the efficiency of organic solar cells by thermal annealing were reported in the literature, with a very wide range of differences on performing the experiments. The positive effects of thermal annealing are the reduction of the free volume and defects at the interface during evaporation of the solvent [73] and enhancement of the interchain interactions [74]. In a bilayer structure, the interdiffusion between the donor and the acceptor was observed [75]. In this way the fullerene molecule is brought within the exciton diffusion radius of the polymer, resulting in a highly efficient charge separation. Thermal annealing of polymer-polymer donor-acceptor blends with subsequent exposure to solvent vapour blends led to a significant increase of the charge carrier photogeneration efficiency [76]. Lee *et al.* [77] reported

* By a good solvent is meant a solvent in which with sufficient stirring and heating, the polymer can dissolve to concentrations of several percent w/v without gelation

the positive effect of heat treatment on a polymer film for improving the quantum efficiency due to the change of morphology at the polymer and electrode interface.

The way how thermal annealing is applied varies in the literature, and different effects are reported. It is known that P3HT crystallises as a result of thermal annealing, which can have a positive effect on the transport of holes [78]. Other investigations, which refer to polythiophene copolymers, indicated a strong increase in the external quantum efficiency of photogenerated charge carriers by performing the thermal annealing under chloroform vapors [79]. Mild thermal treatment i.e., for a period of 30 min at a temperature of 55°C [80] subject to P3HT:fulleropyrrolidine based solar cells, leads to an overall efficiency of 0.6%, while, in the case of P3HT:PCBM based solar cells, the thermal treatment of 4 min at 75°C together with an applied voltage (2.7V) reportedly yielded an efficiency of 3.5% at white light illumination intensity of 80mW/cm² [81].

There is a demand on additional studies to clarify the effects of thermal annealing and the evaluation of an optimum set of the crucial treatment parameters, annealing time and temperature. What has been demonstrated by differential calorimetry measurements is that by annealing at temperatures higher than the melting point of P3HT (see **appendix 2**), a sort of crystalline liquid state for the pure P3HT occurs [82]. In this case, the main chain is irreversibly deteriorated and, by cooling, the initial structure cannot be obtained again. The twisting of the main chain is supposed to happen between two thiophene rings which lose coplanarity, the band gap increases and therefore the conductivity decreases. This fact was theoretically recognized in a blue shift in the absorption spectrum of polythiophene and in its thermochromism [83].

Furthermore, at temperatures higher than 100°C, the content of O_2 in P3HT could no longer be detected due to a dedoping process, and the organic absorber became protected against deterioration [84] .

The following experiments related to thermal annealing were performed and the results and conclusions are discussed below:

- **absorption measurements**
- **test on the persistence of improved electrical performance of P3HT:PCBM based solar cells upon thermal annealing**
- **morphology investigations**
- **optimization of the amount of PCBM acceptor in the P3HT:PCBM based solar cells**

5.2 Absorption measurements

5.2.1 Experimental

Absorption spectra of both pure compounds (P3HT, PCBM) and the P3HT:PCBM mixture were measured before and after thermal annealing.

5.2.2. Results and discussions

The absorption spectrum of P3HT thin films prepared from different solvents shows no change even after one hour of thermal annealing, except for the P3HT prepared from chloroform solution. In this case, a very small increase in the absorption spectrum occurs after 1 hour of thermal treatment at T_a = 130°C (**Figure 5.3**).

For pure PCBM, two spin coated films were tested before and after thermal annealing (**Figure 5.4**). In the first case of using chloroform/toluene as a solvent, a red shift occurs in the absorption spectrum, larger than in the case of using chloroform. Due to the fact that toluene is not a good solvent for PCBM, large domains are built in the material, having as main result a red shift in the absorption spectrum due to PCBM crystallisation. (The result related to the occurrence of PCBM clusters will be discussed in detail in the paragraph 5.6)

The preparation methods used for the P3HT:PCBM based solar cells are indicated in the **appendix 2**. The best results were obtained with the **recipe 2** in which the solvent used was waterfree pure chloroform. Therefore, further investigation on the absorption spectrum for P3HT:PCBM blend will refer to this particular solvent. (**Figure 5.5**)

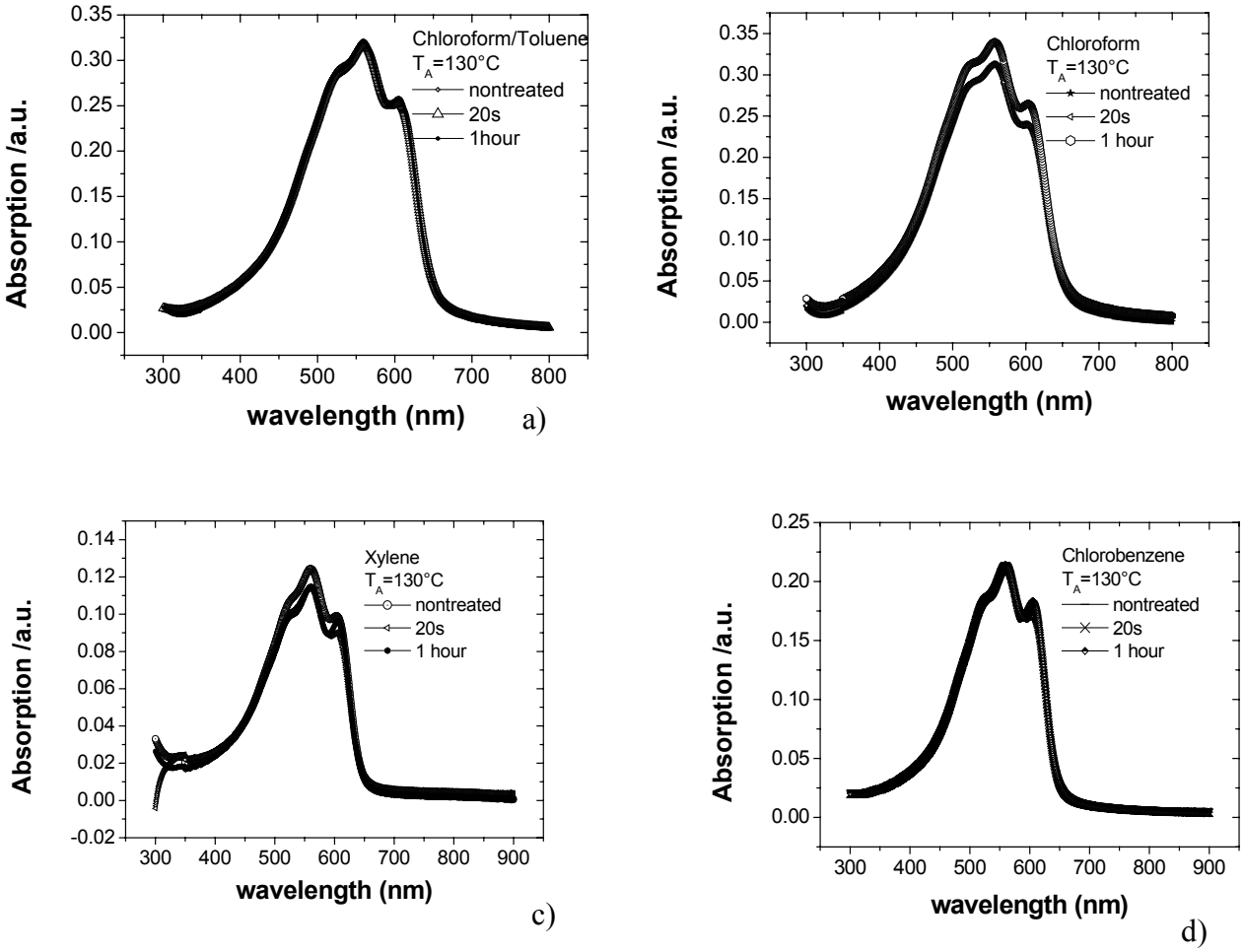

FIGURE 5.3: Absorption spectra of pure P3HT films spin coated from solutions prepared from different solvents before and after annealing.a) chloroform/toluene b) chloroform c) xylene d) chlorobenzene

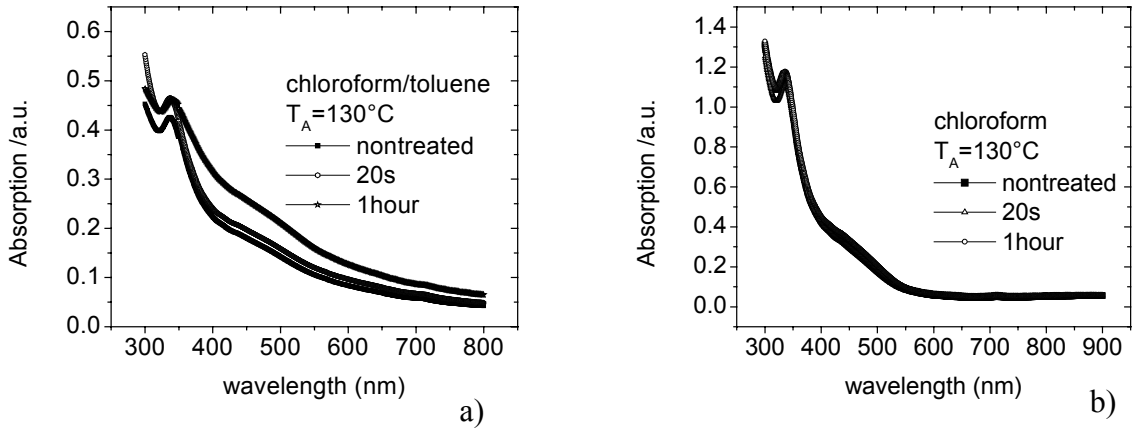

FIGURE 5.4 : Absorption spectrum for pure PCBM films spin coated on glass from a solution of a)chloroform:toluene b) chloroform before and after annealing. The annealing time and temperature are indicated in the legend.

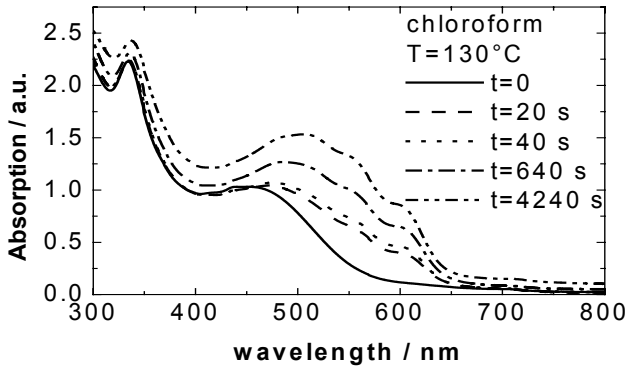

FIGURE 5.5: Absorption spectra of a P3HT:PCBM composite film prepared from chloroform solution as cast (blue line) and after four successive thermal annealing steps, as indicated in the legend. The P3HT:PCBM weight ratio was 1:2.

For the P3HT:PCBM mixture in **Figure 5.5**, two peaks are distinguished in the absorption spectrum of the nontreated film. The peak around 335 nm stems from PCBM, while the peak at 440 nm represents the contribution of P3HT. Upon annealing, the PCBM peak remains unchanged, whereas in the region of P3HT absorption, a pronounced red shift becomes evident (the peak at 440nm in the case of the nontreated cell shifts to 507nm after 1 hour of thermal annealing).The absorption band edge is even larger, it exceeds 100nm. The apparent modification of the P3HT:PCBM absorption spectrum can be attributed to the particular thermochromic properties of P3HT and to the molecular diffusion of PCBM in the polymer matrix [87].This issue will be addressed later on. After one hour of thermal annealing, the overall spectrum of the P3HT:PCBM film looks different compared to the untreated case, i.e, the region around the absorption peak of PCBM extends towards longer wavelengths, and also the height of the peak increases. The absorption shoulder around 620nm supposed to result from interchain interactions becomes higher and more pronounced [74].

5.3 Test on the persistence of improved electrical performance of P3HT:PCBM based solar cells upon thermal annealing

While comparing the performance of thermally treated organic solar cells, attention should be paid on conditions under which the annealing experiment was performed. Different annealing times and temperatures, together with the heating and cooling rates determine in different ways the morphological modification of the organic active layer, with important consequences upon the electrical performances of organic photovoltaic devices.

For example, by cooling a polymer from a temperature higher than its melting point, T_m towards its glass transition temperature, T_g (defined as temperature below which the amorphous/crystalline structure of the polymer is completely frozen), the transition from liquid to solid state might take place in different ways depending on the cooling rate. If the cooling rate is low, this process takes place slowly, so nucleation centers have time to be formed, followed at the end by large crystals. Contrary, if the cooling rate is high, the liquid phase persists till at once it transforms in the solid state around the glass transition temperature. In this case no crystals are formed. This process is illustrated in **Figure 5.6** [88].

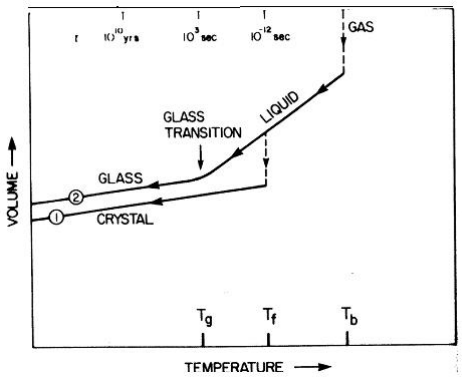

FIGURE 5.6: Dependence of the free volume on temperature. By decreasing the temperature, the polymer undergoes a transition from the liquid to the solid phase. The corresponding temperature is the glass transition temperature. (Reprinted from the reference [88])

How long and at which temperature the thermal annealing is performed, these are very important parameters. The improvement of the electrical performances of P3HT based solar cells upon annealing occurs over a large range of temperatures, starting from T_a = 50°C till higher temperatures closer to the melting point.

5.3.1 Experimental

The following experiments have as main aim to test the thermal annealing procedure on P3HT:PCBM based solar cells at different time and temperatures of thermal annealing. The stability i.e, persistence over a long period of time of the improved parameters of the P3HT:PCBM based cells is shown in the **Figure 5.7**.

A P3HT:PCBM based solar cell was produced in a weight ratio P3HT:PCBM = 1:1, following the preparation procedure mentioned in the **appendix 2 (recipe 2)**. The cell was thermally annealed at T_a = 95°C in many steps, each step corresponding to 20 s annealing time.

The J-V curves (**Figure 5.7**) were measured after each annealing step, in order to register the modification of the main electrical parameters of the cell.

5.3.2 Results and discussion

Figure 5.7 and **table 5.1** show the influence of thermal annealing upon the electrical characteristics of P3HT:PCBM based solar cells.The main striking effect which can be noticed at once, is the strong improvement of the initial nontreated J-V shape of the curve upon thermal annealing. After thermal treatment, the overall trend of the J-V curve approached the ideal Shockley diode characteristics. The short circuit current density increased after every annealing step, correlated with the increase of the fill factor. At the same time, the series resistance decreases considerably (for dark and illuminated curves), while a definite increase of the parallel resistance can be noticed just in the case of the dark curves. For the illuminated curves, the parallel resistance increased at the last annealing step. In the most experimental curves obtained so far for the annealed solar cells, it can be noticed a compromise between the improvement of the short circuit current and the increase of the shunt resistance, i.e, an increase in the J_{sc} is in the most cases obtained on cost of a smaller R_p indicating the presence of shunts.

Figure 5.8, shows the variation of the main parameters with annealing time. While V_{oc} presents a very small increase, remaining almost constant during the annealing procedure, the other parameters J_{sc}, fill factor and η are sensitive to thermal treatment, demonstrating a strong increase compared to the reference values of a nontreated cell.

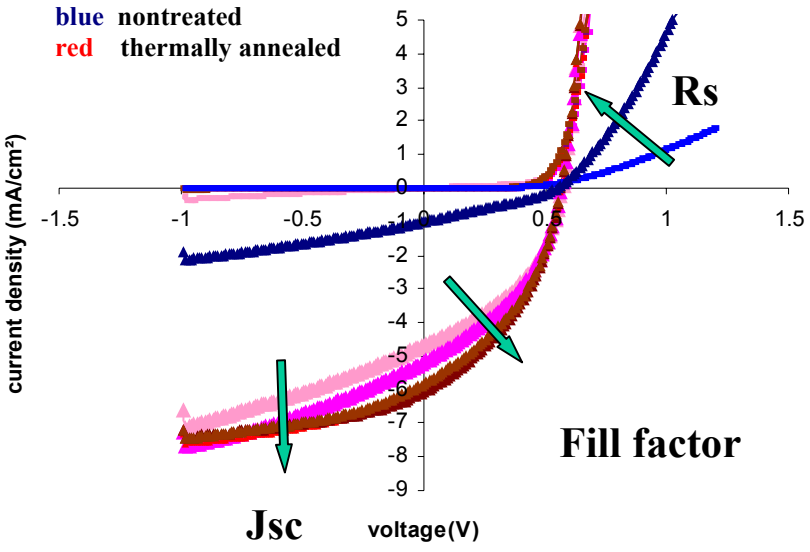

FIGURE 5.7 Detailed view of J-V dark and illuminated curves of P3HT:PCBM based solar cell nontreated (blue curves) and after every annealing step (20s at 95°C) (red curves). The cell was fabricated at a P3HT:PCBM weight ratio =1:1

Table 5.1 Electrical parameters of P3HT:PCBM based solar cells before and after succesive steps of thermal annealing (dark and under illumination 100mW/cm²)

measured at: 290°C	100mW/cm²						dark	
	J_{sc} (mA/cm²)	U_{oc}(V)	FF(%)	η (%)	R_s (ohm*cm²)	R_p (ohm*cm²)	R_s (ohm*cm²)	R_p (ohm*cm²)
Nontreated	1.02	0.551	29.57	0.17	55.35	523.60	296.30	43703.70
20s 95°C	4.68	0.573	41.97	1.13	3.03	311.25	3.67	4033.03
20s 95°C	5.20	0.573	39.88	1.19	3.67	263.00	4.89	54995.11
20s 95°C	5.89	0.573	40.26	1.36	3.67	221.97	8.00	79992.00
20s 95°C	6.09	0.573	39.91	1.39	3.83	221.81	4.40	175995.60
20s 95°C	5.83	0.562	40.71	1.33	4.19	321.74	4.89	28382.21

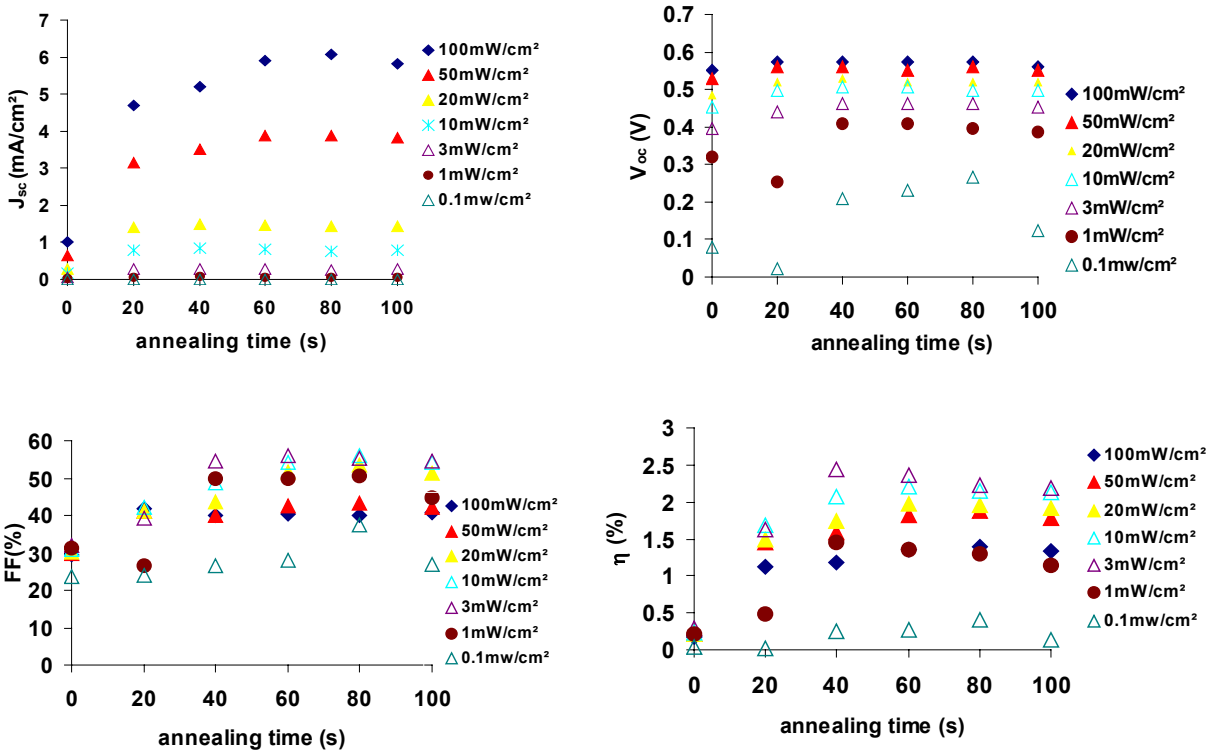

FIGURE 5.8: Dependence of the main parameters: short circuit current density (J_{sc}), open circuit voltage (V_{oc}) , fill factor FF(%) and η (%) on the annealing time

Other annealing experiments confirmed similar conclusions. P3HT:PCBM based solar cells annealed every 2 min., and whose main parameters (J_{sc} and V_{oc}) were monitored after each annealing step over a time interval longer than 2 hours, have shown the persistence of the improved electrical parameters.

Figure 5.9 shows J_{sc} and V_{oc} normalized to the corresponding values of the reference nontreated P3HT:PCBM based solar cell. What can be noticed is that at lower annealing

temperatures (in this case T_a= 85°C and 115°C), immediately after 2 min of thermal treatment, the short circuit current density, J_{sc} increased almost 3 times compared to its reference value before treatment. In the last case, i.e. for (T_a= 140°C), the same effect exists but is weaker.
This is an indication of the morphology improvement of the organic bulk heterojunction material, having as main result a better transport of the charge carriers. At the same time, the open circuit voltage (V_{oc}) decreases in the first 2 cases (T_a= 85°C and 115°C) while at T_a =140°C, an opposite behaviour is noticed.

The conclusion of this experiment is that the main effect of the thermal annealing happens in a short time interval (< 2min tested), and, this positive effect persists over a long period of time.

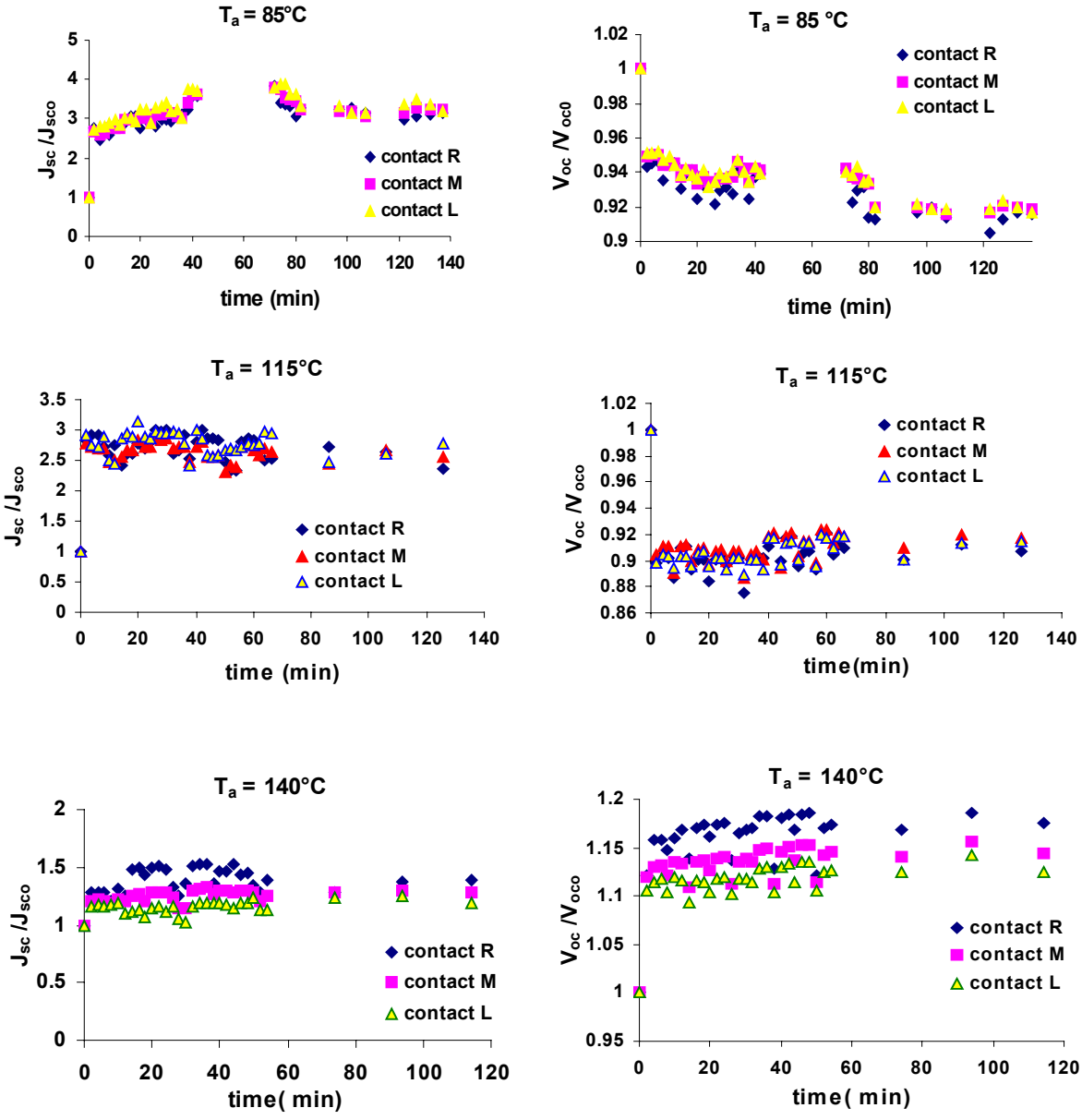

FIGURE 5.9: Dependence of the normalised short circuit current density and normalised open circuit voltage with annealing time for P3HT:PCBM based solar cells annealed at 85°C, 115°C and 140°C. (J_{sc0}, V_{oco} reference values before annealing, J_{sc}, V_{oc} values after annealing)

5.4 Morphology measurements

This experiment was intended to be a preliminary test on the morphological modifications of the P3HT:PCBM organic absorber, induced by the thermal annealing. The main conclusions from this experiment support the results of the **paragraph 5.6.**

5.4.1 Experimental

Two recipes were used for the preparation of P3HT:PCBM based solar cells. The details of the preparations are indicated in the **appendix 2**. In the **recipe 1** of this appendix, the solvent was a mixture chloroform/toluene, while in the second case, pure chloroform was used as a solvent **(recipe 2)**. Chloroform has a fast evaporation rate which almost does not allow the self organisation of the polymer chains in the thin film during spin coating procedure. The result was a non homogeneous surface of the thin absorber film, and sometimes, after spin coating, the whole surface of the ITO substrate was not covered by the organic film. This problem was overcome by a trick in the spin coating procedure. The organic solution is released from the pipette after the spin coater has already started. This procedure determines a uniform spreading of the chloroform based solution on the ITO substrate.

The second case was to use a mixture chloroform/toluene based solution. Toluene swells the polymer without dissolving it, while chloroform dissolves the polymer. By varying the ratio between these 2 solvents one can control the ratio between PCBM diffusion through the swollen matrix and the mutual dissolution of polymer and PCBM [90]. The mixture toluene/chloroform was used also in polythiophene:PCBM based solar cells by other groups [91]. In both cases, the use of waterfree solvents avoids the absorption of the O_2 and the degradation of the active layer.

Related to the solubility of PCBM in different solvents, reports [92] from the literature indicate a better solubility of PCBM in chlorobenzene and chloroform than in toluene. In the last case large PCBM clusters are formed [93]. This previous experience with PCBM obtained by other research groups, was the main incentive for morphological investigations in the present case of P3HT:PCBM blend used as organic absorber for solar cells.

5.4.2 Results and discussion: Atomic Force Microscopy, (AFM)

Thin films of pure organic compounds (P3HT, PCBM), and of the P3HT:PCBM blend, prepared following the two above mentioned recipes based on toluene/chloroform and chloroform respectively, were investigated at the AFM microscope, under different conditions (nontreated and thermal annealed films). The thermal annealing was realized by heating the substrate at T_a = 130°C (maximum heating time was 1 hour). The following conclusions are derived from these experiments:

- **pure P3HT**:

For P3HT thin films in both cases, prepared from pure chloroform (**Figure 5.10 b), d)**) or chloroform/toluene solution (**Figure 5.10 a), c**)), the AFM images are similar, showing a surface quite uniformly spread on the substrate with small aggregates, due probably to a not complete dissolution of the polymer. Even after 1 hour of thermal annealing, the general aspect of the

surface does not change. P3HT is known as a semicrystalline polymer [82]. Basically, the crystal of P3HT is formed by aligned chains which are stacked on top of each other, with the thiophene rings forming a planar alternating up-down conformation, and the alkyl side chains pointing perpendicularly to the stacking direction. The fact that no additional crystallization effect was noticed after thermal annealing in the P3HT film, can be attributed to the fact that probably, the crystals are small to be perceived even at higher resolutions and, on the other hand the amorphous part might dominate.

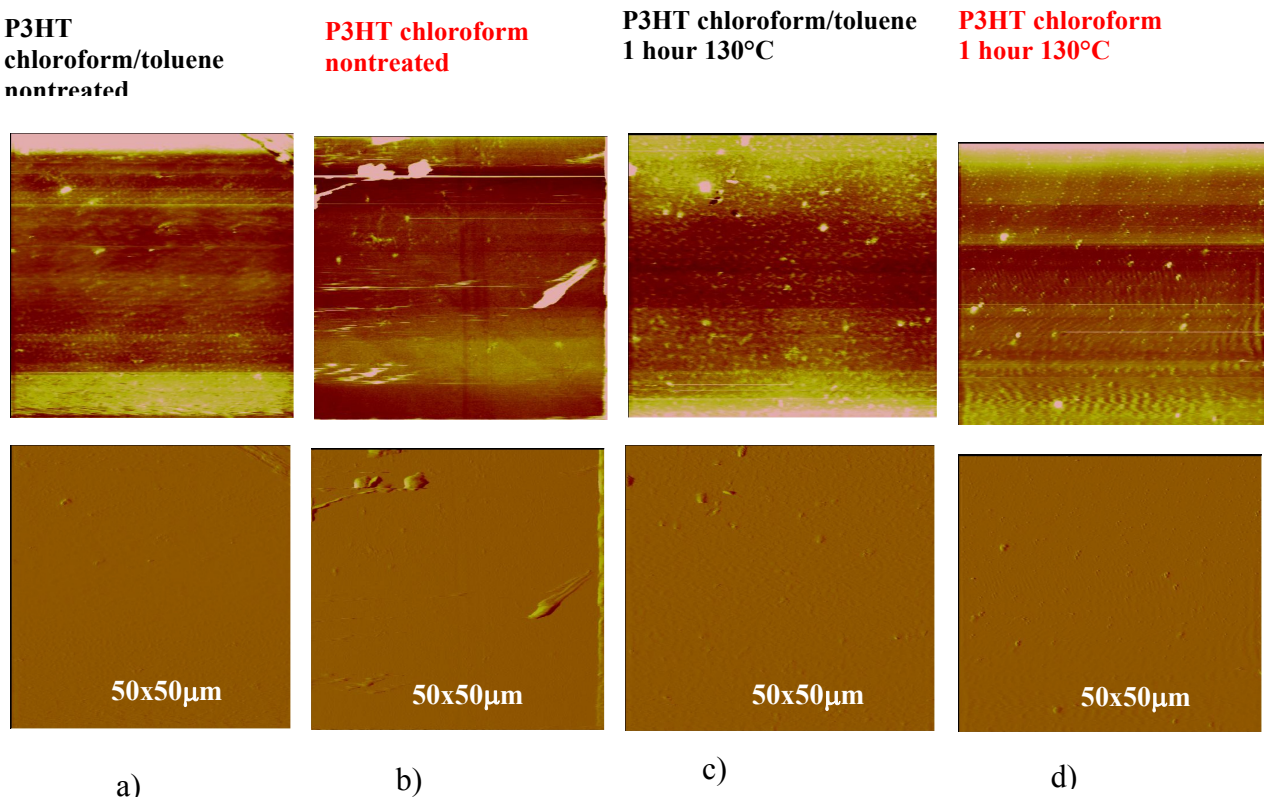

FIGURE 5.10: AFM images in tapping mode, topography (top) and phase (bottom) of the P3HT absorber surface prepared from 2 different solutions (chloroform pure and chloroform/toluene) in 2 different cases (nontreated and thermal annealed 1hour at $T_a = 130°C$)

- **Pure PCBM**

Thin PCBM films show different aspects of the surface, depending on the solvent used. In the case of using chloroform (**Figure 5.11 d), e)**), the PCBM surface is homogeneous but, after one hour of thermal annealing, it shows a trend to crystallisation. A large difference can be reported in the case of using chloroform/toluene as a solvent (**Figure 5.11 a), b), c**)). The nontreated PCBM film indicates a phase separation which becomes more pronounced after thermal treatment. Comparing the images corresponding for the two cases of using as solvent chloroform and chloroform/toluene mixture respectively, it can be clearly noticed, that by increasing the annealing time, the PCBM clusters increased in size. After 1 hour of thermal

treatment at T_a = 130°C, the PCBM clusters reached a height of approximatively 200nm. This morphology difference induced by the solvent can be explained by the already mentioned poor solubility of PCBM in toluene.

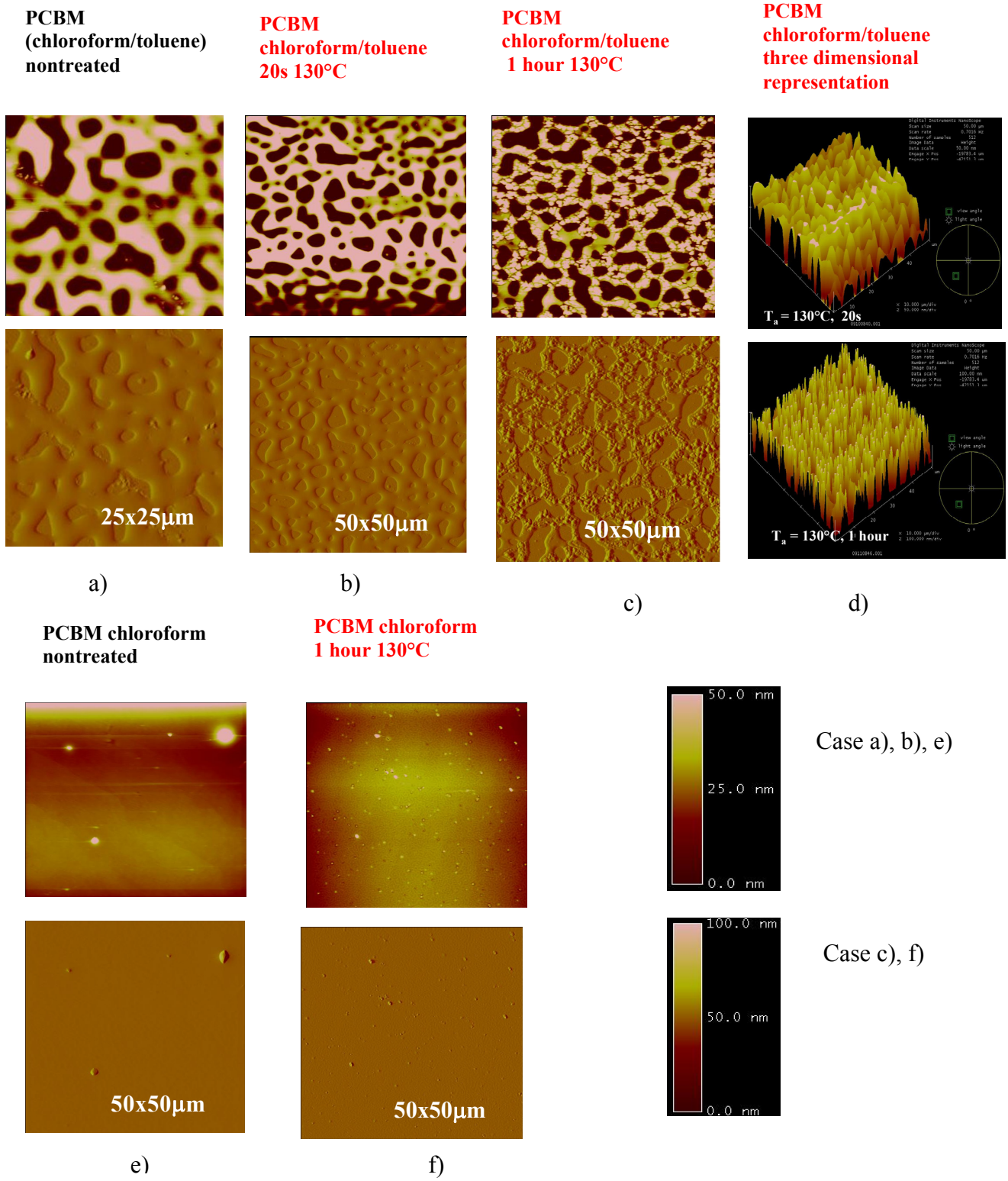

FIGURE 5.11: AFM images in tapping mode, topography (top) and phase (bottom) of the PCBM absorber surface prepared from 2 different solution (chloroform pure and chloroform/toluene) nontreated and thermal annealed

- **P3HT:PCBM**

The main effect of thermal annealing is the morphological modification of the organic layer. Generally, the phase separation within the blend starts already in the solution, but is interrupted for the moment by the film formation during the spin coating process. The spin coated film represents a frozen-in picture. The thermal annealing procedure allows for further modifications of the morphology of PCBM:P3HT blends, as the thermodynamically driven phase separation goes on. The above process consists of two steps: (a) Heating is done at a certain annealing temperature, above the glass transition temperature (T_g), of the polymer (information about T_g for P3HT is indicated in **appendix 2**). During this step, the organic compounds (in our case fullerene) may diffuse in the polymer matrix, aided by the increasing of the free volume of the latter and, hence, by the decreasing of its molar specific density; This results in closer contact and possibly more favorable electrical interaction between the corresponding segments and domains of these molecules (b) By cooling down to the initial temperature, the free volume decreases (i.e., the specific molar density increases), finally freezing in the morphology again below the effective T_g of the mixture. Depending on the duration and the concentration, PCBM crystallises in distinct geometrical and peculiar shapes, with structures of greater than 500 nm observed.

In the case of the P3HT:PCBM blend, the first difference between films prepared following the 2 recipes occurred even in the nontreated case. The relatively uniform surface in the case of using pure chloroform as a solvent, is different from the general aspect of the surface in the case of chloroform/toluene solution, where the density of aggregates is quite high and can be easily noticed. After 20s thermal treatment at T_a = 130°C, in both cases, the first distinct crystals occurred, followed by the increasing in size and density over the whole surface after 1 hour of annealing (**Figure 5.12**). The presence of the PCBM crystals and their large size of 500nm were confirmed also by the Scanning Electron Microscope (SEM) images presented in **Figure 5.13.**

It should be emphasised that the above thermally induced diffusion does not involve a chemical reaction between P3HT and PCBM. The relevant effect one can assume is the formation of the structurally better ordered P3HT phase with the stronger interchain interaction [74]. If the particular case of a P3HT:PCBM blend prepared from pure chloroform solution is analysed, evidence for this effect can be derived from the shape of the absorption spectrum (**Figure 5.5**). There, we reveal a clear and distinct red shift in the spectrum of the annealed mixture relative to the spectra of the starting pure components (see for P3HT **Figure 5.3a** and for PCBM **Figure 5.4b**). Of particular note remains the significant increase in the wavelength region, controlled by the absorption peak of P3HT following the course of annealing relative to the untreated case. Such effect might be due to a modification of the ordering within the polythiophene phase. Before annealing, the polythiophene is present in a less planar, so called, "yellow phase" caused by a large amount of the "hindering" fullerene in the blend, with the absorption maximum around 450 nm. (Note, the PCBM absorption contributes to the overall absorption in this range, too (**Figure 5.4b**), however, its contribution is much smaller.) During annealing, the more planar backbone structure of the P3HT is formed ("red phase") in course of the molecular diffusion of PCBM. In case of pure P3HT (**Figure 5.3a**), the red phase with its characteristic absorption with maximum at 560 nm and partially resolved vibronic structure is formed already during spin coating procedure.

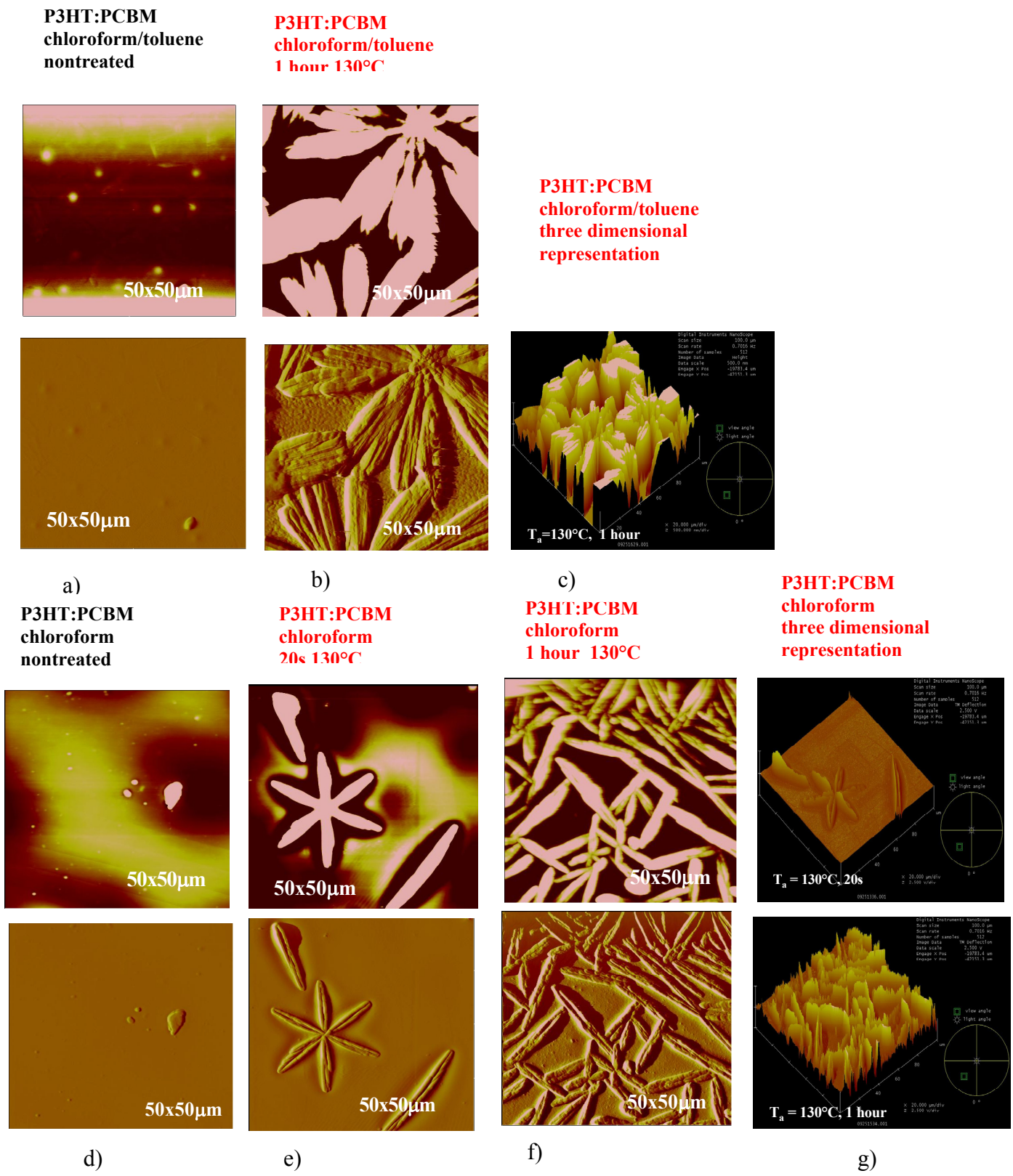

FIGURE 5.12: AFM images in tapping mode topography (top) and phase (bottom) of the P3HT:PCBM absorber surface prepared from 2 different solution (chloroform pure and chloroform/toluene) nontreated and thermal annealed

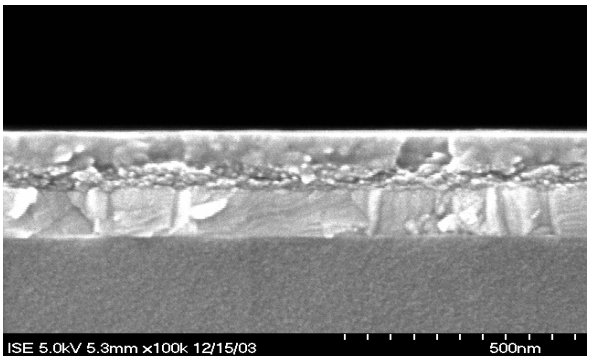

a)

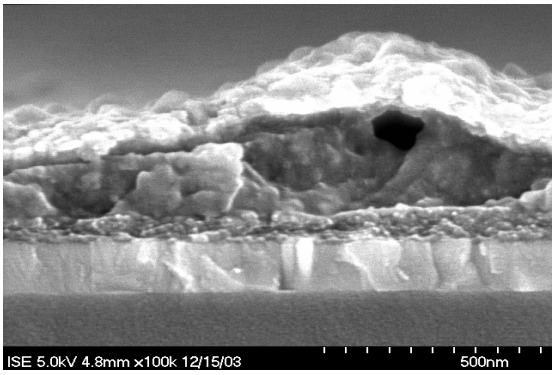

b)

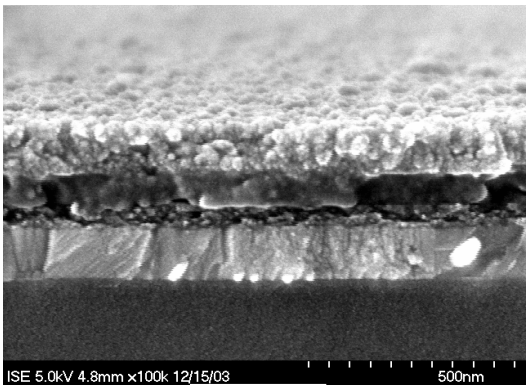

c)

FIGURE 5.13: Scanning Electron Microscope images of P3HT:PCBM organic films show the building of huge clusters (>500nm) after thermal annealing (case b, c) attributed to PCBM crystallisation compared to the untreated case a)

5.5 Optimization of the amount of the PCBM acceptor in the P3HT:PCBM based solar cells

Different opinions in literature have been expressed concerning the optimum portion of the acceptor in the blend heterojunction mixture.

For PPV:PCBM based devices, the most efficient cell was fabricated by using a weight ratio MDMO-PPV:PCBM=1:4, i.e., with 80% PCBM [81]. van Duren et al. demonstrated that phase separation in MDMO-PPV:PCBM sets in at 50% PCBM, leading to an improved electron transport, reduced recombination and, hence, to optimal performance at 80% PCBM. Above 50% PCBM, the domains of rather pure PCBM are formed in a matrix of the non-phase-separated blend [94]. No annealing was applied to blends discussed above. In the case of polythiophene-fullerene based solar cells the optimum ratio of donor and acceptor is unclear. Dittmer et al. [78], working on P3HT:perylene dye blend based solar cells, pointed out that perylene crystal domains are formed and become larger with increasing dye concentration. The thermal annealing of blends leads to a further increase of crystalline perylene domains in size, positively influencing the solar cell performance. At 80% of perylene dye in the blend, a maximal external quantum efficiency was obtained. Whereas the small perylene domains act as electron trap centres, direct electron transport paths are formed upon increasing the crystal size, hence, the photocurrent becomes larger.The simple conclusion is that large crystals give rise to better transport properties.

From these experimental findings the following conclusion comes out: The control over the phase separation is not only governed by the acceptor concentration itself, but is strongly influenced by the thermal annealing too.

5.5.1 Experimental

The present experiment had as main aim the optimization of the PCBM acceptor in the blend and elucidation of its role played in the morphology and electrical performances of annealed P3HT:PCBM based solar cells.

P3HT was used in the preparation of organic solar cells as a donor, combined with the PCBM as acceptor, in P3HT:PCBM weight ratios of 1:0.7, 1:0.8, 1:0.9, 1:1, 1:1.5, 1:2, 1:3. The details of the preparation procedure are indicated in the **appendix 2, recipe 2**. The solar cells were annealed at T_a = 130°C for 20s.

5.5.2 Results and discussion

- **External quantum efficiency of photogenerated charge carriers, (EQE)**

Figure 5.14 compares EQE spectra of ITO/PEDOT:PSS/P3HT:PCBM solar cells with different P3HT:PCBM weight ratios of 1:1, 1:1.5, 1:2, 1:3, being thermally treated at T_a = 130°C for a period of 20s. The corresponding values of the short circuit current density measured directly and estimated from the EQE curves for the same devices are summarised in **Table 5.2** together with peak values of EQE. In contrast to the results gained for PPV:PCBM based solar cells, where a higher amount of PCBM improves the performance of the device [22], the best performance is obtained in this case for much lower concentration of the fullerene acceptor.

Interestingly, the same tendency in the weight ratio dependence of the EQE spectra of treated and untreated P3HT:PCBM cells is observed (not shown). So far, the following conclusion that is relevant for the effect of thermal annealing can be drawn: in all cases, the EQE strongly increases after thermal annealing, the most pronounced enhancement being achieved for the cell with the P3HT:PCBM weight ratio of 1:1.

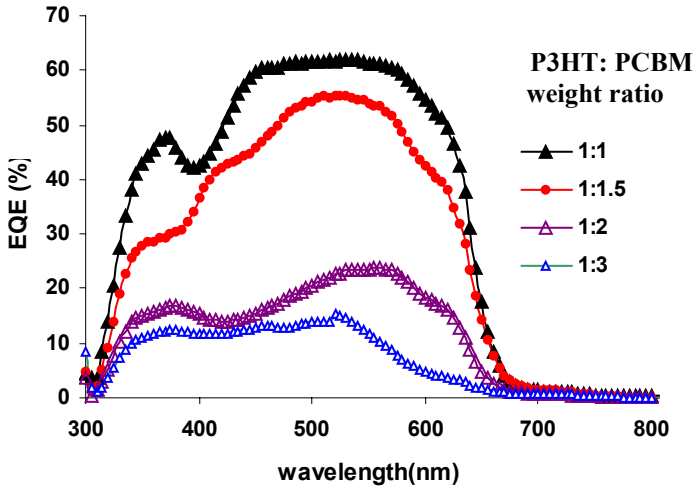

FIGURE 5.14: EQE measurements for P3HT:PCBM based solar cells with different weight ratios of P3HT:PCBM (1:1, 1:1.5, 1:2, 1:3), thermally annealed 20s at T_a = 130°C

Table 5.2 Peak values of external quantum efficiency and short circuit current density both estimated from EQE and measured on P3HT:PCBM based solar cells fabricated with different P3HT:PCBM weight ratios.

P3HT:PCBM weight ratio	max EQE (%)	J_{sc}(mA/cm²) estimated from EQE data	J_{sc}(mA/cm²) measured
1:1	61.7	8.93	7.8
1:1.5	55.48	7.39	5.51
1:2	26.63	2.1	2.99
1:3	14.94	1.42	1.64

- **Absorption spectra**

An interesting effect was observed from the absorption spectra of thermally annealed solar cells fabricated with different P3HT:PCBM weight ratios and illustrated in the **Figure 5.15**. By increasing the amount of PCBM in the blend, the absorption peak in the region around 500 nm of the curve corresponding to P3HT:PCBM weight ratio of 1:1 taken as reference, occurs blue shifted and larger.

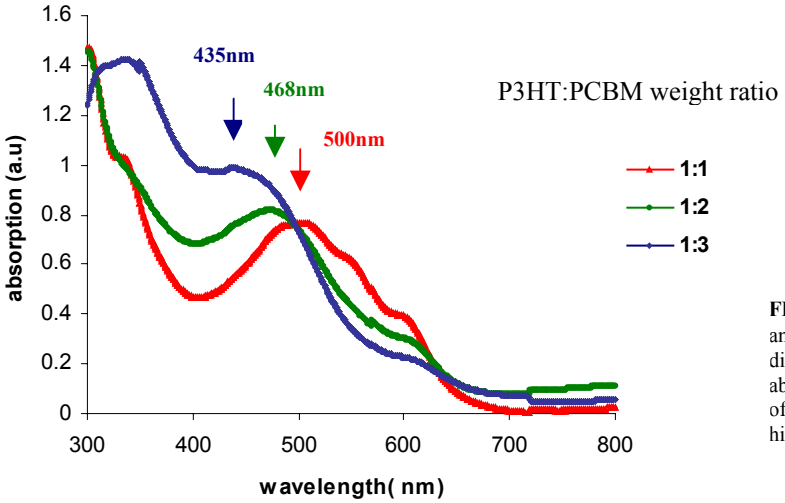

FIGURE 5.15: Absorption spectra of thermally annealed P3HT:PCBM based solar cells with different P3HT:PCBM weight ratios. The absorption peak in the maximum absorption region of P3HT (around 500nm) shows a blue shift at higher PCBM amount in the blend.

- **Atomic force microscopy, (AFM) results**

AFM measurements were performed, in order to understand the morphological differences that were introduced by varying the amount of PCBM in the blend upon annealing. **Figure 5.16** shows the images (phase) taken on the absorber (c), (d) and metallic electrode (a), (b) surfaces of real devices fabricated with the P3HT:PCBM weight ratio of 1:1 and 1:3, respectively. Based on these AFM images, the following conclusions can be summarized: Due to thermal annealing, PCBM crystallises via forming relatively large clusters in the P3HT:PCBM mixture. When comparing the organic absorber surface of the solar cells with the P3HT:PCBM weight ratio of 1:3, 1:2, 1:1.5, and 1:1, both density and size of the crystal grains are larger for the cells with higher PCBM amount (1:3,1:2), whereas they strongly decrease in the other two cases. Towards the P3HT:PCBM weight ratio of 1:1, the pattern of the PCBM crystals changes from a star aspect to isolated small clusters.

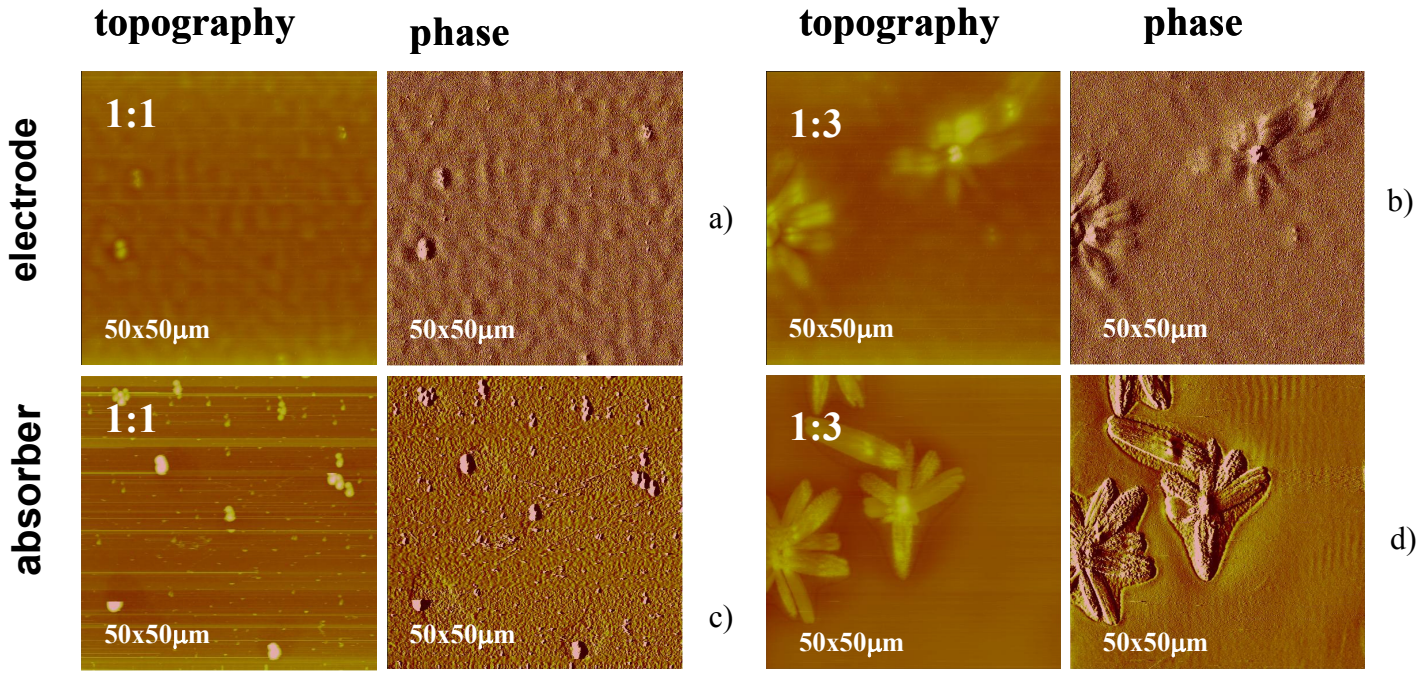

FIGURE 5.16. AFM images in tapping mode (phase) of the P3HT:PCBM absorber surface (c) and (d) as well as of the aluminium electrode (a) and (b) for P3HT:PCBM weight ratio of 1:1 and 1:3, respectively. Scan area 50×50 µm.

AFM images taken on the aluminium contact surface of the cell in **Figure 5.16** (a), (b) show that PCBM clusters, grown on the polymer surface, are not suppressed by the coating metal layer. Furthermore, the metal electrodes obey a wavy structure. The latter is spontaneously formed due to the difference in the thermal expansion coefficients of the organic and the metal layer attached to each other. A similar wavy aspect of the aluminium electrode was recognised in case of annealed polyfluorene light emitting diodes, however, the annealing was done before evaporating the aluminium electrodes, and on heat-treated metal-polymer bilayers. [95]

The spatial distribution of the surface thickness of the PCBM:P3HT blends subject to thermal annealing is extremely inhomogeneous and was found to depend on the PCBM concentration. The overall thickness of the active organic layer varies from less than 100 nm in the amorphous regions to up to 500 nm in the areas where the PCBM clusters are formed. The formation of a cluster in the device areas under the metal electrodes introduces significant mechanical stress on the latter. **Figure 5.17** represents a photograph of three analysed P3HT:PCBM based devices with a P3HT:PCBM weight ratio of 1:1 (case a), 1:2 (case b) and 1:3 (case c), respectively, taken with a digital camera. Therefrom, it is interesting to note that cracks on the aluminium electrodes result from PCBM crystal domains grown under the metal electrode. The cracks are much larger at higher PCBM concentration. AFM images of the areas indicated as bright spots in the **Figures 5.17** (a)-(c) are given in **Figure 5.17** (d) (P3HT:PCBM weight ratio 1:1) and (e) (P3HT:PCBM = 1:3). The patterns observed are similar to those found on the absorber surface (see **Figure 5.16**).

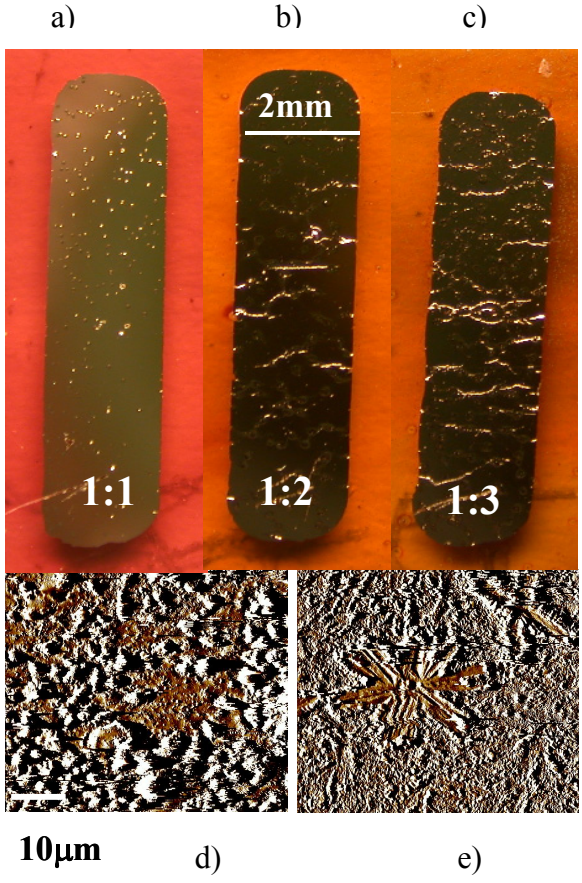

FIGURE 5.17. Photographs of annealed ITO/PEDOT:PSS/P3HT:PCBM/Al solar cells with P3HT:PCBM weight ratio of 1:1 (a), 1:2 (b) and 1:3 (c). T_a=130°C, t=20 s. AFM images (d) and (e) (tapping mode, phase) correspond to cracks on the metal electrodes (a) and (b, c).

From all these findings, the following conclusion comes out: Thermal annealing of blends with a high PCBM concentration has a negative effect on the device performance due to the deterioration of the metallic electrode.

- **J-V results**

In order to confirm the hypothesis of improving the energy conversion efficiency of the solar cell by optimising the amount of PCBM, a series of ITO/PEDOT:PSS/P3HT:PCBM/Al devices was produced with the following P3HT:PCBM weight ratio: 1:0.7, 1:0.8, 1:0.9, 1:1, 1:1.5, 1:2, 1:3. The current density - voltage measurements shown in **Figure 5.18** were performed in the dark and under white light illumination (100mW/cm²) at T=295 K. It becomes obvious that the diode characteristics improve, as the PCBM concentration decreases. The main electrical parameters of the devices in each category are summarised in **Table 5.3**. The functional dependence of the main device parameters, i.e., their mean values together with the standard deviations for the 43 devices investigated, upon variation of the P3HT:PCBM weight ratio is summarised in **Figure 5.19** and **table A1 (appendix 1)**. Obviously, the reduction of the amount of PCBM in the organic mixture has a positive effect on the short circuit current density, and, therefore, the overall power conversion efficiency of the solar cell. No influence on the open circuit voltage was observed. A maximum fill factor of 63% is measured on the device with a P3HT:PCBM weight ratio of 1:1. At a P3HT:PCBM weight ratio below 1:0.9 a gradual decrease of J_{sc} is seen. The conclusion is that the device performance is sensitive against the amount of PCBM with a maximum in the range of the P3HT:PCBM weight ratio between 1:0.9 -1:1. The poor performance of the devices at the P3HT:PCBM weight ratio of 1:2 and 1:3, may be attributed to the formation of PCBM clusters.

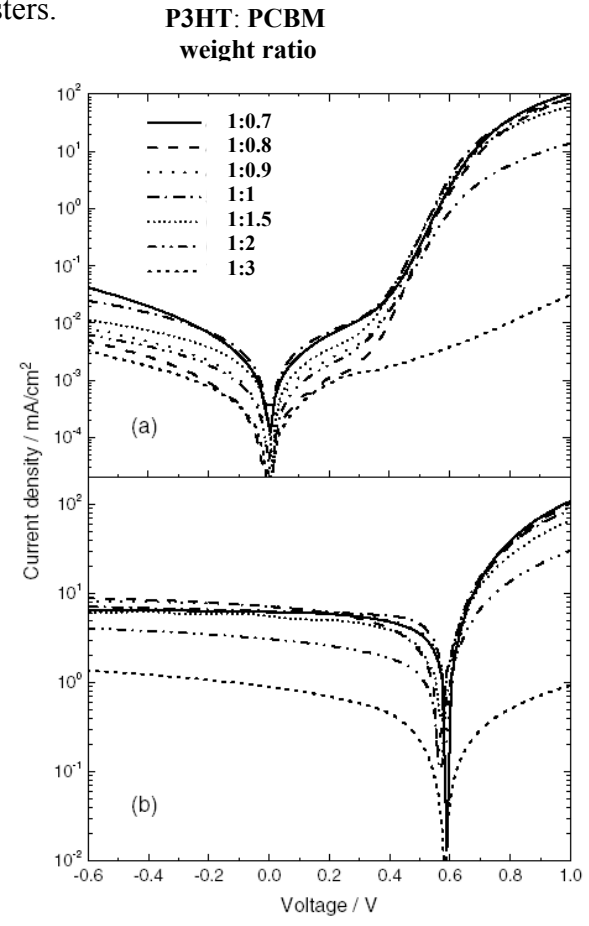

FIGURE 5.18: Current density versus voltage characteristics of annealed ITO/PEDOT:PSS/P3HT:PCBM/Al solar cells in the dark a) and under white light illumination (100mW/cm²) b) for different P3HT:PCBM weight ratios as indicated in the legend. (T=295K)

Table 5.3 Electrical device parameters: short circuit current density, J_{sc}; open circuit voltage,V_{oc} ; fill factor, FF; power conversion efficiency, η ; series resistance, R_S; parallel resistance, R_P (for dark and illuminated devices)[5], as functions of the PCBM concentration. (Data correspond to the Figure 5.18)

	100mW/cm²						dark	
P3HT:PCBM weight ratio	J_{sc}, mA/cm²	V_{oc}, V	FF, %	η, %	R_S, Ohm*cm²	R_P, Ohm*cm²	R_S, Ohm*cm²	R_P Ohm*cm²
1:3	0.9	0.58	35	0.18	423	566	3099	290235
1:1.5	3.08	0.57	43	0.75	9.8	593	22	97756
1:2	5.51	0.576	54.87	1.74	2.66	215.51	2.91	239997
1:1	6.35	0.60	63.2	2.39	3.4	514	3.5	29330
1:0.9	7.23	0.60	45.9	2.01	1.8	298	1.9	93748
1:0.8	7.17	0.58	39.8	1.64	1.6	219	1.6	374998
1:0.7	6.21	0.60	53	1.94	1.9	680	1.8	39472

Figure A1 (Appendix 1) presents the dependence with temperature of the main parameters J_{sc}, V_{oc}, FF and η for the best P3HT:PCBM based solar cell obtained with a P3HT:PCBM weight ratio of 1:1 and indicated with red in the **table A1 (Appendix 1)**. (J_{sc}= 6.35mA/cm², V_{oc}= 0.595V, FF = 63.18%, η = 2.39% at room temperature and 100mW/cm²). In the case of the short circuit current density, J_{sc}, the curve shows at temperatures higher than 250K a saturation trend. Open circuit voltage, V_{oc} reaches a quite high value, 0.8V at 150K. This is an indication of the posibility of even higher voltages at temperatures lower than 150K. The most interesting result is related to the dependence of the fill factor and efficiency with light intensity. A strong increase in both values at high temperatures is expected and corresponds to the experimental results. The maximum in this case at room temperatures occurs at 50mW/cm² and not at 3mW/cm², as it was so far obtained. This result is an indication of an improvement in the transport properties of the organic bulk, as a result of the optimization of the PCBM amount in the solar cell.

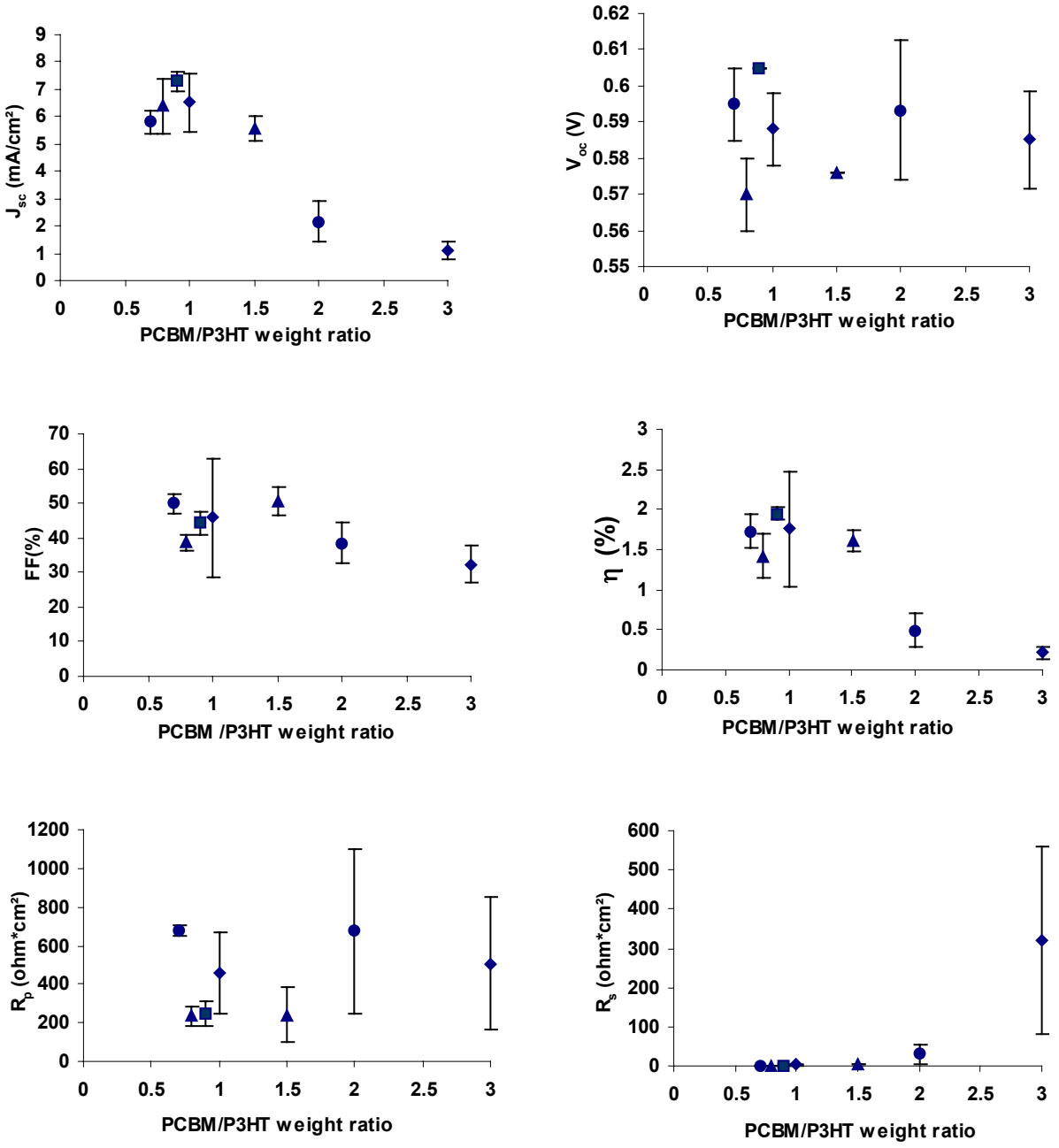

FIGURE 5.19 Short circuit current density (J_{sc}), open circuit voltage (V_{oc}), fill factor (FF), and power conversion efficiency (η) as function of PCBM/P3HT weight ratio.

The following general physical picture can be drawn. Light absorption by P3HT:PCBM composites followed by charge transfer, delocalisation and transport of charge carriers within the bulk heterojunction are sensitive to the amount and size of PCBM clusters. Too low PCBM concentration (below P3HT:PCBM weight ratio 1:0.9) does not enable the required formation of the percolated electron transport paths. In contrast, too high PCBM amount in the blend (above P3HT:PCBM weight ratio = 1:1.5) leads to a partial damage of the absorber-metal interface due

to the formation of voluminous PCBM clusters. The driving force and the physical mechanism behind the PCBM cluster growth are thermal annealing and molecular diffusion, respectively. The optimum amount of PCBM in the blend is found in the range of P3HT:PCBM weight ratio of 1:0.9-1:1. The fullerene surplus at higher concentrations is no longer homogeneously dispersed within the polymer matrix, but diffuses away and creates phase separated clusters. In this way recombination processes in P3HT are enhanced. Apart from the PCBM concentration in the blend, two essential parameters, namely, the annealing temperature and duration, are important. The conclusions of the present work are valid for the particular annealing and preparation conditions used.

Chapter 6

Aspects related to the quality and stability of organic materials

Organic materials used for photovoltaic devices suffer from an inability to remain electrically, chemically or structurally stable for a long period of time. Some systems may degrade within hours or days due to chemical or structural changes. The structure of the organic material itself consists sometimes of pinholes which create an easy way for the diffusion of metallic atoms into the organic bulk, leading to shorts. The repeated passage of the current under high field conditions can cause electrical burning of these shorts.

If an organic material is susceptible to oxidation or reduction under atmospheric conditions, special precautions must be taken to protect the device (for example by encapsulation, working under N_2 atmosphere etc). Potential dopants (oxygen, water, charge transfer agents) need to be considered either detrimental or beneficial.

Another aspect is related to the quality of the organic material, due to the specific conditions under which the synthesis was performed.

These issues will be addressed in this chapter with exemplification of problems occurred in the case of P3HT:PCBM based solar cells.

6.1. Quality of organic material used in the fabrication of photovoltaic devices

Since their first synthesis in 1986 [97], polyalkylthiophene has attracted increased interest, due to the significant improvement in the solubility resulting from the grafting of the flexible hyxdrocarbon chains on the polythiophene backbone.

The fist way [98] of polymerization of 3-alkylthiophene was performed by using as oxidant $FeCl_3$. However this method led to an organic product containing a significant amount of regiochemical defects, about 25%. Therefore, other regiospecific chemical synthetic routes were developed. These methods are: a) McCullogh route [99] and b) Rieke route [100] (**Figure 6.1** case b route B). The polymers obtained as a result of these last two synthesis methods show conductivity levels [99],[13] higher, and improvement in the regioregularity compared to the one obtained by using $FeCl_3$ as oxidant.

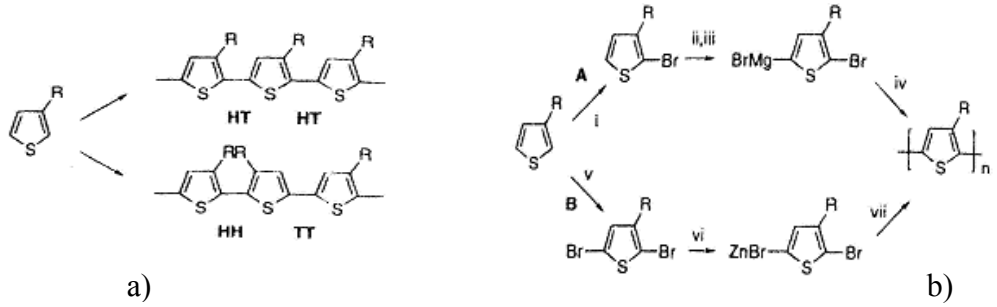

FIGURE 6.1: a) The two specific orientations of the thiophene unit in the polythiophene chain leading to ideal regioregular structure head -to -tail (HT) or to regiorandom structure tail -to -tail (TT)
b)The two regiospecific chemical syntheses leading to regioregular structures of polyalkylthiophene: route A) McCullogh B) Rieke Reprinted from the reference[101]

Generally, the quality of the organic materials is mainly influenced by the chemical synthesis method. Nevertheless, different batches of a polymer fabricated by using the same chemical synthesis method may have different degrees of purity. This is the aspect which will be schown experimentally in the following.

6.2 Experimental

The results of the present study are based on experiments performed with two batches of regioregular P3HT, synthesized after the Rieke method, but purchased from different sources: Aldrich Chemicals AG (batch 1) and Rieke Inc. (batch 2). In the fabrication of P3HT:PCBM based solar cells, PCBM was purchased always from the same source (Groningen University). P3HT:PCBM based solar cells were fabricated following the **recipe 1** from **appendix 2.**

6.3 Results and discussion

Due to the fact that the P3HT from the two batches was obtained as a result of the synthesis following the Rieke route and a high degree of regioregularity is indicated (>99%) in both cases, one should expect comparable results assuming the same recipes were used in the preparation procedure of P3HT:PCBM based solar cells. Surprisingly the experimental results are different. (**Figure 6.2**) In **table 6.1** are indicated the results obtained at room temperature (300K) in the case of P3HT:PCBM solar cells by using P3HT – batch 1 (**table 1a** for a nontreated cell) and P3HT – batch 2 (**table 1b** for a nontreated cell and **table 1c** for the cell from **table 1b** after thermal annealing).

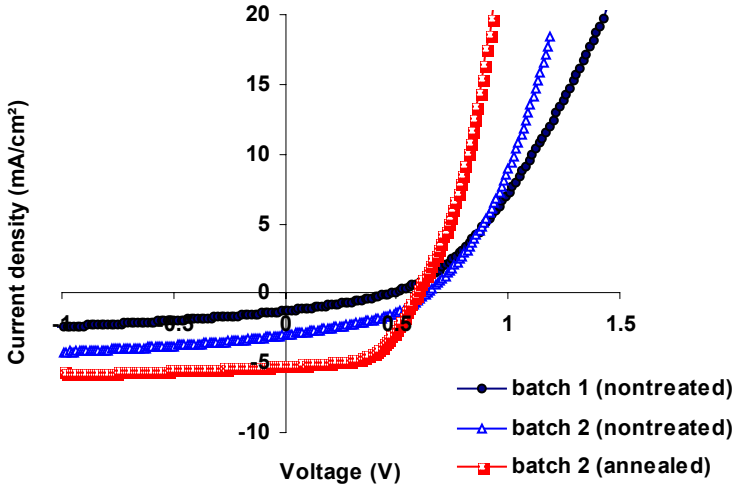

FIGURE 6.2: J-V curves of P3HT:PCBM based cells fabricated with P3HT batch1-nontreated (black curve), P3HT batch 2 –nontreated (blue curve) and P3HT (batch2) thermally annealed (red curve)

Table 6.1 Electrical parameters of P3HT:PCBM based solar cells fabricated with P3HT from two batches a) nontreated (batch 1) b) nontreated (batch 2) c) after thermal annealing (batch 2)

Table 6.1a	P3HT:PCBM nontreated	BATCH 1	ALDRICH AG	
Intensity (mW/cm²)	Jsc(mA/cm2)	Uoc(V)	FF(%)	η (%)
100	1.28	0.48	30.64	0.19
50	0.81	0.45	33.90	0.25
20	0.33	0.42	36.97	0.26
10	0.19	0.405	38.00	0.29
3	0.07	0.36	39.73	0.33
1	0.02	0.3	33.71	0.17

Table 6.1b	P3HT:PCBM nontreated	BATCH 2	RIEKE Inc	
Intensity (mW/cm²)	Jsc(mA/cm²)	Uoc(V)	FF(%)	η (%)
100	2.99	0.639	39.60	0.76
50	1.85	0.628	41.48	0.96
20	0.71	0.606	45.39	0.98
10	0.39	0.595	47.95	1.12
3	0.14	0.562	52.10	1.38
1	0.03	0.518	54.71	0.94

Table 6.1c	P3HT:PCBM annealed	BATCH 2	RIEKE Inc	
Intensity (mW/cm²)	Jsc(mA/cm²)	Uoc(V)	FF(%)	η (%)
100	5.14	0.595	54.51	1.67
50	3.01	0.573	53.52	1.85
20	1.08	0.551	59.99	1.79
10	0.58	0.529	61.65	1.90
3	0.20	0.496	62.34	2.06
1	0.05	0.441	62.08	1.23

The results from **Table 6.1a** and **Figure 6.2** black curve represent the best electrical performance of all P3HT:PCBM based solar cells fabricated with P3HT batch1 which were tested during 1 year. It can be noticed that the solar cell obtained from the P3HT- batch1 gives considerably lower results of the main parameters J_{sc}=1.28mA/cm², FF=30.64% and V_{oc}=0.48% and therefore, a lower efficiency η = 0.19% compared to those given by the solar cell fabricated from the P3HT- batch 2, J_{sc} = 2.99 mA/cm², V_{oc} = 0.639 V, FF = 39.6 %, η = 0.76 %. In the last case after anneling, a considerable increase in the current was obtained, J_{sc}=5.14mA/cm², a higher fill factor, FF = 54.51% and a higher efficiency η = 1.67% at an illumination intensity of 100mW/cm². What is interesting to note is the fact that the maximum value of efficiency is found at 3mW/cm² in all three cases due to the limitation of the bulk transport properties of charge carriers.

Large differences were obtained not in the values of the main parameters (J_{sc}, V_{oc}, FF and η), but also in the overall shape of dependence of these parameters on temperature.

From the **Figures 6.4 and 6.5**, the following conclusions can be summarized:

- Short circuit current density, J_{sc}

In all three cases an increase in the short circuit current density, J_{sc} was noticed. Nevertheless some differences in the overall shape of the curves came out from the experiment (**Figure 6.4**).

For the first P3HT:PCBM based solar cell fabricated with the P3HT - batch1 (**Figure 6.4 case a**), the short circuit current density, J_{sc} increases till it reaches a maximum around 300-320K, followed by a decrease at higher temperatures. This decrease was atributed [102] to the change in the conformation chains of P3HT which, at high temperatures, undergo a transition from a quasiplanar to a nonplanar structure, due to small twists of the monomer units. This assumption is generally valid and was reported [14] many times in the case of conjugated polymers and in the particular case of polythiophene. Nevertheless, this fact cannot explain fully why in the case of the P3HT:PCBM based solar cell fabricated with the P3HT batch 2 (**Figure 6.4 case b**), the short circuit current density increases continuously over the whole range of temperatures. A similar dependence of the short circuit current was reported [103] for OC1C10:PCBM based solar cells.

By performing thermal annealing (2 hours at T_a = 85°C), the short circuit current density, J_{sc} increased even more, and the shape indicates a saturation at high temperatures (>280K) (**Figure 6.4 case c**).

Another explanation of these differences in the dependence of the short circuit current density J_{sc} with temperature is possibly related to the quality of the organic materials from the two batches. It is reported [104], that as a result of the synthesis procedure of polythiophene, Zn and Br impurities remain in the organic material and may act as traps by catching the charge carriers.This fact leads to a lower photogenerated current. In **Figure 6.3** it is indicated the result from Rutherford backscattering spectroscopy (RBS) investigation, which shows Zn and Br impurities present within P3HT and removed afterwards by using a purification procedure.

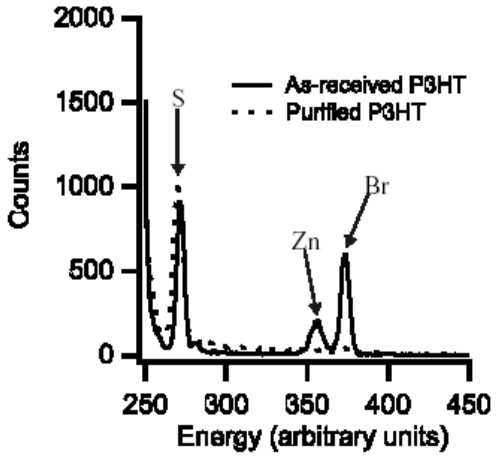

FIGURE 6.3: RBS spectra for the as received and purified P3HT. The spectra have been normalized to the height of the sulphur peak. Indicated are the impurity peaks. Based on the peak positions , these have been assigned to Zn and Br. The low energy region containing the Si and C signals is not shown. (Reprinted from the reference [104])

Another effect, a fragmentation of the polymer chain can occur during the polymerization of the polythiophene as it was mentioned before.

As a general conclusion, the purity degree of different polymer batches must be taken into account, and differences in the results reported by different groups should not be taken as absolute, but related to the specific conditions under which the experiments were performed (materials used, methods of preparation, condition of measurements etc.)

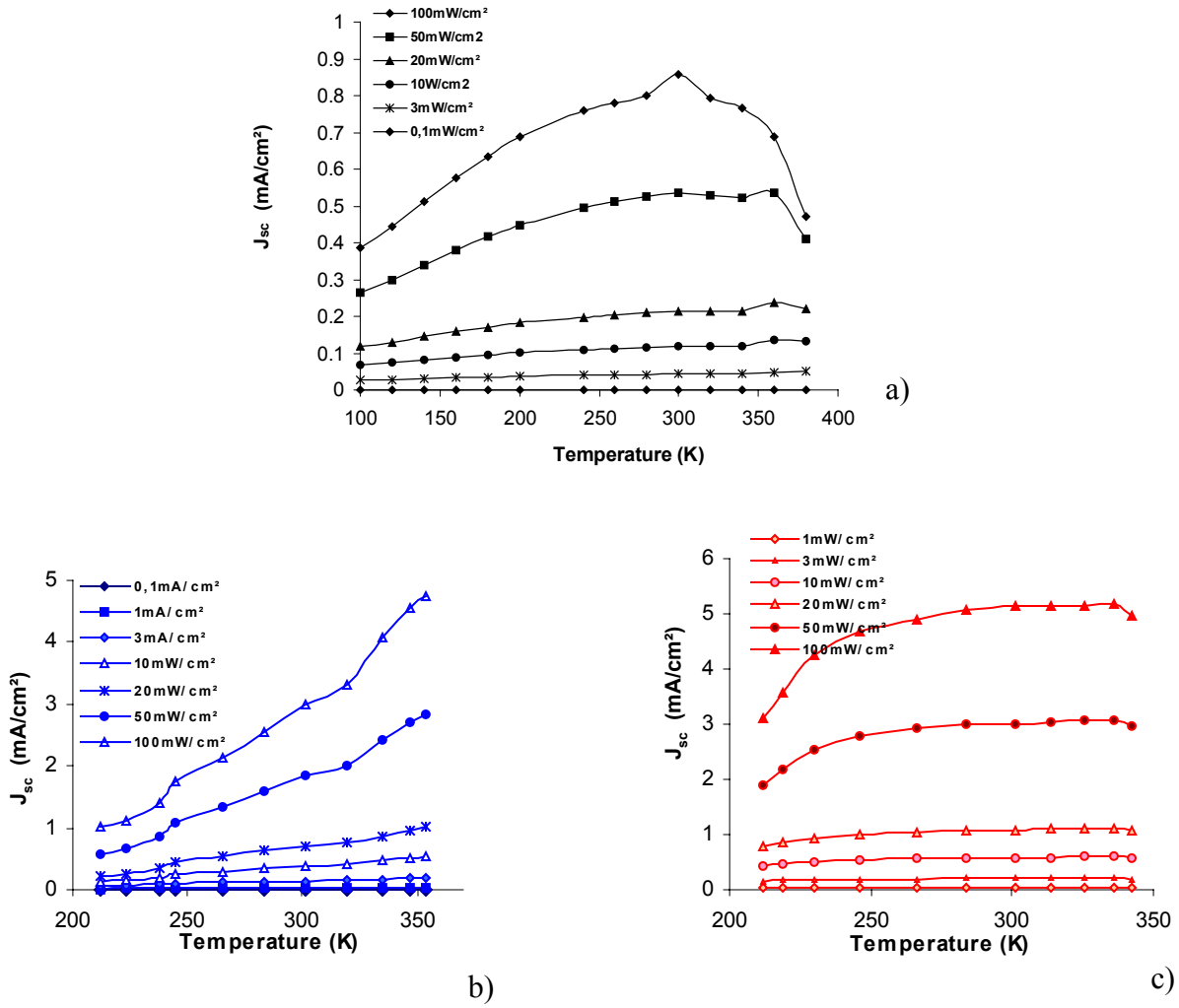

FIGURE 6.4: Dependence of the short circuit current density on temperature for P3HT:PCBM solar cells: a) batch 1 b) batch 2-nontreated c) batch 2 annealed

- Open circuit voltage, V_{oc}

In both P3HT:PCBM based solar cells fabricated with P3HT from both batches, for annealed and non annealed solar cells, the dependence of V_{oc} on temperature is similar and the V_{oc} values in all 3 cases (batch 1 nontreated, batch2 nontreated, batch2 annealed) are comparable to each other (**Figure 6.5**). This is an indication that impurities in the organic materials influence more the bulk transport properties but less V_{oc}.

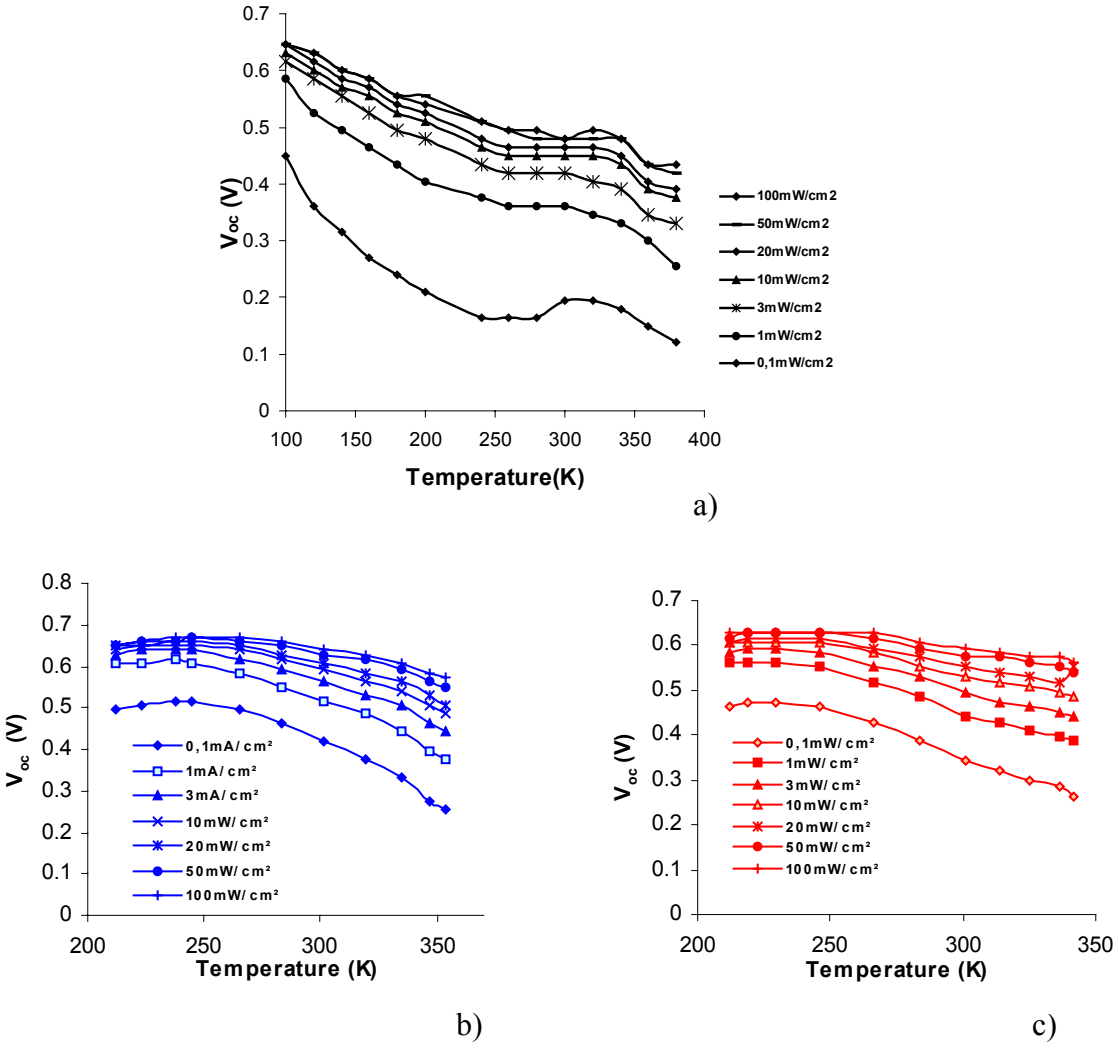

FIGURE 6.5: Dependence of the open circuit voltage on temperature for P3HT:PCBM a) batch 1 nontreated b) batch 2 –nontreated c) batch 2 - annealed

- Efficiency, η (%)

From **Figure 6.6,** it can be noticed that for the cell fabricated with P3HT from the second batch, the maximum of the efficiency which occurs around 3mW/cm² is shifted towards 50mW/cm² at higher temperatures. This result shows the increased transport capability of the organic bulk and is an evidence of a better quality of the P3HT- batch 2 organic material . For the case where the P3HT – batch 1 was used, the maximum of the efficiency remained at 3mW/cm² and the general slope in the decrease of the efficiency with the light intensity takes place more abruptly than in the other two cases. An optimum in the transport of charge carriers through the bulk is reflected in an constant efficiency over the whole range of light intensity.

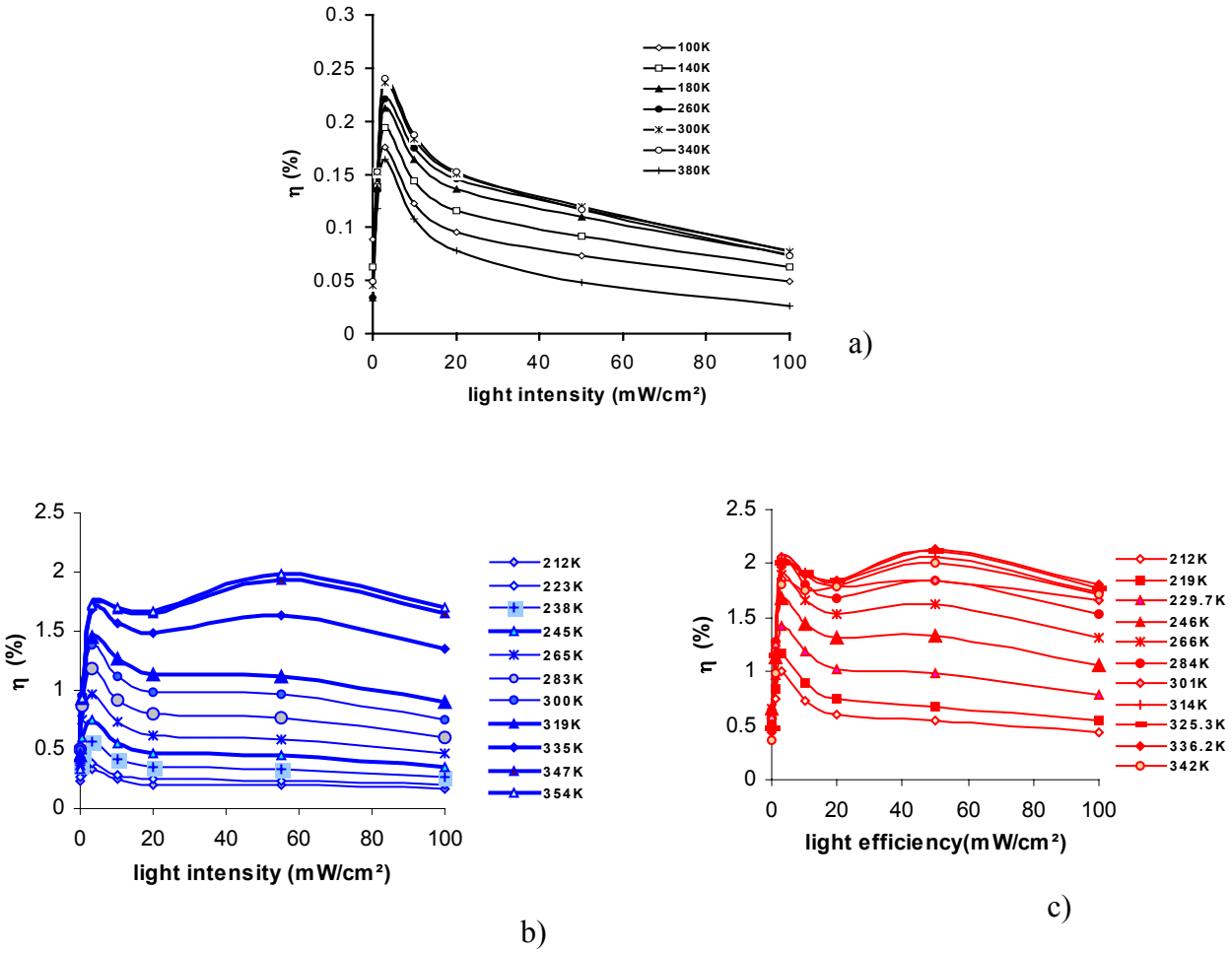

FIGURE 6.6: Dependence of the efficiency on light intensity for P3HT:PCBM based solar cells a) P3HT batch 1 nontreated b) P3HT batch 2- nontreated c) P3HT batch 2- annealed

6.4 Deteriorations at the contact electrode/semiconductor interface

In chapter 2 referring to contacts, the important role played by PEDOT:PSS in extending the life time of the photovoltaic devices, by decreasing the ITO roughness was stressed. The negative aspect of PEDOT:PSS is that it interacts chemically with ITO [105],[106].

Due to the acid nature of PSS, indium is released from the ITO, and is free to diffuse into the PEDOT:PSS layer. This phenomenon is enhanced under O_2, due to the fact that PSS has hydroscopic properties and absorbs water. Studies using Rutherford backscattering spectroscopy have confirmed the diffusion of indium in PEDOT:PSS [107]. PEDOT:PSS can interact directly not only with ITO, but also with glass. In this case Na ions diffuse from the glass into PEDOT. In **Figure 6.7** the time evolution of the In/S and Na/S ratio in a PEDOT:PSS film spin coated on an ITO substrate and on glass respectively is indicated. Another cause of degradation of PEDOT:PSS is triggered not only by the air atmosphere, but also under electrical stress in the absence of air. In this case, the sulphur atoms migrate towards the organic active layer and accumulate at the cathode interface. Additionaly, break bonding effects can lead to a release of oxygen atoms which are very active and can attack the active organic layer.

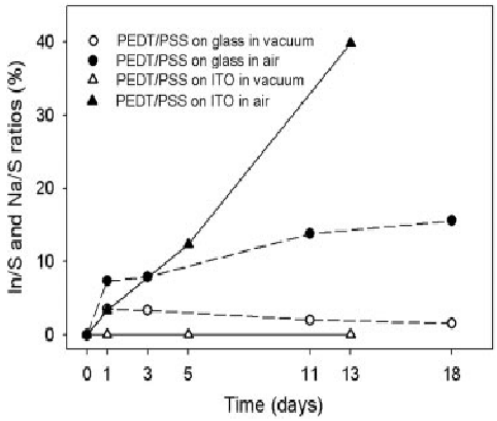

FIGURE 6.7: Time evolution of the In/S and Na/S ratios in a PEDOT:PSS film spin coated on an ITO substrate and on glass under air and vacuum conditions. Reprinted from [10]

For organic light emitting diodes (OLED) based on polyfluorene, black spots are reported [108] to be formed, due to cathode pinhole defects. The pinhole is surrounded by a nonemissive disk in which PEDOT:PSS is locally dedoped to the nonconducting state, while the metal cathode is oxidized.

An example of low performances of P3HT:PCBM based solar cells, which is probably due to the degradation at the electrodes is indicated in **Figure 6.8**. The cell was produced in the glove box and then measured under vacuum conditions at different temperatures. The same measurements repeated at the same temperatures, next day indicated a lower fill factor which decreases considerably the efficiency. The short circuit current density and the open circuit current remained constant.The deterioration is attributed to the instability of the interface organic material/electrodes.

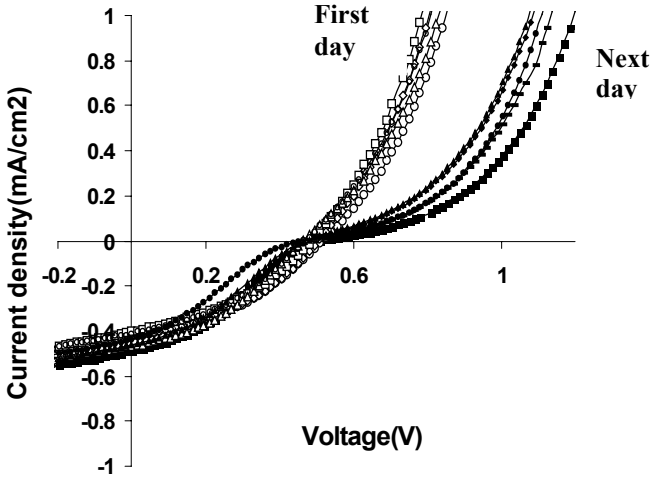

FIGURE 6.8 J-V curve for a P3HT:PCBM based solar cell measured at different temperatures (100mW/cm²). Measurements were taken for the same cell in two days under the same conditions (temperatures and light intensity). In the second day a degradation of the cell occurred, which can be seen in a decrease of the fill factor.

6.5 Light induced degradation

The illumination of conjugated polymers leads to photooxidation, or photobleaching . This deterioration process is enhanced under air atmosphere. Bleaching experiments on PPV, performed by Philips [109] have shown that the photoluminescence and the absorption spectra

decrease, the longer is the exposure time to the air. Additionally, a blue shift occurs in both spectra. This result is explained by the fact that the oxygen interacts chemically with the PPV chain and build carbonyl groups (C=OH) with a strong electron affinity. These carbonyl groups act as traps by catching the electrons. The hole is free to move along the polymer chain, while the electron is trapped and it eventually recombines with a hole in the valence band of the polymer. Thus, photo-oxidation can be interpreted as p-doping the polymer by increasing the number of free holes and enhancing the photoconductivity [110].

In the case of polythiophene no carbonyl groups are formed under O_2 atmosphere. Poly(3 alkylthiophenes) degrade in solution, when exposed to light in the UV vis wavelength region. Degradation takes the form of both reduced π conjugation and chain scission. The former manifests itself as photobleaching, and it is largely the product of the photosensitisation and reaction of a singlet oxygen. Chain scission is initiated by the photolysis of trace amounts of transition metal salts used during the polymerization. Upon π-π^* transitions, poly(3-alkylthiophene) is degraded, and ketone and sulfine groups (C=SO) are formed when exposed to air. The mechanism of exciton dissociation, due to photooxidation is similar to the one which occurs at the interface donor/acceptor. Generally, photooxidation had a futher detrimental effect by building space charge regions and by decreasing the transport of charges through the bulk. Oxygen needs to be excluded from the polymer based devices, to avoid excited state reactions, which lead to self-destruction [111].

Concluding remarks

The aim of this research was the investigation of electrical properties of polymer based solar cells. The materials used were P3HT as a donor, together with the fullerene derivative PCBM as acceptor, combined in a bulk heterojunction structure. The main target in the electrical characterization of polymer based solar cells was the optimization of the main electrical parameters: open circuit voltage, V_{oc}, short circuit current density, J_{sc} together with the fill factor, FF, towards an improved overall power conversion efficiency, η. From all experiments performed, the following conclusions came out:

- Open circuit voltage, V_{oc}

The dependence of V_{oc} with ln(light intensity) shows a linear trend, followed by a saturation region at higher light intensities. The saturation region is determined by the extraction rate of the charge carriers over the barrier formed between the organic bulk and the electrodes. The dependence of V_{oc} on temperature, presented in almost all studied cases a constant decrease in the higher temperature range. This behaviour of V_{oc} observed for P3HT:PCBM based solar cells and reported for other polymer cells was explained based on the general accepted assumption that the theoretical limit of V_{oc} is controlled by the difference $HOMO_{donor}$ - $LUMO_{acceptor}$. Experimentally, V_{oc} versus temperature might deviate from the theoretically expected dependence, as it was shown in chapter 4. (for the particular case when copper was used as metallic electrode). V_{oc} is influenced by the recombination processes in the organic bulk material, which become dominant at lower temperatures. This is the reason why the classical method of determining the theoretical limit of V_{oc} by extrapolating the linear region of $V_{oc} = f(T)$ towards zero temperature, may lead to errors. Therefore, it should be applied with precautions, only in cases when recombination processes al lower temperatures can be neglected and the solar cell is fully saturated with light. Related to this aspect, for the particular case of P3HT:PCBM based solar cells, the value of 1.48V is proposed as theoretical limit for the open circuit voltage, V_{oc} at room temperature. This value was calculated in chapter 2 based on a general formula borrowed from the classical inorganic solar cells, which depends only on material parameters and the temperature of the sun and of the solar cell, respectively.

From the experiment in chapter 3 related to the variation of the metallic electrode for thermally annealed P3HT:PCBM based solar cells, an interesting conclusion came out: V_{oc} is highly sensitive to the variation of the cathode work function. This result led to the conclusion of the absence of Fermi level pinning of the metal electrode upon the Lumo level of the PCBM acceptor. This conclusion is different compared to the one reported in literature, from a similar experiment with PPV:PCBM.

As it was shown in chapter 5, the effect of thermal annealing on V_{oc} is negligible. Therefore, it can be concluded that the V_{oc} is rather insensitive to the morphological modifications induced in the bulk by thermal treatment, and is only governed by the energetics of the organic compounds (donor/acceptor) and by the work functions of the electrodes. The degree of purity of the material does not influence either V_{oc}.

- Short circuit current density, J_{sc}

The short circuit current density, J_{sc} is the main indicator of the transport and photogeneration capabilities of the organic bulk material. The photogeneration of charge carriers in the bulk is reflected by the external quantum efficiency (EQE). From the EQE and the solar spectrum photon flux, J_{sc} given by a cell can be calculated. By using this method, the theoretical limit of the J_{sc} for solar cells based on organic compounds absorbing solar energy in the range 320-800nm was obtained to be 25.98mA/cm². It was shown in chapter 3, that J_{sc} is proportional to the light intensity. At temperatures >300K no bimolecular recombination was found in P3HT:PCBM based solar cells.

The dependence $J_{sc} = f(T)$ shows an increase of J_{sc} with increasing temperature. This result is commonly attributed to a thermally activated hopping mechanism, characteristic to disordered organic materials and always reported not only for P3HT but also for cells based on other polymers (PPV, OC1C10 etc).

- Fill factor, FF and power conversion efficiency, η

The fill factor, FF and the power conversion efficiency, η increase both at higher temperatures. This result illustrates the special feature of organic solar cells to operate better in a warm climate, opposite to the behaviour of conventional inorganic solar cells. The dependence of η on light intensity shows an interesting aspect. The highest η is obtained in the most cases at 3mW/cm², and not at the highest light intensity, as expected. At higher temperatures, this maximum is shifted towards 50mW/cm². This fact represents an evidence for the improvement in the bulk transport properties of the organic material.

The thermal annealing has been proved to be a very efficient method for improving the electrical characteristics of P3HT:PCBM based solar cells. The morphological changes induced in the organic active layer determine a considerable increase of the short circuit current density, J_{sc}. The fill factor, FF improves too, and the overall shape of the J-V curve gets closer to the aspect of an ideal diode characteristic.

For P3HT:PCBM based solar cells, the positive effects of thermal annealing occur in a large range of temperatures up to the melting point of P3HT (the lowest annealing temperature which was tested was 75°C, the highest was 140°C). The electrical parameters of annealed P3HT:PCBM based cells monitored over a long time interval, proved the persistence of the positive effects induced by thermal treatment. The morphological changes in the P3HT:PCBM organic bulk, attributed to the thermochromic properties of P3HT, take place in a short time interval (minimum tested annealing time was 20s). Nevertheless, due to the lack of reliable information about the melting point and the temperature glass transition of both pure organic compounds (P3HT and PCBM) and of the blend, the optimum time and temperature at which thermal annealing should be performed in the case of P3HT:PCBM based solar cells are not indicated here, and still remain an open question.

The last part of chapter 5 consists of a particular experiment related to the optimization of the amount of the PCBM acceptor in the P3HT:PCBM based solar cells. (annealing was performed 20s at $T_a = 130°C$). The results from this experiment clearly proved a better electrical performance for the cells fabricated with a lower PCBM amount in the blend. The optimum P3HT:PCBM weight ratio was found to be in the range 1:0.9-1:1. This result was oposite to the

conclusion known from the literature, from the experience with PPV:PCBM based solar cells where a higher amount of the PCBM acceptor determines a better power conversion efficiency. The reason why high amounts of the PCBM acceptor have a detrimental effect on electrical performances of P3HT:PCBM based solar cells, was clarified by AFM and SEM investigations. AFM images of thin films of the P3HT:PCBM absorber show a crystallisation process of the PCBM acceptor in the blend as a result of thermal annealing. The height of the PCBM clusters were found to be in the range >500nm. The metallic electrode is deteriorated, due to these large PCBM domains and to the difference in the thermal expansion coefficient between the metallic electrode and the organic layer as a result of thermal annealing.

The best thermally annealed P3HT:PCBM based solar cell, was obtained with a P3HT:PCBM weight ratio of 1:1. (J_{sc}=6.35mA/cm², V_{oc}= 0.59V, FF= 63.18%, η = 2.39% under 100mW/cm² white light intensity and at room temperature).

Organic materials can be produced with a different degree of purity as a result of the chemical synthesis. In chapter 6 it was exemplified in what degree the quality of organic materials can affect the electrical performance of the future organic device. Two P3HT:PCBM based solar cells produced with P3HT from different batches can present huge differences in the electrical performances. An important conclusion came out from this experiment: Results in the literature, when compared, should be always related to the specific preparation conditions and to the quality of the organic materials, and therefore should not be generalized or taken as absolute.

APPENDIX 1

Table A1 Electrical parameters of thermally annealed P3HT:PCBM based solar cells fabricated with different P3HT:PCBM weight ratios (dark and illuminated)

100 mW/cm²								dark	
cell	weight ratio P3HT:PCBM	Jsc (mA/cm²)	Uoc (V)	FF (%)	η (%)	Rs (ohm*cm²)	Rp (ohm*cm²)	Rs (ohm*cm²)	Rp (ohm*cm²)
D6L	1:0.7	5.36	0.59	47.53	1.50	1.60	705.95	1.56	83331.77
D6M	1:0.7	6.21	0.59	52.97	1.94	1.92	679.90	1.83	39471.85
D6R	1:0.7	5.87	0.605	49.31	1.75	1.44	645.11	1.44	22057.38
D9L	1:0.8	6.46	0.575	40.49	1.50	1.88	261.00	2.42	124997.58
D9M	1:0.8	5.58	0.56	35.59	1.11	2.08	222.47	2.21	374997.79
D9R	1:0.8	7.17	0.575	39.84	1.64	1.60	218.99	1.63	374998.37
D4L	1:0.9	7.71	0.605	40.04	1.87	2.68	171.74	2.59	124997.41
D4M	1:0.9	6.98	0.605	46.91	1.98	1.74	276.03	1.79	149998.21
D4R	1:0.9	7.23	0.605	45.85	2.01	1.83	298.17	1.88	93748.13
D7R	1:1	5.73	0.584	53.24	1.78	4.00	1760.00	4.19	146662.48
D7L	1:1	6.35	0.595	63.18	2.39	3.38	514.26	3.52	29329.81
D2L	1:1	7.33	0.605	41.10	1.82	2.07	164.14	2.07	33331.26
D2M	1:1	7.11	0.605	42.50	1.83	3.95	216.64	3.75	83329.58
D1M*	1:1	7.8	0.576	49.57	2.22	5.64	184.88	7.38	319992.62
D1L*	1:1	6.17	0.576	34.9	1.24	4	239.03	3.84	87268.88
D5M*	1:1	6.61	0.588	44.95	1.74	2.46	328.57	2.34	68569.09
D5L*	1:1	5.93	0.576	52.96	1.8	2.4	244.00	2.34	43634.02
D5R*	1:1	5.64	0.588	29.321	0.97	3.31	90.8	3.09	95996.90
D4L*	1:1.5	5.11	0.576	50.37	1.48	3.09	392.77	3.2	106663.46
D4M*	1:1.5	5.51	0.576	54.869	1.74	2.66	215.51	2.91	239997.09
D4R*	1:1.5	6.05	0.576	46.86	1.63	3.00	110.9	3.00	191997
D5R	1:2	3.08	0.573	42.50	0.75	9.78	592.96	22.00	97755.78
D5M	1:2	2.83	0.573	41.21	0.67	7.33	498.41	14.67	175985.33
D2L*	1:2	2.1	0.6	41.87	0.5285	10.28	849.41	12.00	359988
D2M*	1:2	1.93	0.588	40.44	0.458	18.00	1263.89	23.52	359976.47
D2R*	1:2	2.09	0.612	30.62	0.3914	60.00	502.50	37.30	239962.69
D6L*	1:2	1.85	0.6	35.55	0.3942	28.00	727.05	28.00	76335.63
D6M*	1:2	1.81	0.6	39.47	0.4292	43.29	561.01	42.21	209957.78
D6R*	1:2	1.58	0.6	36.69	0.348	60.00	407.31	58.74	839941.20
D8L	1:3	0.88	0.573	34.54	0.17	473.12	613.30	3437.50	216562.50
D8M	1:3	0.90	0.584	34.91	0.18	423.08	565.69	3098.59	290234.74
D8R	1:3	0.79	0.584	33.45	0.15	523.81	789.62	2953.02	290380.31
D8L*	1:3	1.25	0.6	28.95	0.21	199.58	365.12	213.8	959786.19
D8M*	1:3	1.42	0.588	36.21	0.301	85.714	637.44	127.32	479872.67
D8R*	1:3	1.39	0.588	32.99	0.2699	133.33	481.06	118.81	479881.18
D9M*	1:3	1.4	0.576	32.43	0.26	157.3	104.37	135.48	839864.51
D9R*	1:3	0.902	0.588	25.4	0.1347	563.75	1769.57	884.21	75479.42

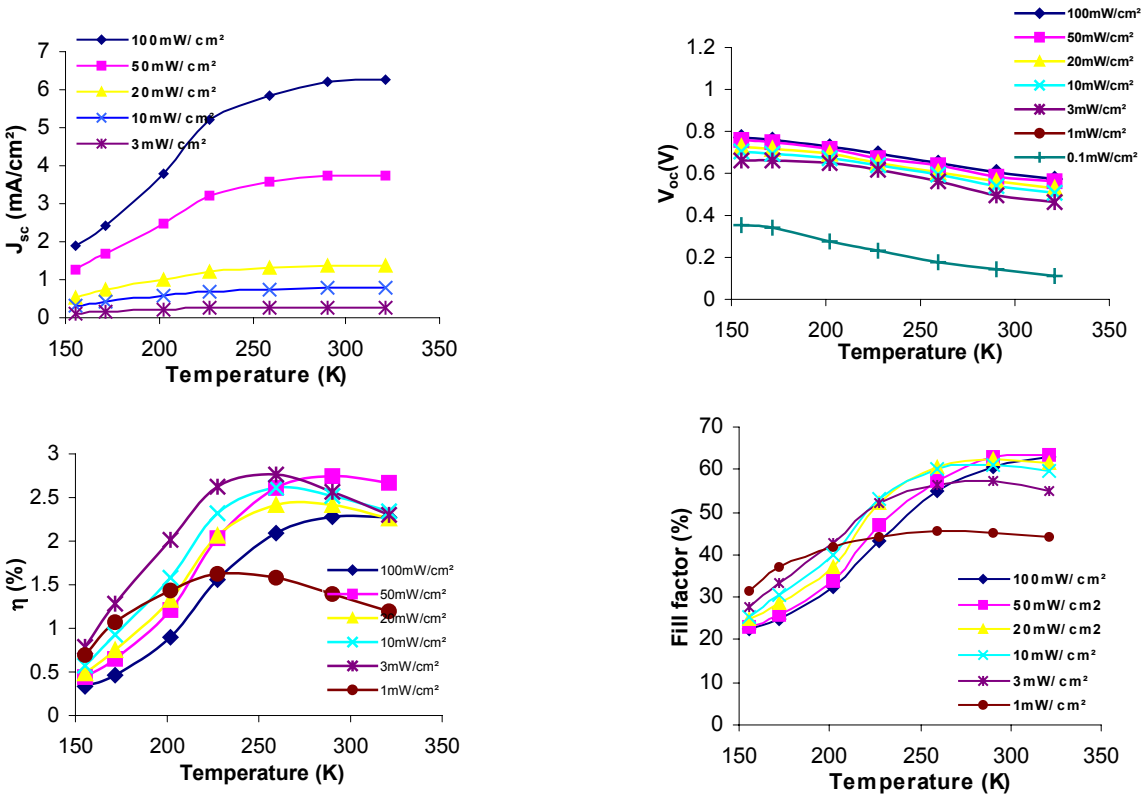

FIGURE A1: Temperature dependence of the main parameters Jsc,Voc, FF and η for the best P3HT:PCBM based solar cell obtained (maximum efficiency obtained 2.39% at room temperature and 100mW/cm²)

Appendix 2

Regioregular poly(3- hexylthiophene 2.5 diyl) (P3HT) synthesized following the Rieke procedure [13] was purchased from Aldrich AG (batch1) and from Rieke Met. Inc. (batch 2), and the fullerene derivative [6,6]-phenyl -C_{61} butyric acid methyl ester, (PCBM) [25] was obtained from the University of Groningen. These organic materials were used as received, without further purification. ITO substrates were etched under O_2 atmosphere 10 min O_2 flow 100%.

Recipe 1:

ITO/PEDOT:PSS/P3HT:PCBM/Al bulk heterojunction solar cells were prepared in a nitrogen atmosphere of a glove box and electrically characterized. First, a thin layer of polyethylenedioxythiophene doped with polystyrene-sulfonic acid (PEDOT:PSS) Baytron P, Bayer AG, Germany was spin coated at 1500 rpm on patterned clean ITO coated glass substrates in order to smoothen the surface of ITO and, hence, avoid possible short circuits due to the spiky roughness of the surface. The PEDOT:PSS solution was spin coated on ITO substrates and then dried at 50°C for 1 hour. An active layer consisting of a mixture of P3HT:PCBM at a 1:2 weight ratio, dissolved in a chloroform–toluene solvent mixture at 0.25 wt% was then spin coated at speed 4000 rpm on top of the dry PEDOT:PSS film to give a thin film of about 100 nm. Finally, 100 nm Al contacts were deposited on the active layer by thermal evaporation at low rate in a high vacuum of better than 10^{-6} mbar in all cases.

Recipe 2 (for the experiment related to the optimization of the PCBM amount in the blend)

Regioregular (P3HT) (batch 2) was used in the preparation of organic solar cells as a donor, combined with the fullerene derivative, PCBM as acceptor, in weight ratios P3HT:PCBM = 1:0.7, 1:0.8, 1:0.9, 1:1, 1:1.5, 1:2, 1:3.

Bulk heterojunction ITO/PEDOT-PSS/P3HT:PCBM/Al solar cells were produced in the following way: The indium tin oxide coated glass substrate ITO (purchased from Merck with surface resistance 20 Ω/□) has been cleaned in standard solvents and dried in a nitrogen flow. Afterwards, the O_2 plasma etched ITO substrates were spin coated with a thin layer of poly(3, 4 ethylenedioxythiophene)poly(styrenesulfonate) (PEDOT-PSS) purchased from Bayer AG. After drying the PEDOT coated substrate for about 30 min at 100°C on a hot plate, a thin layer of the active organic layer P3HT:PCBM was applied on top of the substrate. The solution of P3HT:PCBM was prepared in chloroform at a concentration of 1wt% of P3HT, heated and stirred for more than one day at 50°C and filtered afterwards. Finally, Al electrodes (100nm) was thermally evaporated on the organic active layer under vacuum at high evaporation rate (0.2-0.5nm/s).

The thermal annealing procedure was performed by placing the solar cells on a hot plate at a certain annealing temperature T_a during a certain time interval. The temperature of the hot plate was monitored by using a thermoresistor in order to reduce errors due to the cooling/heating cycle of the hot plate.

Electrical characterization of solar cells:

I-V curves of the P3HT:PCBM solar cells were measured by using an Advantest TR 6143 source /measure unit with the solar cells placed in a nitrogen cooled cryostat, at a vacuum better than 10^{-5}mbar . A 150 W xenon lamp (Osram XB0 150W/XBR) was used as illumination source, with a water filter placed in the light path in order to reduce the IR part of the spectrum. The light intensity was calibrated at 100mW/cm² and filters were used to vary light intensity.

Absorption spectrum of the P3HT:PCBM organic layer before and after annealing was measured by using a Varian Cary 5E ultraviolet-visible spectrometer. External quantum efficiency (EQE) measurements were measured in a lock-in detector after illumination with monochromatic light. AFM measurements were performed with a Digital Instrument Vecco in tapping mode with a resolution of 50μm. Scanning electron microscopy measurements were performed at ISE Freiburg.

All solar cells were produced in the glove box, under nitrogen atmosphere.

Data about P3HT and PCBM

According to Zhao et al. [82] , the glass transition and the melting point temperatures of P3HT are 12°C and 178°C, respectively, whereas Chen et al. [13] determined the melting temperature of 240-245°C for head-to-tail regioregular P3HT, while no indication for a glass transition temperature was given.

For PCBM, no information about the melting point and the T_g was found in literature.

Bibliography

[1] C.B. Hatfield Oil back on the global agenda. Permanent decline in global oil is virtually certain to begin within 20years *Nature* 387, 121 (1997)

[2] Intergovernmental Panel on Climate Change (IPCC) Second Assessment Report Climate Change 1995, (1995) Web site: www.meto.gov.uk

[3] K. Petritsch Organic Solar cells architectures *PhD Thesis* Web site: http://www.solarpassion.com/solar_thesis/thesis_download.htm

[4] United Nations Environment Programme (UNEP) Global Environment outlook (GEO) 2000 Earth scan Publications Ltd, London (2000) Web site: www.unep.org

[5] T. Ito, H. Shirakawa and S. Ikeda *J. Polym. Sci. Chem*. 12, 11 (1974)

[6] C. K. Chiang, Y. W. Park, A. J. Heeger, H. Shirakawa, E. J. Louis and A. G. MacDiarmid *Phys. Rev. Lett.* 39, 1098 (1977)

[7] Press release 10.03.2004 General Electric http://www.heise.de/newsticker/meldung/45391

[8] P. J. Flory Principles of polymer chemistry Book Cornell University Press (1953)

[9] G. J. Kavarnos Fundamentals of photoinduced electron transfer Book Weinheim : VCH (1993).

[10] X. Crispin, S. Marciniak, W. Osikovitz, G. Zotti, F. Louwet, M. Fahlmann, L. Groenendaal, F. de Schryver and W.R. Salaneck Conductivity, morphology, interfacial chemistry and stability of poly(3,4-ethylene dioxithiophene)-Poly(styrenesulfonate): A Photoelectron Spectroscopy Study *Journal of polymer science*: *Part B: Polymer Physics* vol 41, 2561-2583 (2003) Wiley Periodicals Inc. http://www.ifm.liu.se/Surfphys/Xavier/pedot-pssreview.pdf

[11] N.S.Sariciftci Polymeric photovoltaic materials *Current Opinion in Solid State and Materials Science* 4, 373-378 (1999)

[12] H. Sirringhhaus, N. Tessler and R. Friend Integrated optoelectronic devices based on conjugated polymers *Science* vol. 280, page 1741, (1998)

[13] T. Chen, X. Wu, R. D. Rieke Regiocontrolled Synthesis of poly(3-alkylthiophenes) mediated by Rieke Zinc:Their Characterization and Solid State properties *Journal. Am. Chem Soc*. 117, 233-244 (1995)

[14] A. Assadi, C. Svenson, M. Willander and O. Inganäs Field Effect Mobility of Poly(3-hexylthiophene) *Appl. Phys. Lett*. 53, 195 (1988)

[15] T. Yamamoto, A. Morita, Y. Miyazaki, T. Maruyama, H. Wakayama, Z. Zhou, Y. Nakamura, and T. Kanbara Preparation of p- conjugated poly(thiophene-2.5diyl), poly(p-phenylene) and related polymers using Zerovalent Nickel Complexes. Linear structure and properties of the p-Conjugated polymers *Macromolecules* 25, 1214-1223 (1992)

[16] R.W. Lof, M.A. van Veenendaal, B. Koopmans, H.T. Jonkman and G.A. Sawatzky *Phys. Rev. Lett*. 68, 3924 (1992)

[17] B. Mishori, E.A. Katz, D. Faiman and Y. Shapira *Solid State Commun*. 102, 489 (1997)

[18] E.L. Shirley and S.G. Louie Phys. Rev. Lett. 71, 133 (1993)

[19] M.S. Dresselhaus, G. Dresselhaus and P.C. Eklund Science of fullerenes and Carbon nanotubes Book *Academic NewYork (1996)*

[20] N.S. Sariciftci, L. Smilowitz, A.J. Heeger, and F. Wudl *Science* 258, 1474 (1992)

[21] S. Morita, A.A. Zakhidov and K. Yoshino *Solid State Commun.*. 82, 249 (1992)

[22] S.E. Shaheen, C. J. Brabec, N.S. Sariciftci, F. Padinger, T. Fromherz, J.C. Hummelen *Appl. Phys. Lett.* 78, 841 (2001)

[23] P. Peumans and S.R. Forrest *Appl.Phys.Lett*. 79, 126 (2001)

[24] press release 07/01/04 Siemens AG, Germany

[25] J. C. Hummelen, B. W. Knight, F. LePeq, F. Wudl, J. Yao and C. L.Wilkins *Journal Org. Chem*. 60, 532–538 (1995).

[26] L.A.A. Petterson, F. Carlson, O. Inganäs and H. Arwin *Thin Solid Films* 313, 356 (1998)

[27] L. Groenendaal, F. Jonas, D. Freitag, H. Pielartzik and J.R. Reynolds *Adv. Mater*. 12, 481 (2000)

[28] F. Jonas and J. Morrison *Synth. Met*. 85, 1397 (1997)

[29] L.S. Roman, W. Mammo, L.A. Petterson, M.R. Anderson and O. Inganäs *Adv. Mater*. 10, 774 (1998)

[30] W. U. Huynh, J.J. Dittmer and A.P. Alivisatos *Science* 295, 2425 (2002)

[31] G. Greczynski, M. Fahlman and W.R. Salaneck An experimental study of poly(9,9-dioctyl-fluorene) and its interfaces with Li, Al, and LiF *J. Chem. Phys*. 113, 2407-2412 (2000)

[32] V. Lüttge, M. Kluge and G. Bauer Botanik *Book Wiley-VCH Weinheim*

[33] C.J. Brabec, G. Zerza, G. Cerullo, S. De Silvestri, S. Luzatti, J.C. Hummelen and N.S. Sariciftci *Chem. Phys. Lett.* 340, 232, (2001)

[34] R. Friend, J. Burroughes and T. Shimoda Polymer diodes *Physics World* June (1999) p. 35

[35] Fachlexikon der Physik, Verlag Harri Deutsch, 2. Auflage (1989)

[36] S. M. Sze Semiconductor devices: Physics and technology *Book Wiley (2001)*

[37] J. Rostalski and D. Meissner Monochromatic versus solar efficiencies of organic solar cells *Solar Energy Materials & Solar Cells* 61, 87-95 (2000)

[38] W. Ruppel and P. Würfel Upper limit for the conversion of solar energy *IEEE Trans Electron Devices* vol ED 27 p. 877 (1980)

[39] G. L. Araujo Limits to efficiency of single and multiple band gap solar cells in *A. Luque and G.L. Araujo Eds Physical limitations to photovoltaic energy conversion Adam Hilger Bristol p.106, (1990)*

[40] D. Fichou Handbook of oligo- and polythiophene *Book Wiley VCH Weinheim (1999)*

[41] V.D. Mihailetchi, P.W. M.Blom, J.C. Hummelen and M.T. Rispens Cathode dependence of the open circuit voltage of the polymer:fullerene bulk heterojunction solar cells *Journal of Appl. Phys.* 94,10 (2003)

[42] M.A. Green Silicon Solar cells: Advanced principle and practice Centre for Photovoltaic devices and Systems, University of New South Wales (1995).

[43] W. Shockley and H.J. Queisser *J.Appl. Physics* 32, 510 (1961)

[44] M. Munzel Temperatur und intensitätsabhängige elektrische Charakterisierung von Cu(In, Ga) Se2 Dünnschichtsolarzellen *Diplomarbeit Universität Oldenburg (2000)*

[45] P. Schilinsky, C. Waldauf, J. Hauch and C. Brabec Simulation of light intensity dependent current characteristics of polymer solar cells *J. of Appl. Phys*. 95, p. 2816 (2004)

[46] G. Smestad and H. Ries Luminescence and current-voltage characteristics of solar cells and optoelectronic devices Sol En Mat Sol Cells 25, 51-71 (1992)

[47] A. Burk, P.Johnson, W. Hobson and A. Ellis, *J. Appl. Phys*. 59, 1621 (1986)

[48] J. Nelson Organic photovoltaic films in *Current Opinion in Solid State and Materials Science* 6, 87–95 (2002)

[49] N.S. Sariciftci, D. Braun, C. Zhang, V.I. Srdanov, A.J. Heeger, G. Stucky and F. Wudl Semiconducting polymer-buckminsterfullerene heterojunctions: Diodes, photodiodes and photovoltaic cells *Appl. Phys. Lett*. 62, 585 (1993)

[50] H. Kim, S. Jin, H. Suh and K. Lee Origin of the open circuit voltage in conjugated polymer fullerene photovoltaic cells – *in press*

[51] C.J. Brabec, A. Cravino, D. Meissner, N.S. Sariciftci, T. Fromherz, M.T. Rispens L. Sanchez and J.C. Hummelen Origin of the open circuit voltage in plastic solar cells *Adv. Funct. Mater*. 11, 374 (2001)

[52] C.J. Brabec, A. Cravino, D. Meissner, N.S. Sariciftci, M.T. Rispens, L. Sanchez, J.C. Hummelen and T. Fromherz The influence of materials work function on the open circuit voltage of plastic solar cells *Thin Solid Films* 403, 368–372 (2002)

[53] C.J. Brabec, N.S. Sariciftci, and J.C. Hummelen Plastic solar cells *Adv. Funct. Mater* 11:15–26 (2001)

[54] C. M. Ramsdale, J. A. Barker, A. C. Arias, J. D. MacKenzie, R. H. Friend, and N. C. Greenham The origin of the open circuit voltage in polyfluorene – based photovoltaic devices *J. Appl. Physics* 92, 8 (2002)

[55] D. Braun and A.J. Heeger Visible light emission from semiconducting polymer diodes *Appl. Phys. Lett*. 58, 1982 (1991)

[56] P. Bröms, J. Birgersson, N. Johnsson, P. Lögdlund and W.R. Salaneck Calcium electrodes in polymer LED`s *Synth. Met*. 74, 179 (1995)

[57] A. Gadisa, M. Svensson, M. R. Andersson and O. Inganäs Correlation between oxidation potential and open circuit voltage of composite solar cells based on blends of polythiophene/fullerene derivative *Appl. Phys. Lett.* 84, 9, p. 1609 (2004)

[58] A. J. Campbell, D. D. C. Bradley and D. G. Lidzey *J. Appl. Phys*. 82, 6326 (1997)

[59] A.J. Campbell, M.S. Weaver, G.D. Lidzey and D.D. C. Bradley Bulk limited conduction in electroluminiscent polymer devices *J. Appl. Phys.* 84, 12, (1998)

[60] D. Seanor Electrical properties of polymers Academic Press, New York 1982

[61] F.N. Hooge and D. Pockler *Phys. Chem. Solids* 25, 977 (1964)

[62] P. Schilinsky and C. Waldauf Recombination and loss analysis in polythiophene based bulk heterojunction photodetectors *Appl. Phys. Lett.* 81, 20, (2002)

[63] S.C.J. Merskers, P.A. van Hall, A.J. Spiering, J.C. Hummelen, A.F.G. van der Meerand and R.A. Janssen Phys. Rev. B, 61, 9917 (2000)

[64] V. Dyakonov, I. Riedel, C. Deibel, J. Parisi, N.S. Sariciftci and J.C. Hummelen Electronic properties of polymer – fullerene solar cells *Mat.Res.Soc.Symp.Proc*. 665, (2001)

[65] E. A. Katz, D. Faiman, S. M. Tuladhar, J. M. Kroon, M. M. Wienk, T. Fromherz F. Padinger, C. J. Brabec and N. S. Sariciftci Temperature dependence of the photovoltaic device parameters of polymer – fullerene solar cells under operating conditions *J. Appl. Phys.* 90, 10, p. 5343, (2001)

[66] U. Lemmer and E.O. Göbel Photoluminiscence spectroscopy as a probe for disorder and excitonic effects in organic and inorganic semiconductors in *Primary photoexcitations in conjugated polymers : Molecular Exciton versus Semiconductor Band Model - Book, edited by N. S. Sariciftci World Scientific Publ. , Singapore (1997)*

[67] B.G. Streetman Solid State Electronic Devices *Book Prentice Hall (1990)*

[68] K. Emery, J.Burdick, Y.Caiyem, D.Dunlavy, H.Field, B.Kroposki, T.Moriarty, L.Ottoson, S.Rummel, T.Strand and M.W.Wanlass- *Proceedings of the Spec. Conference* p.1275, (IEE-1996)

[69] E. Moons Conjugated polymer blends: linking film morphology to performance of light emitting diodes and photodiodes *J.Phys: Cond. Matter*. 14, 12235 (2002)

[70] By good solvent we mean a solvent in which with sufficient stirring and heating, the polymer can dissolve to concentrations of several percent w/v without gelation

[71] B. J.Schwartz Conjugated polymers as molecular materials: How chain conformation and film morphology influence energy transfer and interchain interactions *Annu. Rev. Phys. Chem*. 54:141-72 (2003)

[72] Z. Bao, A. Dodabalapur, and A. Lovinger Soluble and processable regioregular poly(3-hexylthiophene) for thin film field effect transistor applications with high mobility *Appl. Phys. Lett*. 69, 26, 4108 (1996)

[73] T. Ahn and H. L. Sien-Ho Ha Effect of annealing of polythiophene derivative for polymer light-emitting diode *Appl. Physics Lett*. 80, 3 (2002)

[74] P.J. Brown, D. S. Thomas, A. Köhler, J. Wilson, J. Kim, C. Ramsdale, H. Sirringhaus, and R. H. Friend Effect of interchain interactions on the absorption and emission of poly(3 hexylthiophene) *Phys. Rev. B*. 67, 064203 (2003)

[75] M. Drees, K. Premaratne, W. Graupner, J. R. Heflin, R. M. Davis, D. Marciu and M. Miller Creation of a gradient polymer-fullerene interface in photovoltaic devices by thermally controlled interdiffusion *Appl. Phys. Lett*. 81, 24, (2002)

[76] R. Pacios and D.D.C. Bradley *Synth.Met*. 9149, 1 (2001)

[77] T. W. Lee and O. O. Park *Macromolecules* 11, 801 (2000)

[78] J. Dittmer, E. Marseglia and R. Friend Electron trapping in dye/polymer blend photovoltaic cells *Adv. Mater*. 12, 1270 (2000)

[79] F. Zhang, M. Svensson, M. Andersson, M. Maggini, S. Bucella, E. Menna and O. Inganas Soluble polythiophene with pendant fullerene groups as double cable materials for photodiodes *Adv. Mater* 13, 1871 (2001)

[80] N. Camaioni, G. Ridolfi, G. Casalbore-Miceli, G. Possamai and M. Maggini The effect of a mild thermal treatment on the performances of poly(3-alkylthiophene)/Fullerene solar cells *Adv. Mater* . 14, 1735 (2002)

[81] F. Padinger, R. Rittberger and N. Sariciftci Effect of postproduction Treatment on plastic solar cells *Adv. Funct. Mater* 13, (2003)

[82] Y. Zhao , G. Yuan, P. Roche and M. Leclerc A calorimetric study of the phase transitions in poly(3- hexylthiophene) *Polymer* 36, 2211 (1995)

[83] C. Yang, F. P. Orfino and S. Holdcroft A Phenomenological Model for Predicting Thermochromism of regioregular and Nonregioregular poly(3-alkylthiophenes) Macromolecules 29, 6510 (1996)

[84] B. A. Mattis, P. C. Chang, V. Subramarian Effect of thermal cycling on performance of poly(3-hexylthiophene) transistors *Mat. Res.Soc. Symp.Proc*. 771 (2003)

[85] T. Arai , Y. Mukarami, H. Suematsu, K. Kikuchi, Y. Achiba and I. Ikemoto Resistivity of single crystal C_{60} and effect of O_2 *Solid State Commun.* 84 , 827-829 (1992)

[86] R. Pacios and D.D.C. Bradley Charge separation in polyflourene composites with internal donor/acceptor heterojunctions *Synth. Metals* 9149, 1-5 (2001)

[87] B.L. Lucht, W.B. Euler and O.J. Gregory *Polymer Preprints* 43, 59 (2002)

[88] R. Zallen The physics of amorphous solids *Book* John Wiley &Sons Inc 1983

[89] P. Peumans, S. Uchida and S.R. Forrest Efficient bulk heterojunction photovoltaic cells using small-molecular –weight organic thin films *Nature* 425, 158, (2003)

[90] D. Godovsky, L. Chen, L. Pettersson, O. Inganas, M. Andersson and J.C. Hummelen The use of combinatorial materials development for polymer solar cells *Adv. Mater. Opt. Electron*. 10, 47-54 (2000)

[91] C. J. Brabec, C. Winder, M. C. Scharber, N. S. Sariciftci, J. C. Hummelen, M. Svensson and M. R. Andersson Influence of disorder on the photoinduced excitations in phenyl substituted polythiophene *J. Chem. Phys.* 115,7235, (2001)

[92] T. Martens, J. D'Haen, T. Munters, Z. Beelen, L. Goris, J. Manca, M. D'Olieslaeger, D. Vanderzande, L. De Schlepper and R. Andriessen *Synth. Met*. 138, 243 (2003)

[93] H. Hoppe, M. Niegemann, C. Winder, A. Hinsch, J. Kraut, R. Hiesgen, D. Meissner and N.S. Sariciftci Nanoscale morphology of conjugated polymer/fullerene based bulk heterojunction solar cells in press

[94] J. K. J. van Duren, X. Yang, J. Loos, C. W. T. Bulle-Lieuwma, A. B. Sieval, J. C. Hummelen, and R. A. J. Janssen *Proceedings of SPIE* Vol. 5215 Organic Photovoltaics IV, (Ed: Z.H. Kafafi, P.A. Lane)

[95] J. Kim, J. Lee, C. W. Han, N. Y. Lee, and I. J. Chung *Appl. Phys. Lett*. 82, 4238 (2003)

[96] J. Kim and H. H. Lee *Journal Polym. Sci*., *Part B: Polym. Phys*. 39, 1122 (2001)

[97] M. Sato, S. Tanaka, and K. Kaeriyama *J.Chem Soc*. , *Chem Commun* 873,(1986)

[98] R. Sugimoto, S. Takeda , H.B. Gu and K. Yoshino, *Chem. Express* 1, 635 (1986)

[99] R.D. Mc Cullough and R.D. Lowe *Journal. Chem Soc, Chem.Commun* 70 (1992)

[100] T.A. Chen and R.D. Rieke Journal Am. Chem. Soc. 114,10 (1992)

[101] J. Roncali Synthetic principles for bandgap control in linear π- Conjugated systems Chem. Rev. 97, 173-205 (1997)

[102] D. Chirvase, Z. Chiguvare, M.Knipper, J.Parisi, V.Dyakonov and J.C. Hummelen Temperature dependent characteristics of poly(3 hexylthiophene)-fullerene based heterojunction solar cells *J. Appl.Phys*. 93, 3376, (2003)

[103] I. Riedel, J. Parisi, V. Dyakonov, L. Lutsen, D. Vanderzande and J.C. Hummelen Effect of temperature and illumination on the electrical characteristics of polymer-fullerene bulk heterojunction solar cells *Adv. Funct. Mater*.14, 38, (2004)

[104] M.M. Erwin, A.V. Kadavanich1, J. McBride, T. Kippeny, S. Pennycook, and S.J. Rosenthal Material characterization of a nanocrystal based photovoltaic device *Eur. Phys. J. D* **16**, 275-277 (2001)

[105] F. Nüesch ,L. Rothberg ,E. Fortsythe ,Q. Le ,Y. Gao *Appl Phys. Lett.* 74, 880 (1999)

[106] K.W. Wong ,H.L. Yip,Y. Luo, K.Y. Wong, W.M. Lau, K.H. Low, H.F.Chow, Z.Q. Gao, W.L. Yeung , C.C. Chang *Appl. Phys. Lett*. 80, 2788 (2002)

[107] M.P.D. Jong, L.J.V. Ijzendoorn and M.J. Voigt *Appl. Phys. Lett*. 77, 2255, 2000

[108] J.S.Kim, P.K. Ho, C.E. Murphy, N. Baynes and R.H. Friend *Adv Mater*. 14, 206 (2002)

[109] M. C. Vissenberg Optoelectronic properties of disordered organic materials *PhD thesis*

[110] H. Antoniadis, L.J. Rothberg, F. Papadimitrakopoulos, M.Yan and M.E. Galvin Enhanced carrier photogeneration by defects in conjugated polymers and its mechanism *Phy. Rev. B* 50,14911, (1994)

[111] M.Yan, L.J.Rothberg, F. Papadimitrakopoulos, M.E. Galvin and T.M. Miller Defect quenching of conjugated polymer luminescence *Phys. Rev. Lett.* 73, 744 (1994)

[112] J. C. Hummelen, B. W. Knight, F. LePeq, F. Wudl, J. Yao, and C. L.Wilkins, *J. Org. Chem.* 60, 532 (1995)

[113] I. Riedel, N. Martin, F. Giacalone, J.L. Segura, D. Chirvase, J. Parisi and V. Dyakonov Polymer solar cells with novel fullerene based acceptor *Thin Solid Films* 451-452, 43 (2004)

[114] C. Waldauf and P. Schilinsky *Thin Solid Films* 451-452, 503 (2004)

[115] J. Simon and J.J. Andre Molecular Semiconductors: Photoelectrical Properties and Solar Cells *Book* (Springer, Berlin, 1985)

[116] M. Grätzel and J. E. Moser Solar Energy conversion in *Electron transfer in chemistry Book* edited by Vincenzo Balzani

[117] http://www.nature.com/nsu/000921/000921-5.html

List of publications

1) D. Chirvase, Z.Chiguvare, M.Knipper, J.Parisi, V.Dyakonov, and J.C.Hummelen Electrical and optical design and characterisation of regioregular poly(3-hexylthiophene-2.5diyl)/fullerene- based heterojunction polymer solar cells *Synth. Met*. 138, 299-304 (2003)

2) D. Chirvase, Z. Chiguvare, M. Knipper, J. Parisi, V. Dyakonov, and J. C. Hummelen Temperature dependent characteristics of poly(3 hexylthiophene)-fullerene based heterojunction organic solar cells *J. of Appl. Phys*. 93, 3376 (2003)

3) D. Chirvase, J.Parisi, J.C.Hummelen, and V.Dyakonov Influence of nanomorphology on the photovoltaic action of polymer-fullerene composites *Nanotechnology* 15,1317-1323 (2004)

Conferences

1) European Research Conference on Photovoltaic Devices: High efficiency solar cells Portugal, Tomar, september 2001 poster presentation

2) EUROMAP meeting Hasselt, Belgium october 2001 talk (30min)

3) EUROMAP meeting Linz, Austria, april 2002, talk (30min)

4) E-MRS Spring meeting Strasbourg 18-21 June 2002 poster presentation and article 1) (see list of publications)

5) EUROMAP meeting Madrid, Spain, october 2002

6) EUROMAP meeting Milano, Italy, mai 2003, talk (30 min)

7) EUROMAP meeting Kassel, Germany, october 2003, talk (30min)

8) EUROMAP meeting Madrid, Spain, june 2004, talk (30min)

Erklärung gemäss $8(2) der Promotionsordnung

Hiermit erkläre ich, dass ich diese Arbeit selbständig verfasst und nur die angegebenen Hilfsmittel benutzt habe.

Oldenburg, den 13.12.2004

Unterschrift

Curriculum vitae

Name: Chirvase
Christian name: Dana
Date and place of birth: 02.09.1967
Nationality: romanian
e-mail: chirvase_dana@yahoo.com

Education

2000- present – Carl von Ossietzky University Physics Faculty Oldenburg, Germany, PhD candidate in the field of organic based solar cells

1998-1999 – Carl von Ossietzky University, Physics Faculty Oldenburg, Germany, DAAD Scholarship for the postgraduated course "Renewable Energies", Master Degree specialization Windenergy und solar Photovoltaics.

1986- 1991 – University Politehnica Bucharest, Energy Faculty, Romania, graduated as electrical engineer

1982-1986 – Mihai Viteazul secondary school, Bucharest, Romania specialization mathematics and physics.

1974- 1982 – primary school (Bucharest, Romania)

Professional experience

- **October 1991- December 1995: Romanian Electricity Authority (RENEL) within the Energy Research and Modernizing Institut (ICEMENERG) Bucharest, Romania**

- **December 1995 – August 1998 Romanian Electricity Authority (RENEL) in the frame of Studies, Research and Engineering Group (GSCI)**

- **August 1998 – September 1999: Carl von Ossietzky University Oldenburg, Germany**

- **October 1999-December 2000: SC ELECTRICA. SA. Power Distribution Company (Marketing Department – Measurement and Energy Quality Systems).**

- **December 2000 – 2004: Carl von Ossietzky University Oldenburg, Physics Faculty Department for Energy and Semiconductor Research**

Oldenburg, 10. 10. 2004